AD A094533

NRL Memorandum Report 4438

A Comparison of Two-Step Time Integration Schemes for the Finite Element Advection Equation

LEVEL II

MICHAEL L. MORRELL

Department of Civil Engineering
Clemson University
Clemson, South Carolina

RICHARD A. SKOP and GEORGE A. KERAMIDAS

Applied Mechanics Branch
Marine Technology Division

RK023901

RK023014

January 19, 1981

DTIC
SELECTED
FEB 0 5 1981

E

NAVAL RESEARCH LABORATORY
Washington, D.C.

81 2 05 042

REPORT DOCUMENTATION PAGE		READ INSTRUCTIONS BEFORE COMPLETING FORM
1. REPORT NUMBER NRL Memorandum Report 4438	2. GOVT ACCESSION NO. *AD--A094*	3. RECIPIENT'S CATALOG NUMBER *533*
4. TITLE *(and Subtitle)* A COMPARISON OF TWO-STEP TIME INTEGRATION SCHEMES FOR THE FINITE ELEMENT ADVECTION EQUATION		5. TYPE OF REPORT & PERIOD COVERED Interim report on a continuing problem
		6. PERFORMING ORG. REPORT NUMBER
7. AUTHOR*(s)* Michael L. Morrell,* Richard A. Skop, and George A. Keramidas		8. CONTRACT OR GRANT NUMBER*(s)*
9. PERFORMING ORGANIZATION NAME AND ADDRESS Naval Research Laboratory Washington, DC 20375		10. PROGRAM ELEMENT, PROJECT, TASK AREA & WORK UNIT NUMBERS 61153N, RR0230141 0273-0-1
11. CONTROLLING OFFICE NAME AND ADDRESS Office of Naval Research Washington, DC 22217		12. REPORT DATE January 19, 1981
		13. NUMBER OF PAGES 92
14. MONITORING AGENCY NAME & ADDRESS*(if different from Controlling Office)*		15. SECURITY CLASS. *(of this report)* Unclassified
		15a. DECLASSIFICATION/DOWNGRADING SCHEDULE

16. DISTRIBUTION STATEMENT *(of this Report)*

Approved for public release; distribution unlimited.

17. DISTRIBUTION STATEMENT *(of the abstract entered in Block 20, if different from Report)*

18. SUPPLEMENTARY NOTES

*Clemson University

19. KEY WORDS *(Continue on reverse side if necessary and identify by block number)*

Advection   Finite Elements
Advection Equation   Transport Processes
Fluid Mechanics

20. ABSTRACT *(Continue on reverse side if necessary and identify by block number)*

Numerical studies of two explicit, two-step time integration techniques for the one dimensional, constant velocity finite element advection equation have been conducted for both square hill and cosine hill density distributions. One of these integration techniques, the Godunov scheme, is first order accurate in time while the other, the Lax-Wendroff scheme, is second order accurate in time. The results show that, overall, the "best" numerical solutions are obtained by combining a

(Continued)

DD **FORM 1473** EDITION OF 1 NOV 65 IS OBSOLETE
1 JAN 73
S/N 0102-014-6601

i

20. ABSTRACT (Continued)

central weighted first-step Lax-Wendroff time integration with parabolic spatial discretization either in its full or condensed $[M]$ matrix form. Both the standard and central weighted first-step Godunov time integrations are found to be numerically diffusive. This diffusivity tends to override whatever spatial discretization is used. However, the positivity property possessed by the Godunov schemes can be valuable for many applications.

CONTENTS

A COMPARISON OF TWO-STEP TIME INTEGRATION SCHEMES FOR THE FINITE ELEMENT ADVECTION EQUATION

1. INTRODUCTION

Nonlinear hyperbolic equations of the form

$$\frac{\partial \vec{\rho}}{\partial t} + \text{div}(\vec{V} \vec{\rho}) = \vec{F}(\vec{V}, \vec{\rho}) \qquad (1.1)$$

where $\vec{\rho}$ is a vector of conserved quantities, $\vec{V}$ is the velocity field, and $\vec{F}$ is a given functional, describe flow behavior in subjects ranging from hydraulics to gas dynamics. Finite difference techniques that had been applied to the solution of Equation (1.1) were examined in detail by Roache [1] in his classic text *Computational Fluid Dynamics* published in 1972. More recent finite difference attacks on Equation (1.1) have been reviewed by Sod [2] and by Book, et al. [3]. As is evident from these references, finite difference solutions of Equation (1.1) have reached a high level of sophistication and accuracy. The most significant criticism that can be leveled against these techniques is the difficulty encountered in treating complex flow boundaries. This is especially true for the most accurate methods that rely on the use of a "staggered" mesh.

A natural way of handling complex flow boundaries is through finite element discretization of the spatial derivatives in Equation (1.1). In these finite element methods (for an excellent introduction see the text by Baker [4]) the space of concern is divided into a large number of sub-spaces over each of which the dependent flow variables are approximated by shape functions. Complex flow boundaries fall naturally out of the discretization as constraints on the shape function coefficients of boundary elements.

1

Before blindly applying finite element methods to the solution of Equation (1.1), however, it is necessary to evaluate their ability to replicate some simple flow behaviors predicted by Equation (1.1). To this end, we examine in this report numerical solutions of the simple, constant velocity, advection equation

$$\frac{\partial \rho}{\partial t} + V \frac{\partial \rho}{\partial x} = 0 \tag{1.2}$$

that becomes, upon finite element spatial discretization,

$$[M]\{\dot{R}\} + V[K]\{R\} = 0. \tag{1.3}$$

Here, [M] and [K] are matrices that depend on the specific discretization, $\{R\}$ is a column matrix representing the node point values of the "density" ρ, and the dot denotes ordinary differentiation with respect to time. For practical computational purposes, two requirements can be imposed on the time integration technique used to advance Equation (1.3):

1. It should require knowledge of $\{R\}$ only at the node points. This requirement is imposed to preserve the strongest attributes of the finite element method, namely, ease of establishing grids for complex geometric boundaries and ease of handling boundary conditions.

2. It should be explicit to ensure fast, efficient calculations. This requirement really stems from Equation (1.1) where an implicit integration scheme would mandate the solution of large, nonlinear sets of algebraic equations at each time step.

The problems of concern are a) what combination of spatial discretization and time integration "best" models the true advection solution and b) whether "best" is good enough. Within bounds, the latter concern is, of course, fairly subjective.

In the subsequent sections of this report, we undertake numerical experiments using both linear and parabolic spatial discretizations of Equation (1.2) combined with two basic, two-step time integration schemes for Equation (1.3). One of these schemes is first order accurate (in a Taylor series sense) while the other is second order accurate. Following the convention of Sod [2], we refer to the first scheme as a Godunov type scheme and the second scheme as a Lax-Wendroff type scheme. We also

consider the effects of [M] matrix condensation [4] on the numerical solution. This popularly used technique obviates the need for performing an inversion of the large [M] matrix. In addition, two first step weightings of the basic time integration schemes are studied. Such weightings are used commonly in finite difference methods [1] to average the influence of adjacent nodes. One weighting gives zero weight to the node under consideration and is termed the "smoothed" weighting. The second weighting, based on symmetry considerations, is termed the "modified" weighting.

All told, twenty four different combinations of spatial discretization and time integration are applied to the advection of both a smooth cosine hill density distribution and a discontinuous square hill density distribution. For the most part, those combinations that employ a parabolic spatial discretization yield more accurate solutions than those that employ a linear spatial discretization. This result is similar to some recent findings of Leonard [5] that indicate even-ordered finite differencing to be more accurate than odd-ordered finite differencing. Overall, the "best" representation of the true advection solution is obtained from the combination of parabolic spatial discretization and modified Lax-Wendroff time integration. This time integration combined with the condensed parabolic [M] matrix formulation also gives quite acceptable numerical solutions. The modified Godunov time integration combined with either the full or condensed parabolic spatial discretization, while highly diffusive, does possess some positivity properties that can be useful in certain applications.

We conclude the report by examining time step (Courant number) stability questions for the more promising combinations of spatial discretization and time integration.

2. PROBLEM DEFINITION

Let the density of a certain substance be denoted by $\rho(x,t)$. This substance is being advected downstream (x-direction) at a constant velocity V. Requiring that the substance be conserved leads to the advection equation:

$$\frac{\partial \rho}{\partial t} + V \frac{\partial \rho}{\partial t} = 0. \tag{2.1}$$

Normally this equation is applied to a finite (or infinite) length in the x-direction, thus permitting mass to flow out at the boundaries. This would confuse the evaluation of the integration schemes, in that the resulting errors could either be in the scheme itself or the system could be losing mass. In order to avoid the possibility of gaining or losing mass, the x domain of Equation (2.1) is taken as a continuous loop.

Consider now that the x-direction is a continuous loop, hereafter called a racetrack. The domain of x is $0 \leqslant x \leqslant L$. By this we mean that the point $x = L$ is the same as the point $x = 0$ as shown in Figure 2.1. For our subsequent numerical studies, we take $L = 48$ (arbitrary units of distance).

Two initial conditions are considered: (a) a cosine hill between x_1 and x_2,

$$\rho(x,0) = F(x) = \begin{cases} 1 & x \leqslant x_1 \text{ and } x \geqslant x_2 \\ \dfrac{3}{2} - \dfrac{1}{2} \cos \dfrac{2\pi(x - x_1)}{x_2 - x_1} & x_1 < x < x_2 \end{cases} \tag{2.2}$$

and (b) a square hill also between x_1 and x_2,

$$\rho(x,0) = F(x) = \begin{cases} 1 & x \leqslant x_1 \text{ and } x \geqslant x_2 \\ 2 & x_1 < x < x_2 \end{cases}. \tag{2.3}$$

These initial conditions are shown in Figure 2.2 for $x_1 = 8$ and $x_2 = 18$.

The exact solution to Equation (2.1) is expressed as

$$\rho(x,t) = F(x - Vt) \tag{2.4}$$

where F is the initial density distribution given by Equation (2.2) or (2.3). Note that the values of x in Equation (2.4) must reflect the racetrack domain and the racetrack boundary condition

$$\rho(0,t) = \rho(L,t). \tag{2.5}$$

Although the exact solution is near to being trival, the numerical solution is extremely challenging as witnessed by the literature (see References).

3. FINITE ELEMENT FORMULATION

The Finite Element Method is a technique which divides the space domain into subdomains, called elements. Over each element the density is approximated by

$$\tilde{\rho}^e\,(x,t) \,=\, \sum_{i=1}^{K}\, R_i^e(t)\, N_i(x) \tag{3.1}$$

where $\tilde{\rho}^e(x,t)$ is the approximation of $\rho(x,t)$ over the element e, $R_i^e(t)$ are a set of discrete values at nodes (or grid points) on the boundaries or within the element, and $N_i(x)$ (which are taken to be the same form for each element) are a set of interpolation polynomials, also called shape functions, of order $K - 1$ where K is the number of nodes per element. The following subsections will define these symbols for each shape function assumed; i.e., linear and parabolic.

In general the approximate solution will be in error and will not satisfy Equation (2.1). Thus we can write,

$$\frac{\partial \tilde{\rho}^e}{\partial t} \,+\, V\, \frac{\partial \tilde{\rho}^e}{\partial x} \,=\, E^e(x,t). \tag{3.2}$$

For any assumed $\tilde{\rho}^e$ we seek a solution for R_i^e which will minimize $E^e(x,t)$. There are several techniques to do this; however, Galerkin's method is used here. The method requires that the error $E^e(x,t)$ be orthogonal with $N_i(x)$ for each element; therefore,

$$\int_0^{L^e} E^e(x,t)\, N_i(x)\, dx \,=\, 0 \quad i = 1,\, \ldots,\, K \tag{3.3}$$

where L^e is the element length. Substitution of Equation (3.1) into (3.3) gives the classic Finite Element discretization equation

$$[M^e]\, \{\dot{R}^e\} \,+\, V\, [K^e]\, \{R^e\} \,=\, \{0\} \tag{3.4}$$

where

$$[M^e] \rightarrow m_{ij}^e = \int_0^{L^e} N_i(x)\, N_j(x)\, dx \qquad i,j = 1,\, \ldots,\, K \tag{3.5}$$

$$[K^e] \rightarrow k_{ij}^e = \int_0^{L^e} N_i'(x)\, N_j(x)\, dx \qquad i,j = 1,\, \ldots,\, K \tag{3.6}$$

$$\{R^e\} = \{R_1^e\ R_2^e\ \ldots\ R_K^e\}^T$$

$$\{\dot{R}^e\} = \{\dot{R}_1^e\ \dot{R}_2^e\ \ldots\ \dot{R}_K^e\}^T$$

The prime denotes spatial differentiation and the dot denotes ordinary time differentiation.

5

When equation (3.4) is written for each element and connectivity between elements is considered then the global system of equations to be solved is

$$[M]\{\dot{R}\} + V[K]\{R\} = \{0\} \tag{3.7a}$$

where

$$\{R\} = \left\{R_1 R_2 \dots R_N\right\}^T \tag{3.7b}$$

Here $[M]$ and $[K]$ are the assembled mass and advection matrices and N is the total number of nodal values (degrees of freedom) in the system.

3.1 Linear Elements

Linear finite elements are developed by using a linear shape function with the coefficients expressed in terms of nodal values. Thus for the linear element we have from Equation (3.1) with $K = 2$:

$$\tilde{\rho}^e(x, t) = R_1^e N_1 + R_2^e N_2$$

where

$$N_1 = 1 - (x/L^e) \tag{3.8}$$
$$N_2 = (x/L^e)$$

and where R_1^e is the density at $x = 0$ and R_2^e is the density at $x = L^e$. (Again, L^e is the element length). Integrating Equation (3.5) with the shape function of Equation (3.8) defines the mass matrix for $i,j = 1$ to 2:

$$[M^e] = \frac{L^e}{6} \begin{bmatrix} 2 & 1 \\ 1 & 2 \end{bmatrix}. \tag{3.9}$$

Likewise, integrating Equation (3.6) after differentiating Equations (3.8) defines the advection matrix for $i,j = 1$ to 2:

$$[K^e] = \frac{1}{2} \begin{bmatrix} -1 & 1 \\ -1 & 1 \end{bmatrix}. \tag{3.10}$$

Now Equation (3.4) can be written for a linear element.

$$\frac{L^e}{6} \begin{bmatrix} 2 & 1 \\ 1 & 2 \end{bmatrix} \begin{Bmatrix} \dot{R}_1^e \\ \dot{R}_2^e \end{Bmatrix} + \frac{V}{2} \begin{bmatrix} -1 & 1 \\ -1 & 1 \end{bmatrix} \begin{Bmatrix} R_1^e \\ R_2^e \end{Bmatrix} = \begin{Bmatrix} 0 \\ 0 \end{Bmatrix} \tag{3.11}$$

The assembled mass and advection matrices appearing in Equation (3.7) are given, for the linear element discretization, in Appendix A.

3.2 Parabolic Elements

Parabolic finite elements are developed by using parabolic shape functions with coefficients expressed in terms of nodal values. For this element a node at the mid-point is established in addition to the nodes at the ends. Equation (3.1) is written for $K = 3$:

$$\bar{\rho}^e(x,t) = R_1^e N_1 + R_2^e N_2 + R_3^e N_3$$

where

$$N_1 = 1 - 3(x/L^e) + 2(x/L^e)^2$$
$$N_2 = 4(x/L^e) - 4(x/L^e)^2 \tag{3.12}$$
$$N_3 = - (x/L^e) + 2(x/L^e)^2$$

and where R_1^e, R_2^e and R_3^e are the densities at $x = 0$, $x = L^e/2$, and $x = L^e$, respectively. Integrating Equation (3.5) with the above shape functions defines the mass matrix for $i,j = 1, 2, 3$:

$$[M^e] = \frac{L^e}{30} \begin{bmatrix} 4 & 2 & -1 \\ 2 & 16 & 2 \\ -1 & 2 & 4 \end{bmatrix} \tag{3.13}$$

Likewise, integrating Equation (3.6) after differentiating Equations (3.12) defines the advection matrix for $i,j = 1, 2, 3$:

$$[K^e] = \frac{1}{6} \begin{bmatrix} -3 & 4 & -1 \\ -4 & 0 & 4 \\ 1 & -4 & 3 \end{bmatrix}. \tag{3.14}$$

Now Equation (3.4) can be written for the parabolic element:

$$\frac{L^e}{30} \begin{bmatrix} 4 & 2 & -1 \\ 2 & 16 & 2 \\ -1 & 2 & 4 \end{bmatrix} \begin{Bmatrix} \dot{R}_1^e \\ \dot{R}_2^e \\ \dot{R}_3^e \end{Bmatrix} + \frac{V}{6} \begin{bmatrix} -3 & 4 & -1 \\ -4 & 0 & 4 \\ 1 & -4 & 3 \end{bmatrix} \begin{Bmatrix} R_1^e \\ R_2^e \\ R_3^e \end{Bmatrix} = \begin{Bmatrix} 0 \\ 0 \\ 0 \end{Bmatrix}. \tag{3.15}$$

The assembled mass and advection matrices appearing in Equation (3.7) are given, for the parabolic element discretization, in Appendix B.

3.3 Condensed [M] Matrix Formulation

Equation (3.7) can be rewritten formally as

$$\{\dot{R}\} = [M]^{-1}[K]\{R\} \tag{3.16}$$

where $[M]^{-1}$ denotes the inverse of $[M]$. Generally, $[M]$ is a large, sparse matrix and the calculation of $[M]^{-1}$ (which is a full matrix) can be very time consuming. The process of condensing the mass matrix, or lumping the mass at the diagonal terms, is a popular procedure [4] for avoiding this time consuming inversion.

Hence, the condensed mass matrix $[M_c]$ is defined by

$$[M_c] \rightarrow \begin{cases} m_{cii} = \sum_{j=1}^{N} m_{ij} & i = 1, \ldots, N \\ m_{cij} = 0, \; i \neq j & i,j = 1, \ldots, N \end{cases} \tag{3.17}$$

where the m_{ij} are the entries in $[M]$ and N is the rank of $[M]$. The matrix $[M_c]$ now replaces $[M]$ in Equation (3.7) and Equation (3.16) is replaced by

$$\{\dot{R}\} = - V[M_c]^{-1}[K]\{R\}. \tag{3.18}$$

We note that this condensation is mass preserving.

4. TIME INTEGRATION SCHEMES

There are many methods available for advancing Equation (3.16) [or (3.18)] in time. For reasons explained in the Introduction, the focus of this report deals with the two-step methods of Lax-Wendroff and Godunov (see Reference [2]).

4.1 Standard Two-Step

Consider that the value of the nodal densities at time step n are known $\{R^n\}$. The solution at the $n + 1$ time step is sought. The time increment is Δt. Then the standard two-step method can be written as:

$$\text{1st step} \quad \{R^{n+\alpha}\} = \{R^n\} + \alpha \, \Delta t \{\dot{R}^n\} \tag{4.1a}$$

and

$$\text{2nd step} \quad \{R^{n+1}\} = \{R^n\} + \Delta t \{\dot{R}^{n+\alpha}\} \tag{4.1b}$$

where α is a fraction of the time step. The time derivative $\{\dot{R}^n\}$ is determined from Equation (3.16) [or (3.18)] using $\{R^n\}$ and subsequently $\{\dot{R}^{n+\alpha}\}$ is determined from Equation (3.16) [or (3.18)] using $\{R^{n+\alpha}\}$ from Equation (4.1a).

8

The two well-known methods embodied in equations (4.1) are the Lax-Wendroff method when $\alpha = 1/2$ and the Godunov method when $\alpha = 1$. The Lax-Wendroff method first estimates the time derivative at the mid-point of the time step then uses the value to step ahead to $n + 1$. The Godunov method first estimates the time derivative at a full step and uses this estimate to step ahead to $n + 1$.

Equations (4.1) are referred to in this report as the *standard* two-step methods. Because the standard two-step methods update a nodal value only as a function of its previous value, it seems plausible that introducing a weighting matrix to average the influence of adjacent nodes might improve numerical accuracy. Such averaging is used frequently in finite difference methods [1]. This weighting matrix should have a general form so as to be problem independent. Two such weighting matrices are employed herein.

4.2 Smoothed Two-Step

The first weighting matrix is termed the "smoothed" weighting matrix. The terms in the smoothed weighting matrix, $[W_s]$, are determined from the entries m_{ij} in the global mass matrix $[M]$:

$$[W_s] \rightarrow \begin{cases} w_{sii} = 0 & i = 1, \ldots, N \\ w_{sij} = \dfrac{m_{ij}}{C_i}, i \neq j & i, j = 1, \ldots, N \end{cases}$$

$$C_i = \sum_{\substack{j=1 \\ j \neq i}}^{N} m_{ij}. \tag{4.2}$$

The quantity C_i is the sum of all terms in row 'i' of $[M]$ except the diagonal term. Note that the sum across row 'i' of $[W_s]$ is unity so that $[W_s]$ is mass conserving.

The weighting matrix is used only in the first step. Thus the *smoothed* two-step method is written as:

$$\text{1st step} \quad \{R^{n+\alpha}\} = [W_s]\{R^n\} + \alpha \, \Delta t \{\dot{R}^n\}$$

and

$$\text{2nd step} \quad \{R^{n+1}\} = \{R^n\} + \Delta t \{\dot{R}^{n+\alpha}\}. \tag{4.3}$$

The smoothed Lax-Wendroff method is obtained by letting $\alpha = 1/2$ in Equation (4.3); and the smoothed Godunov method is obtained by letting $\alpha = 1$ in Equation (4.3).

4.3 Modified Two Step

The second weighting matrix is termed the "modified" weighting matrix. The terms in the modified weighting matrix $[W_m]$, are determined from $[M]$: the global mass matrix:

$$[W_m] \rightarrow w_{mij} = \frac{m_{ij}}{C_i} \quad i, j = 1, \ldots, N$$

$$C_i = \sum_{j=1}^{N} m_{ij}. \tag{4.4}$$

Now C includes the diagonal term m_{ii} and the sum across row 'i' of $[W_m]$ is again unity.

The weighted matrix is again used only in the first step. Thus the *modified* two-step method is written as:

$$\text{1st step} \quad \{R^{n+\alpha}\} = [W_m]\{R^n\} + \alpha \Delta t \{\dot{R}^n\}$$

and

$$\text{2nd step} \quad \{R^{n+1}\} = \{R^n\} + \Delta t \{\dot{R}^{n+\alpha}\} \tag{4.5}$$

The modified Lax-Wendroff method is obtained by letting $\alpha = 1/2$ in Equation (4.5); and the modified Godunov method is obtained by letting $\alpha = 1$ in Equation (4.5).

5. NUMERICAL RESULT

Numerical computations were performed to evaluate the ability of the various solution schemes to replicate the true advection solution. There are several measures by which to ascertain the adequacy of a particular scheme: one being the eyeball. A second measure used herein is the average absolute error; hereafter called simply the Error given by

$$\text{Error} = \frac{1}{N} \sum_{i=1}^{N} |\rho - \bar{\rho}| \tag{5.1}$$

where ρ is the exact solution, $\bar{\rho}$ is the approximate solution, and N is the number of nodes. This quantitative measure is used to compare the schemes. The scheme with the smallest Error is the "best"

numerical model. At which value this error becomes intolerable is still subjective. However by observing the density distributions at a given time and the associated Error, an acceptable range can be established.

As mentioned previously, the length of the racetrack was set at $L = 48$ (arbitrary units of distance) and the initial location of the cosine hill and square hill density distributions [Equations (2.2) and (2.3)] was between $x_1 = 8$ and $x_2 = 18$. The advection velocity was set at $V = 1$ unit of distance/s. Hence, the density distribution is advected once around the track every 48 s.

In Section 5.1, the results obtained using the linear finite element spatial discretization are presented. Section 5.2 contains the results obtained using the parabolic finite element spatial discretization. These results are based on a time period of 96 s (two cycles around the track) and are compared in Section 5.3. The effect of time step size on the better solution schemes is studied in Section 5.4. Finally, Section 5.5 presents results for long time periods. The density distribution is allowed to travel around the track for 480 s (ten cycles).

5.1 Linear Elements

The development of the linear finite element (linear FEM) spatial discretization is given in Section 3.1 and Appendix A. We take the length of each element as $L^e = 1$ unit of distance. Thus, there are 48 elements on the track. Node 1 corresponds to $x = 0$ while node $N + 1 = 49$ corresponds to $x = L$. Since the track is closed, the number of degrees of freedom $N = 48$.

Based on some trial calculations, a time step $\Delta t = 0.2$ s was selected to study the time integration schemes. The Courant number, equal to $V \Delta t / L^e$, is 0.2 for the linear element.

Figures 5.1.1 to 5.1.6 present results of the advected cosine hill density distribution for the three Lax-Wendroff methods (standard, smoothed, and modified) and the three Godunov methods using the linear FEM. Figures 5.1.7 to 5.1.12 contain similar results using the condensed linear mass matrix formulation (linear CFM). It is worthwhile to point out that the linear CFM spatial discretization is

equivalent to standard central differencing. The time periods in each figure are 24 s, 48 s, 72 s, and 96 s or 1/2, 1, 1-1/2, and 2 cycles around the track. The exact solution is superimposed on the graphs of the advected hill. Using a time step of 0.2 s means at 96 s the solution has gone through 480 time steps.

The first item to notice from Figure 5.1.1 is that the standard Lax-Wendroff method does an excellent job of advecting the cosine hill. From Figure 5.1.13 (a) the Error at 96 s is 1.4%. Looking at the other linear FEM figures, the remaining time integrators tend to diffuse the hill. This is numerical diffusion due to the nature of the two-step method. The standard Godunov scheme is the only one which shows no oscillations. Both the standard Lax-Wendroff scheme and standard Godunov scheme "track" the hill (do not lead or lag), but the latter has a 50% reduction of the peak value at 96 s. Figures 5.1.13 (a) and (b) show that the smoothed integrator is the poorest, the standard is the best, and the modified is in between. Using the Error and the density graphs, value judgements can be made on goodness.

The graphs of the six time integration schemes combined with the linear CFM method indicate all of these techniques to be diffusive and to lag behind the true position of the hill. Figure 5.1.13 (c) and (d) contain the associated Errors for the linear CFM. First note that the order, best to poorest, is the same as in Figures 5.1.13 (a) and (b), i.e, standard, modified, and smoothed. From the Error graph the standard Godunov is the best of the linear CFM methods with a 10% Error at 96 s. If the Error graphs for linear FEM were over-laid on those for linear CFM, all of the respective FEM techniques would have less error than the associated CFM technique. However, the difference is small except for the standard Lax-Wendroff. Careful observations will reveal that the standard finite difference techniques (linear CFM) do reasonably well compared to the respective linear FEM techniques.

Whereas the cosine hill density distribution represents a "smooth" function, that is Equation (2.2) and its first derivative are continuous functions, the square hill density distribution presents a more severe test for the solution procedures.

12

The square hill solutions using the linear FEM are presented in Figures 5.1.14 to 5.1.19 and the associated Error graphs in Figures 5.1.26 (a) and (b). After observing these, it is noted that none do as well as they did for the cosine hill. The smallest Error is now around 14%. There are similarities between the two propagated hills. The two standard time integration schemes still track the hill accurately. The standard Lax-Wendroff scheme is the least diffusive (has the sharpest front) but has the largest amplitude oscillations away from the hill. The standard Godunov scheme diffuses the hill but to a large extent damps out the oscillations. From observing the propagated hill graphs and the Error graphs, we see that modified Lax-Wendroff and Godunov methods give results comparable to the standard methods. The smoothed integrator is still the poorest by a sizeable margin.

Turning now to the linear CFM method, Figures 5.1.20 to 5.1.25 contain results of the advected square hill and the associated Error graphs are in Figures 5.1.26(c) and (d). First note that the propagated hill does not look any worse than the associated linear FEM hill. Next note from the Error graph that the relative positions of the time integration schemes are the same as previously observed. The smoothed method is still the poorest and the standard and the modified methods give nearly the same Error.

Comparing linear FEM and linear CFM using the standard and modified integrators shows that at 96 s the Errors are approximately 16% (FEM) and 22% (CFM) using Lax-Wendroff methods and 15% (FEM and CFM) using Godunov methods. After reviewing the associated propagated hill, there is not much difference between the respective FEM and CFM methods. For example, using the standard Lax-Wendroff scheme, the propagated hills for FEM and CFM have the same quality of tracking the hill and maintaining the sharpness of the front.

5.2 Parabolic Elements

The development of the parabolic finite element spatial discretization is given in Section 3.2 and Appendix B. We take the length of each element as $L^e = 2$ units of distance. Thus there are 24 elements on the 48 unit long track. Recalling that each parabolic element has a mid-point node, there are

13

still therefore 48 nodal degrees of freedom. By using 24 parabolic elements a direct comparison can be made with 48 linear elements on the basis of equal "computational effort."

The advection velocity remains at $V = 1$ unit of distance/s and the time step remains at $\Delta t = 0.2$ s. The Courant number based on element length, $V\Delta t/L^e$, is 0.10 for the parabolic element. There is a question as whether the element length or distance between node points is the appropriate length scale for defining the Courant number. Based on the latter length scale, the Courant number remains 0.20.

The graphs for the smoothed time integration schemes are not included for the parabolic element. From observations discussed in Section 5.1, it was shown to be the poorest method. In addition, the smoothed Lax-Wendroff scheme in combination with the parabolic spatial discretization becomes unstable in a short time period. Error values greater than 100% were found in less than 24 s.

Advection of the cosine hill is again studied first. Figures 5.2.1 to 5.2.4 contain the parabolic FEM solutions. The Error graphs are in Figures 5.2.9(a) and (b). Both the standard and modified Lax-Wendroff time integrations do an excellent job of tracking the hill and its amplitude, with the modified method having the smallest Error, 1.4%. Both Godunov methods track the hill but the amplitude is reduced by numerical diffusion. The Error graphs show virtually no difference between the standard and modified Godunov methods.

The parabolic CFM solutions for the advected hill are shown in Figures 5.2.5 to 5.2.8. The associated Error graphs appear in Figures 5.2.9(c) and (d). For the two Lax-Wendroff methods, parabolic CFM does remarkably well, giving an Error of 2% for the standard and 4% for the modified. Also, both Godunov methods give results nearly identical to those obtained with parabolic FEM. Thus, the condensing of the mass matrix to avoid the time consuming inversion process is extremely advantageous for the problem of the cosine hill.

Turning now to the advection of the square hill, the parabolic FEM results appear in Figures 5.2.10 to 5.2.13. The Error graphs are in Figures 5.2.18 (a) and (b). As with linear elements, the

14

advected solution for the square hill is not as accurate as that for the cosine hill. All the parabolic FEM schemes track the hill well. The standard Lax-Wendroff method, which gave good results with the linear element and the parabolic element for a cosine hill now is tending to loose stability at 96 s. The modified Lax-Wendroff scheme remains stable and tracks the position and amplitude of the hill reasonably well. The Godunov methods retain the characteristics of diffusivity and positivity that have been previously observed.

Figures 5.2.14 to 5.2.17 contain results of the parabolic CFM solutions for the advected square hill. The Error graphs are displayed in Figures 5.2.18 (c) and (d). From the graphs of the advected hills there does not seem to be much difference in the tracking abilities of either CFM or FEM combined with the modified Lax-Wendroff scheme or either Godunov scheme. It is worthwhile to note that, for the standard Lax-Wendroff scheme, the CFM is stable while the FEM is diverging by the end of 96 s.

After examination of the four sets of Error graphs in Figure 5.2.18, it is seen that the modified Lax-Wendroff scheme combined with parabolic FEM has the least Error, 8% at 96 s. The associated parabolic CFM has an Error of 12% at 96 s, not a significant difference. Upon reviewing the advected square hills for these two combinations, no significant difference is found. Both combinations track the position and amplitude of the hill reasonably well. Both produce peak amplitudes that are approximately 10% greater than they should be and both give roughly the same degree of sharpness of the hill front.

5.3 Comparison of Linear and Parabolic Elements

In Table 5.3.1, the errors generated by the various spatial discretization/time integration schemes at 96 s (two cycles) are summarized. The "smoothed" methods are not included in the table since their performances were markedly inferior to the other methods in advecting the density distribution.

From the table, we see that the numerically diffusive, standard Godunov time integration scheme overrides whatever spatial discretization is used. The same is true of the modified Godunov scheme

15

except in combination with linear CFM. For the linear discretizations, we also not that the Godunov schemes tend to outperform the Lax-Wendroff schemes.

Turning our attention to the modified Lax-Wendroff time integration scheme, we not diminishing errors as we proceed from linear CFM to linear FEM to parabolic CFM to parabolic FEM. This latter combination produces the least overall error for both the cosine hill and square hill advection problems.

The results for the standard Lax-Wendroff scheme are mixed. Linear FEM and parabolic CFM spatial discretization give equivalent errors that are substantially below those obtained with linear CFM. However, this time integration in combination with parabolic FEM performs poorly for square hill advection.

5.4 Time Step Size Study

To insure that the results of the previous sections were not biased by the selection of $\Delta t = 0.2$ s and also to examine the effects of time step size on the stability and accuracy of the advected solution, a study of time step variation was undertaken for some of the better performing numerical models.

For the cosine hill density distribution, we considered the standard Lax-Wendroff, linear FEM combination and the modified Lax-Wendroff, parabolic FEM combination. The Error graphs as a function of time step size are given in Figure 5.4.1.

For the standard Lax-Wendroff, linear FEM scheme, we see that the error decreases as Δt decreases from 0.5 s to 0.1 s. However, there is no significant difference between the errors for $\Delta t = 0.2$ s and $\Delta t = 0.1$ s; and, in fact, an asymptotic error of around 1% appears to have been reached.

In contrast to the decreasing Error with decreasing Δt, the modified Lax-Wendroff, parabolic FEM scheme appears to have a minimum error at around $\Delta t = 0.25$ s. The differences in error for time steps ranging from $\Delta t = 0.1$ s to $\Delta t = 0.33$ s are not meaningful, however. For $\Delta t = 0.5$ s, this scheme still yields an acceptable error as compared to the previous scheme that becomes unstable. The

16

advection of the cosine hill with $\Delta t = 0.5$ s is shown in Figure 5.4.2. The computational effort here is 2/5th of that required for $\Delta t = 0.2$ s.

Turning now to the square hill, the effects of time step size on six of the eight combinations of Lax-Wendroff time integration and spatial discretization were examined. The Errors for linear FEM are shown in Figure 5.4.3, and for linear CFM in Figure 5.4.4. We see from these figures that $\Delta t = 0.2$ s is representative of the general behavior of each scheme. We also not that, as with the cosine hill, the standard Lax-Wendroff scheme gives decreasing error with decreasing Δt, while the modified Lax-Wendroff scheme appears to have a minimum error at an intermediate Δt.

The Error results for parabolic FEM are given in Figure 5.4.5. The same comments as made above are applicable except we note that using a time step $\Delta t = 0.1$ s in conjunction with standard Lax-Wendroff, parabolic FEM provides a stable solution.

5.5 Time Duration Study

As a final check on the performance of the better methods, the density distributions were numerically advected ten times (480 s) around the racetrack. Hence, for $\Delta t = 0.2$ s, there were 2400 steps in the time integration.

Examining the results for the cosine hill first, Figures 5.5.1 and 5.5.2 show, respectively, the advected solutions for the standard Lax-Wendroff, linear FEM scheme and for the modified Lax-Wendroff, parabolic FEM scheme. After ten cycles around the track, the performance of the latter scheme is seen to be superior to the performance of the former scheme. The Error graph for this problem is shown in Figure 5.5.3. A 4% error after ten cycles around the track is exceptional performance for an explicit numerical advector.

For the square hill, the modified Lax-Wendroff scheme was the only time integrator used. The advected solutions for this time integrator in combination with linear FEM, linear CFM, parabolic FEM, and parabolic CFM are shown in Figures 5.5.4 to 5.5.7, respectively. After ten cycles, it is seen

that the linear FEM and linear CFM combinations have washed out most of the information contained in the original square hill. The parabolic FEM and parabolic CFM combinations, meanwhile, continue to excellently track the location of the hill. In both cases, the hill has lost its sharp front but still has a distinct front. The peak amplitude is 10% greater than it should be. Very few oscillations occur away from the hill. For both cases, the Error after 480 s is about 10%.

Finally, in Figure 5.5.8, the advected square hill for the modified Lax-Wendroff, parabolic FEM scheme with $\Delta t = 0.33$ s is shown. The solution is again quite satisfactory. The Error graph comparing $\Delta t = 0.2$ s and $\Delta t = 0.33$ s is given in Figure 5.5.9.

6. CONCLUSIONS

Numerical studies of explicit time integration techniques for the finite element advection equation have been conducted. The results have shown that, overall, the "best" numerical solutions are obtained by combining the modified Lax-Wendroff time integration with parabolic spatial discretization either in its full or condensed $[M]$ matrix form. Both the standard and modified Godunov time integrations have been shown to be numerically diffusive. This diffusivity tends to override whatever spatial discretization is used. However, the positivity property possessed by the Godunov schemes can be valuable for certain applications.

Many numerical questions remain for future studies to resolve. These include the abilities of the better schemes to integrate coupled sets of nonlinear hyperbolic equations and to handle multidimensional problems. This latter issue can grow exponentially since we have shown the better schemes to involve nonlinear shape functions. Many analytical questions regarding the stability and phase properties of the various schemes also need to be answered.

7. ACKNOWLEDGMENTS

8. REFERENCES

[1]   P.J. Roache, 1972 Computational Fluid Dynamics. Albuquerque, New Mexico: Hermosa Publishers.

[2]   G.A. Sod, 1978 Journal of Computational Physics 27, 1-31. A survey of several finite difference methods for systems of nonlinear hyperbolic conservation laws.

[3]   D.L. Book, et.al., 1979 Naval Research Laboratory Memorandum Report 4095 (Washington, DC). Recent developments in computational techniques for applied hydrodynamics.

[4]   A.J. Baker, 1979 Finite Element Computational Fluid Mechanics. Knoxville, Tennessee: The University of Tennessee at Knoxville.

[5]   B.P. Leonard, 1979 in Finite Element Methods for Convection Dominated Flows. New York, New York: American Society of Mechanical Engineers. A survey of finite differences of opinion on numerical muddling of the incomprehensible defective confusion equation.

Appendix A
LINEAR ELEMENT MATRICES

Let the x domain be subdivided into N linear finite elements each of length L^e. The nodes are numbered consecutively from 1 to $N + 1$ as x increases from 0 to L. The element mass $[M^e]$ and advection $[K^e]$ matrices are given by Equations (3.9) and (3.10).

On recalling that nodes 1 and $N + 1$ represent the same point (racetrack boundary condition), the assembled mass $[M]$ and advection $[K]$ matrices for the N degree of freedom system are found as

$$[M] = \frac{L^e}{6} \begin{bmatrix} 4 & 1 & & & & & & 1 \\ 1 & 4 & 1 & & & & & \\ & 1 & 4 & 1 & & & & \\ & & & & & & & \\ & & & & & 1 & 4 & 1 \\ & & & & & & 1 & 4 & 1 \\ 1 & & & & & & & 1 & 4 \end{bmatrix} \begin{matrix} 1 \\ 2 \\ 3 \\ \cdot \\ \cdot \\ \cdot \\ N-2 \\ N-1 \\ N \end{matrix}$$

$$
[K] = \frac{1}{2}
\begin{bmatrix}
0 & 1 & & & & & & -1 \\
-1 & 0 & 1 & & & & & \\
 & -1 & 0 & 1 & & & & \\
 & & & & & & & \\
 & & & & & & & \\
 & & & & & & & \\
 & & & & -1 & 0 & 1 & \\
 & & & & & -1 & 0 & 1 \\
1 & & & & & & -1 & 0
\end{bmatrix}
\begin{matrix}
1 \\ 2 \\ 3 \\ \cdot \\ \cdot \\ \cdot \\ N-2 \\ N-1 \\ N
\end{matrix}
$$

Appendix B
PARABOLIC ELEMENT MATRICES

Let x domain be subdivided into N parabolic finite elements each of length L^e. The nodes are numbered consecutively from 1 to $2N + 1$ as x increase from 0 to L. The even numbered nodes correspond to element mid-point nodes. The element mass $[M^e]$ and advection $[K^e]$ matrices are given by equations (3.13) and (3.14).

On recalling that nodes 1 and $2N + 1$ represent the same point (racetrack boundary condition), the assembled mass $[M]$ and advection $[K]$ matrices for the $2N$ degree of freedom system are found as

$$[M] = \frac{L^e}{30}
\begin{bmatrix}
8 & 2 & -1 & & & & & & -1 & 2 \\
2 & 16 & 2 & 0 & & & & & & \\
-1 & 2 & 8 & 2 & -1 & & & & & \\
 & 0 & 2 & 16 & 2 & 0 & & & & \\
 & & & & & & & & & \\
 & & & & -1 & 2 & 8 & 2 & -1 & \\
 & & & & & 0 & 2 & 16 & 2 & 0 \\
-1 & & & & & & -1 & 2 & 8 & 2 \\
2 & & & & & & & 0 & 2 & 16
\end{bmatrix}
\begin{matrix}
1 \\ 2 \\ 3 \\ 4 \\ \\ 2N-3 \\ 2N-2 \\ 2N-1 \\ 2N
\end{matrix}$$

with column labels $1\quad 2\quad 3\quad 4\quad \cdots\quad 2N-3\quad 2N-2\quad 2N-1\quad 2N$

22

$$[K] = \frac{1}{6} \begin{array}{cccccccccc} 1 & 2 & 3 & 4 & & . & . & . & 2N-3 & 2N-2 & 2N-1 & 2N \\ \end{array}$$

	1	2	3	4				2N-3	2N-2	2N-1	2N	
	0	4	-1						1	-4		1
	-4	0	4	0								2
	1	-4	0	4	-1							3
		0	-4	0	4	0						4
												.
												.
				1	-4	0	4	-1				2N
					0	-4	0	4	0			2N-2
	-1					1	-4	0	4			2N-1
	4						0	-4	0			2N

TABLE 5.3.1

Percent errors at 96s (two cycles) with a time step $\Delta t = 0.2s$.

	linear FEM				linear CFM			
	SLW	MLW	SG	MG	SLW	MLW	SG	MG
cosine hill	1	14	9	10	18	20	10	12
square hill	16	14	15	16	21	24	15	19

	parabolic FEM				parabolic CFM			
	SLW	MLW	SG	MG	SLW	MLW	SG	MG
cosine hill	3	1	9	9	2	4	9	9
square hill	33	8	15	15	15	12	15	15

$$x = 0 = L$$

x

V

x_1

x_2
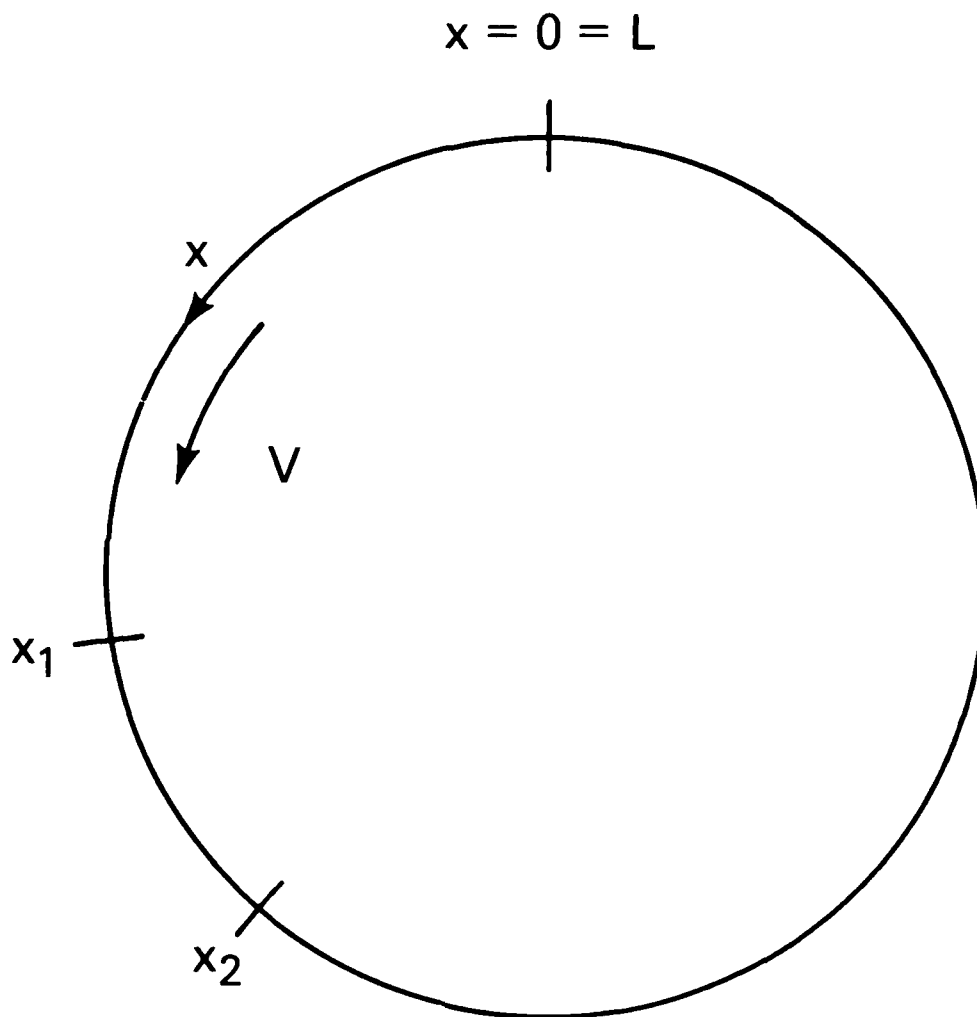
Fig. 2.1 — Domain of x
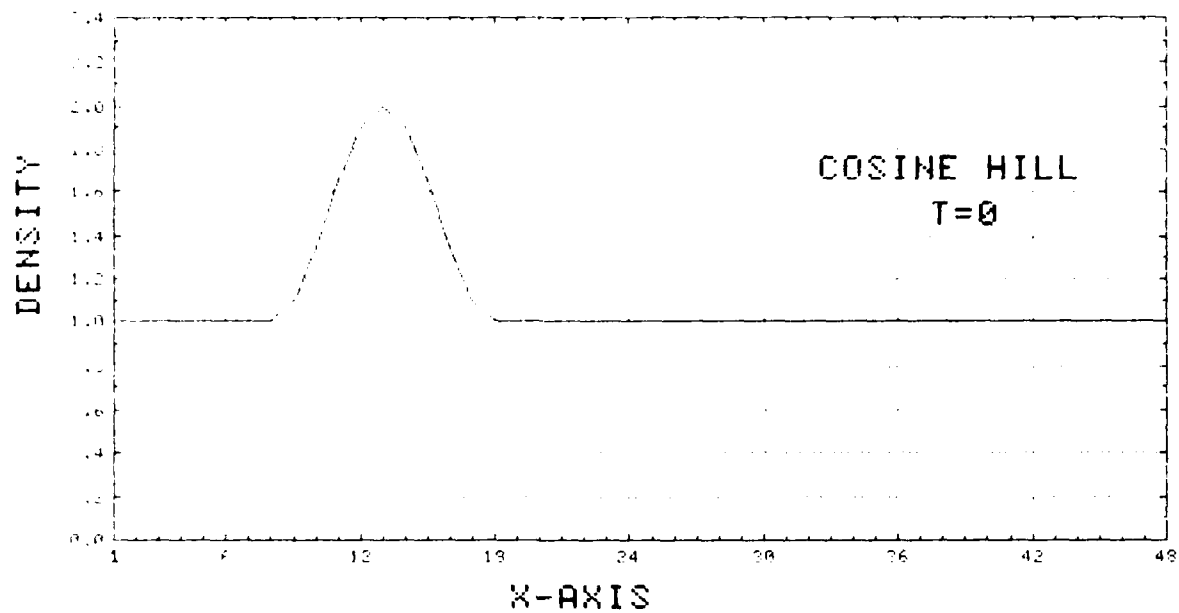
(a)
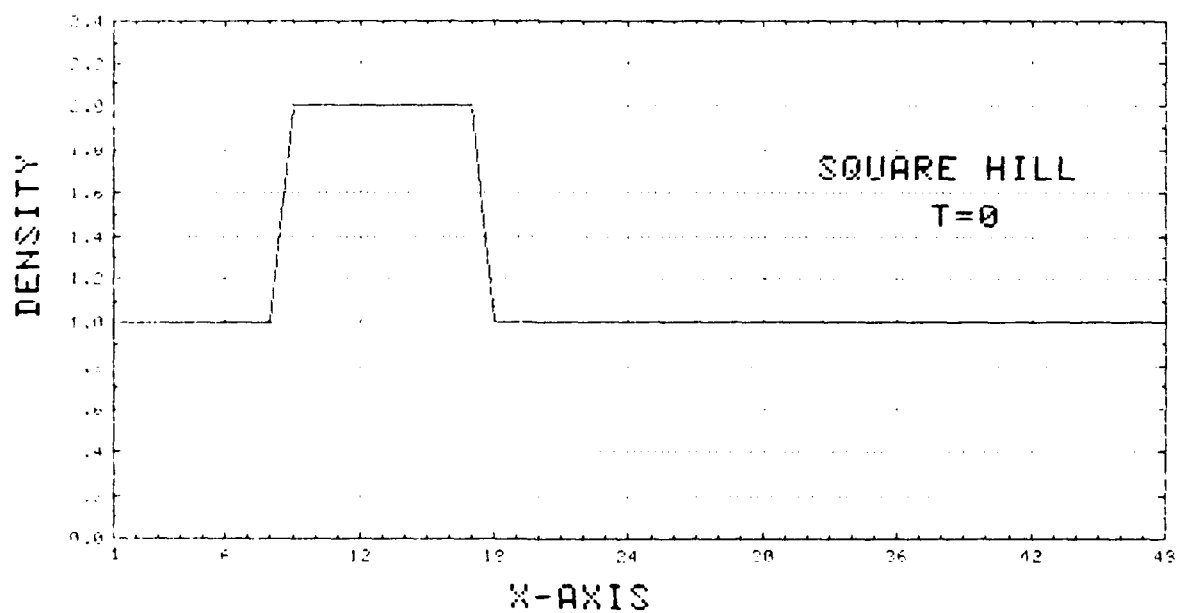
(b)

Fig. 2.2 — Initial conditions: (a) cosine hill, (b) square hill
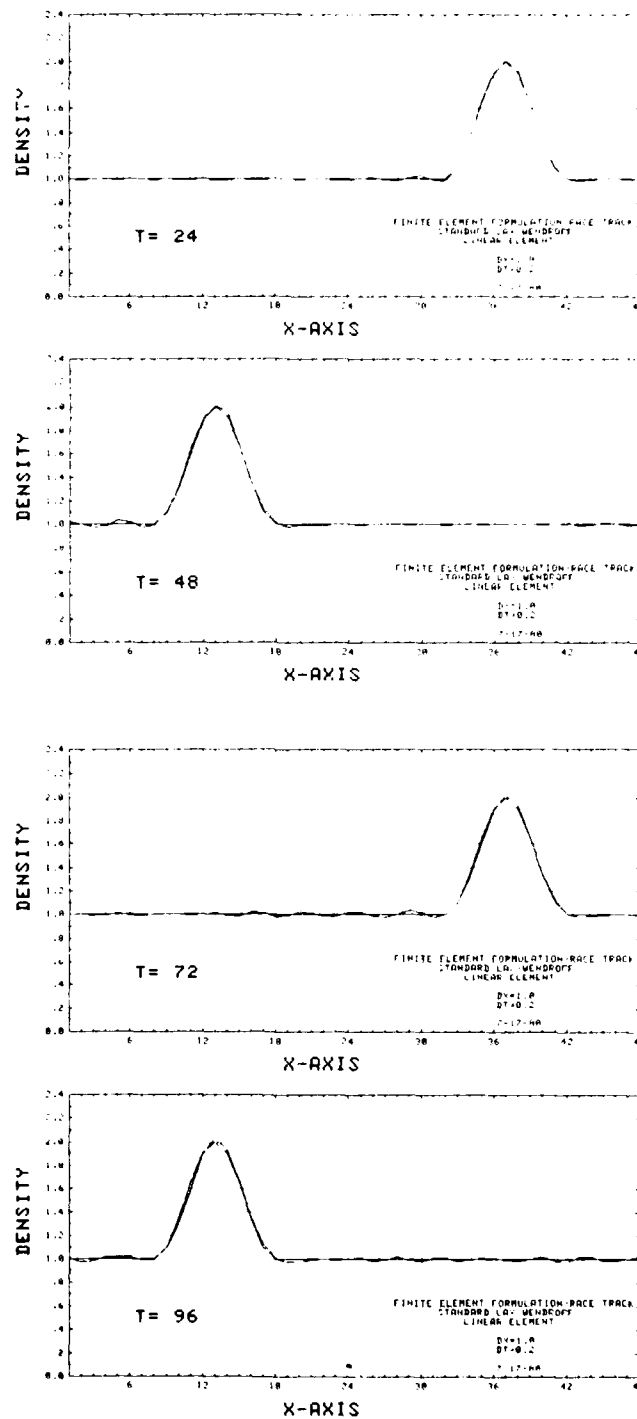
Fig. 5.1.1 — Advected cosine hill: standard Lax-Wendroff, linear FEM
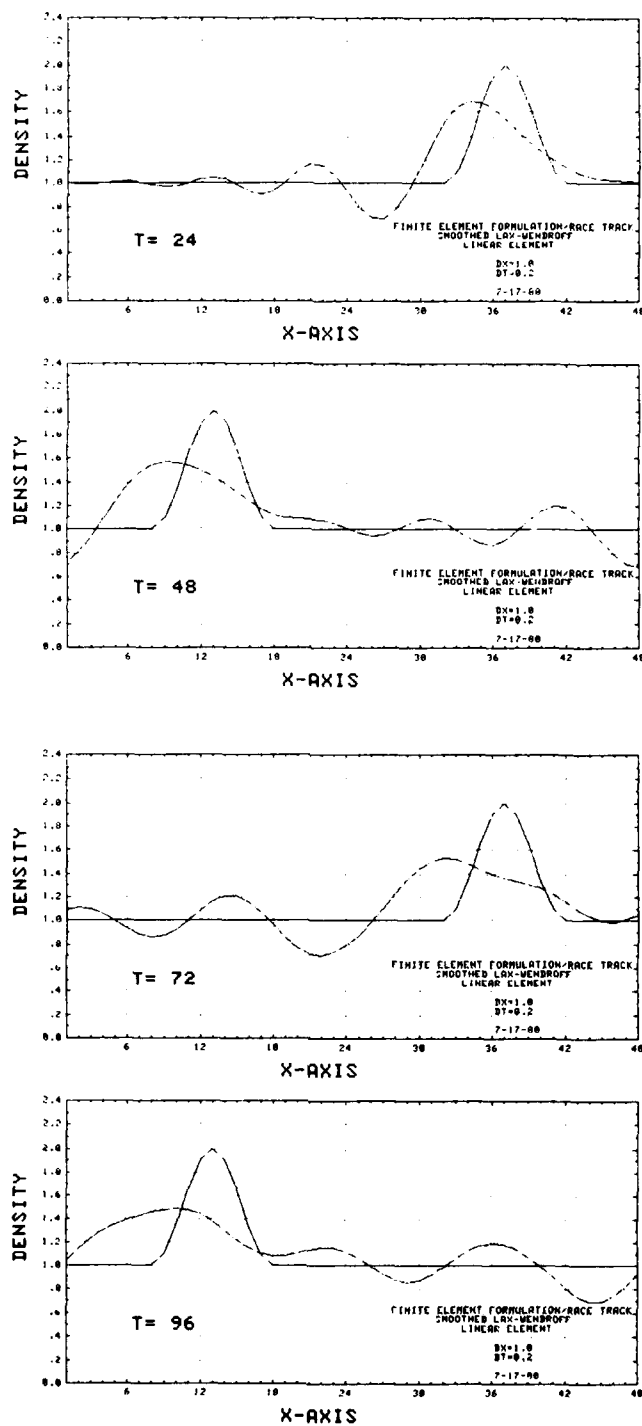
Fig. 5.1.2 — Advected cosine hill: smoothed Lax-Wendroff, linear FEM
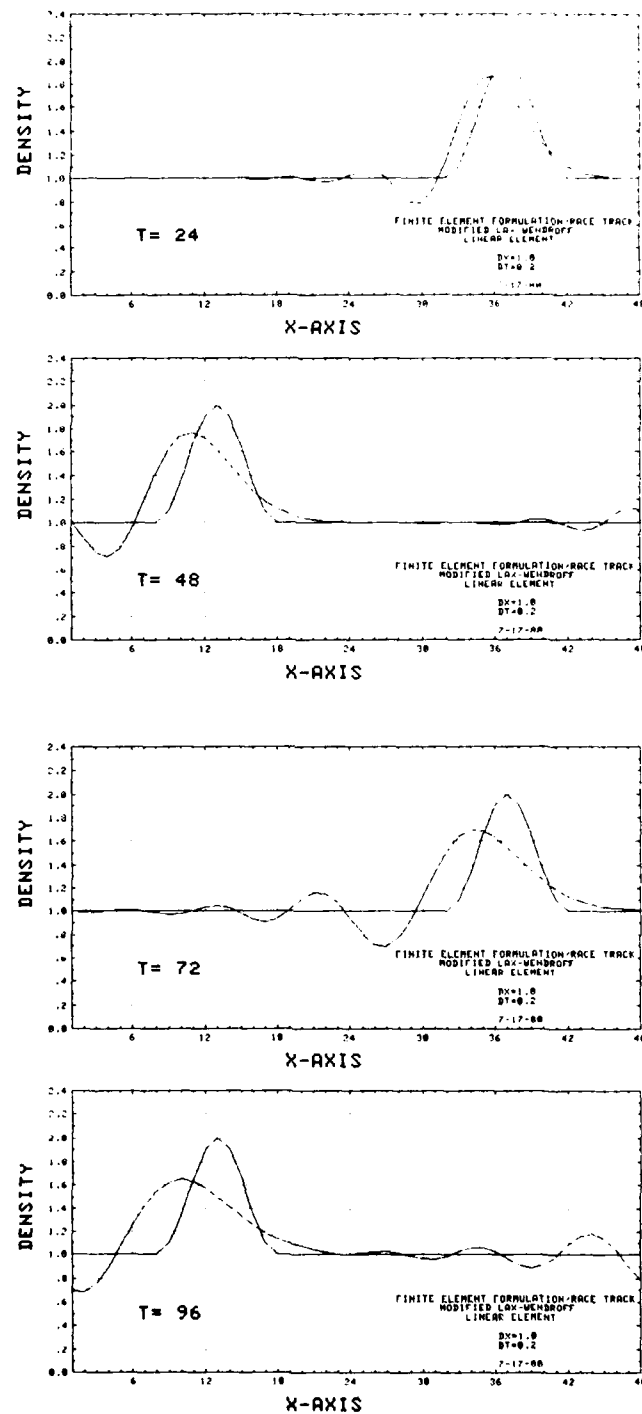
Fig. 5.1.3 — Advected cosine hill: modified Lax-Wendroff, linear FEM
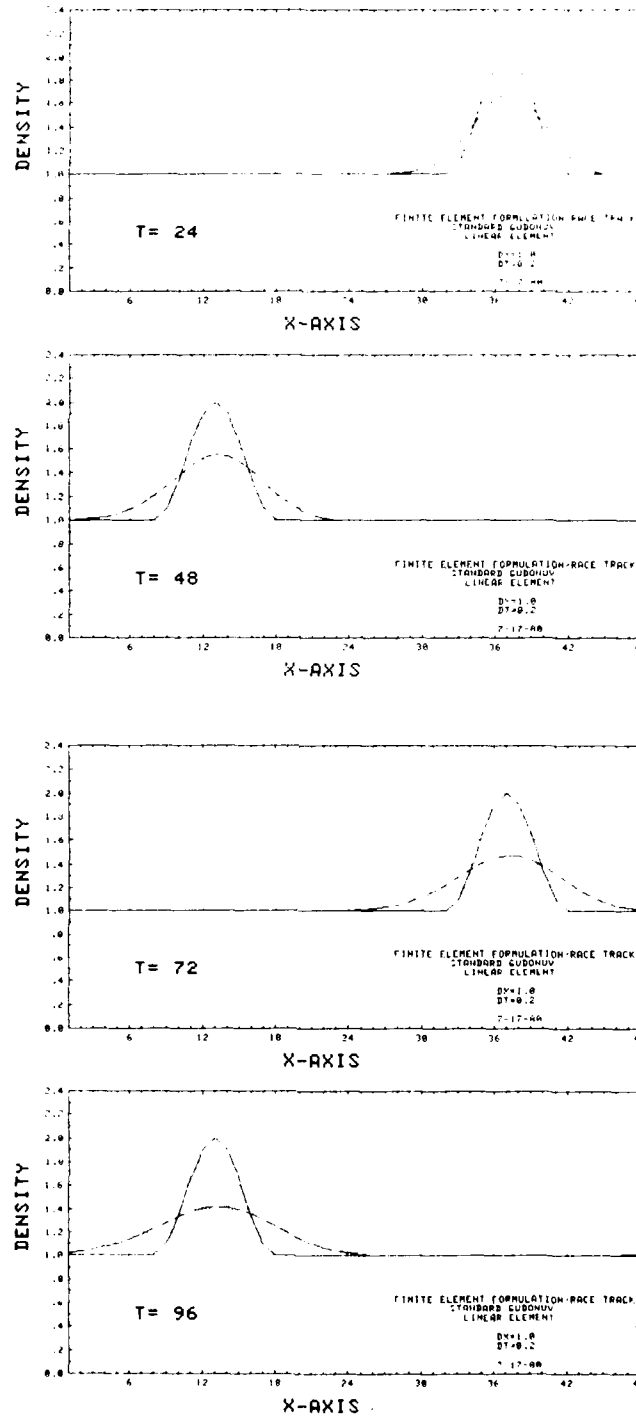
Fig. 5.14 — Advected cosine hill: standard Godunov, linear FEM
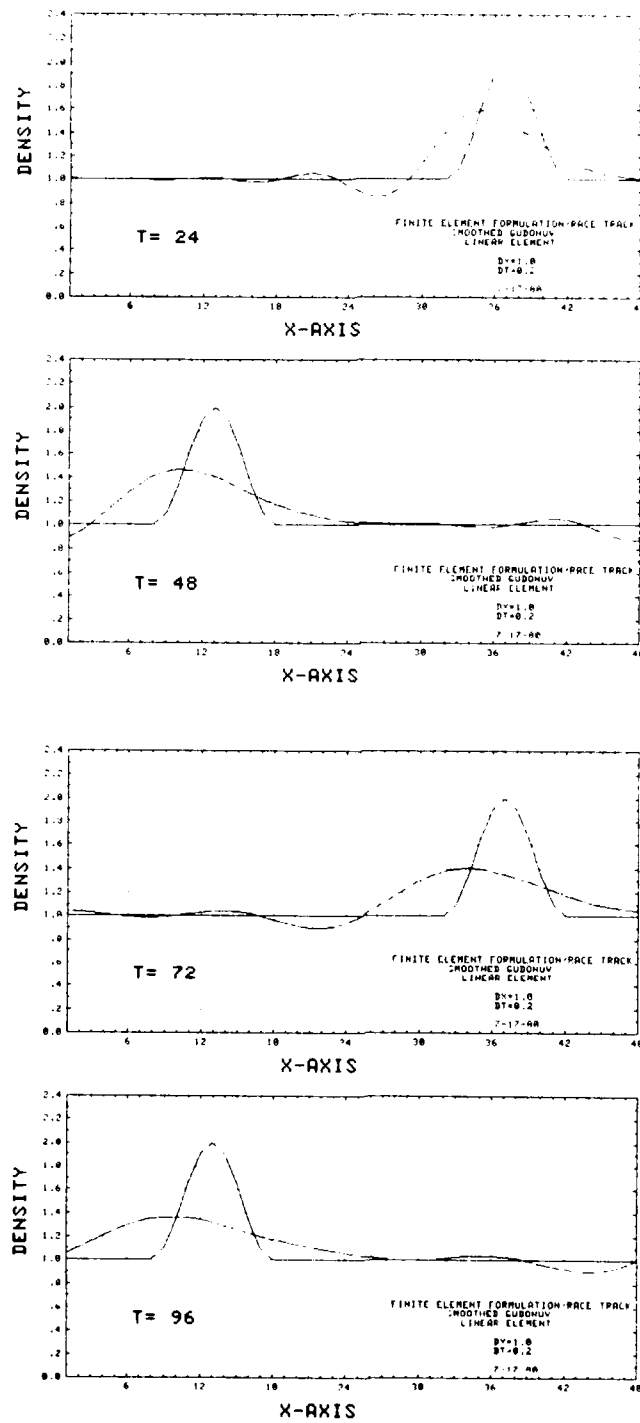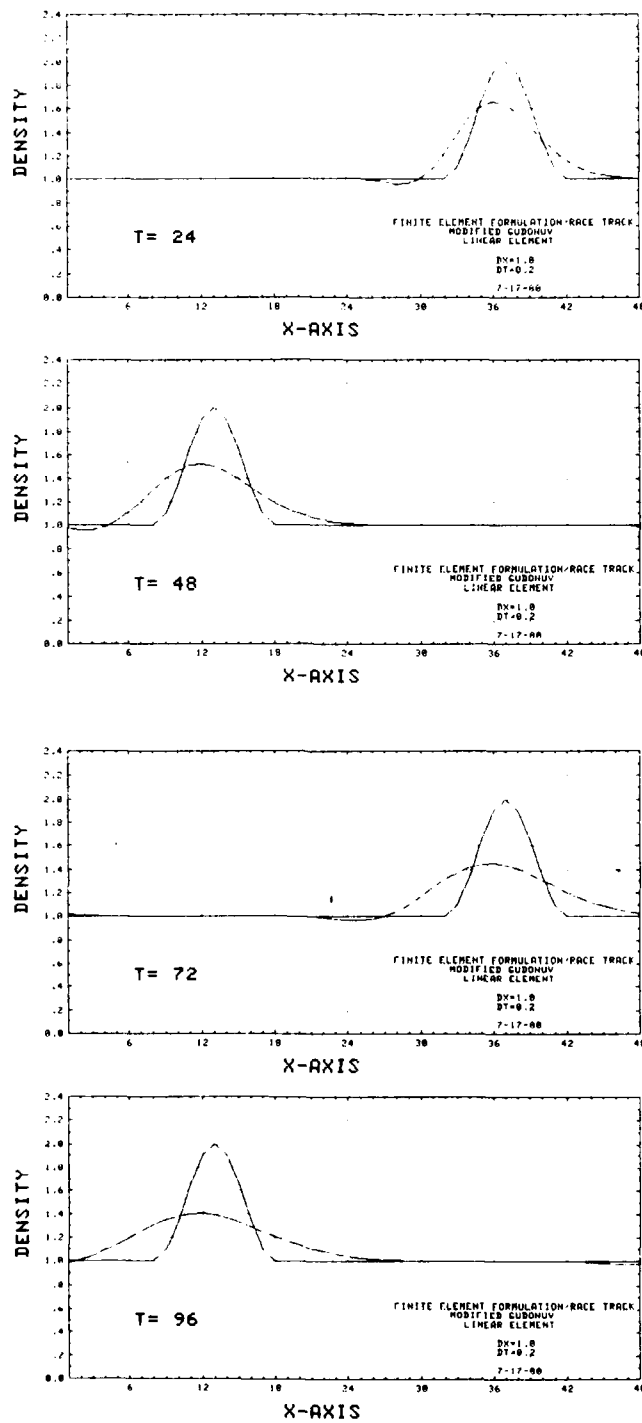
Fig. 5.1.5 — Advected cosine hill, smoothed Godunov, linear FEM

Fig. 5.1.6 — Advected cosine hill: modified Godunov, linear FEM
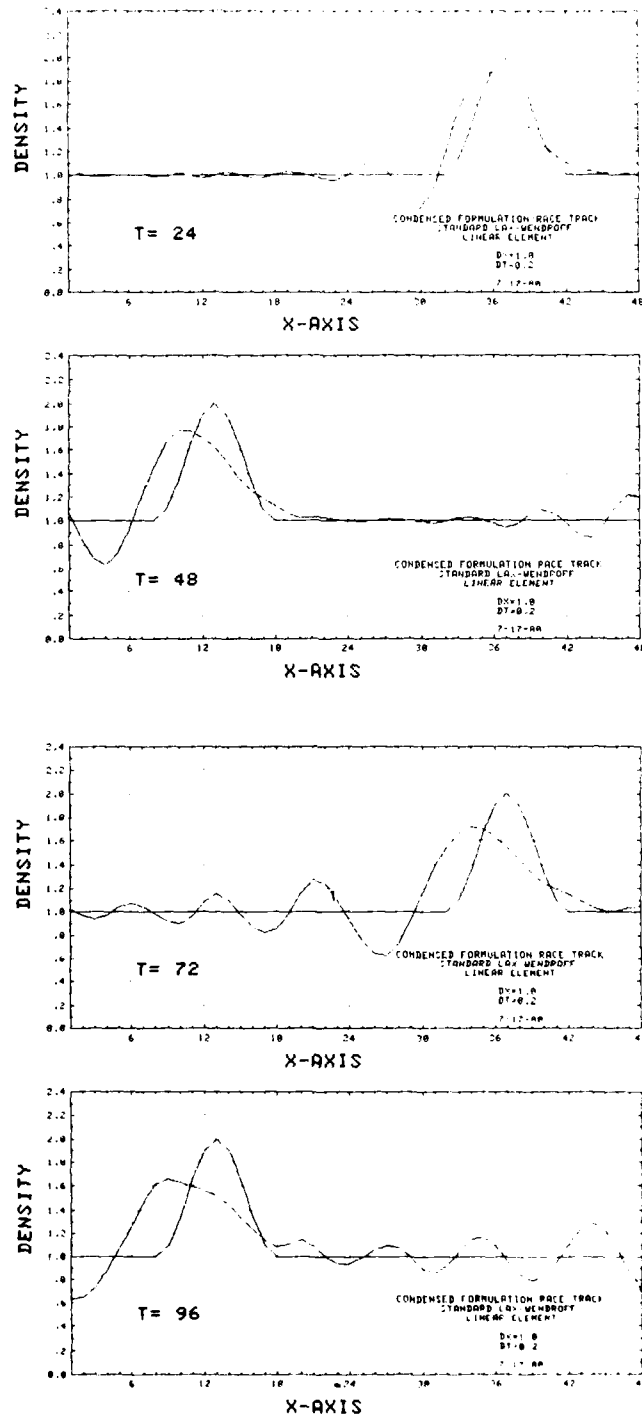
Fig. S.17 — Advected cosine hill: standard Lax-Wendroff, linear CFM
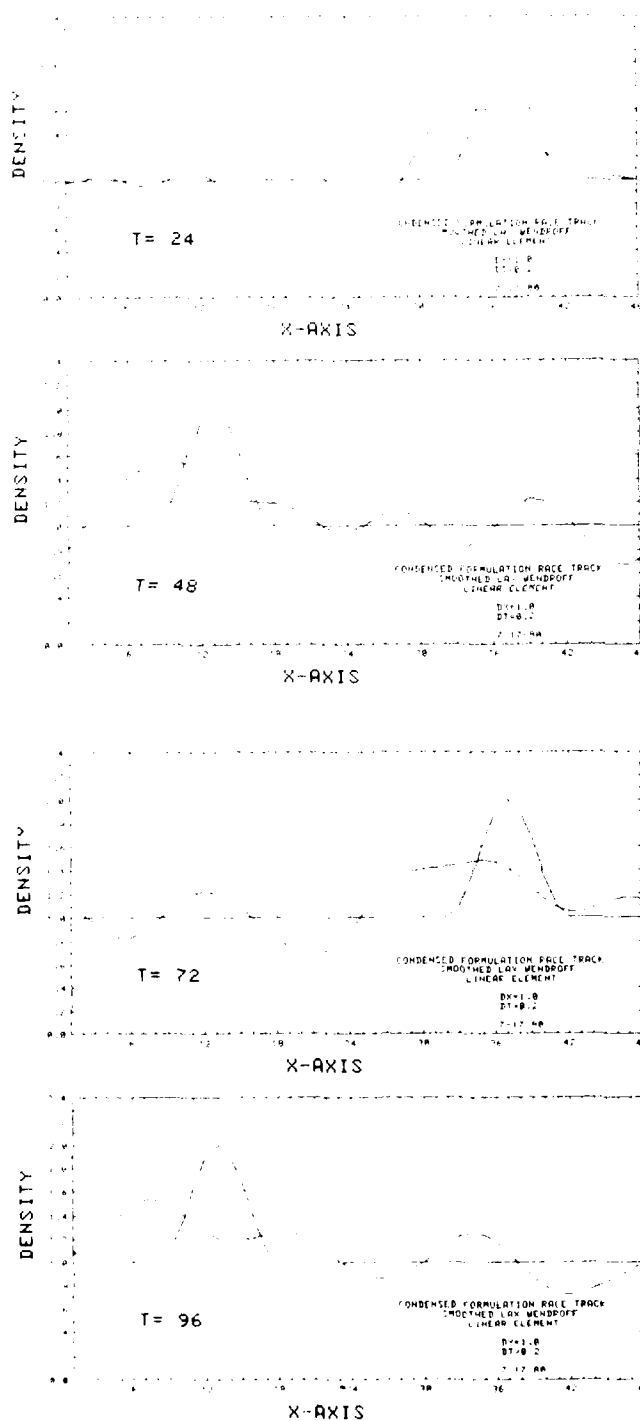
Fig. 3.18 — Advected cosine hill, smoothed Lax-Wendroff,
linear CEM
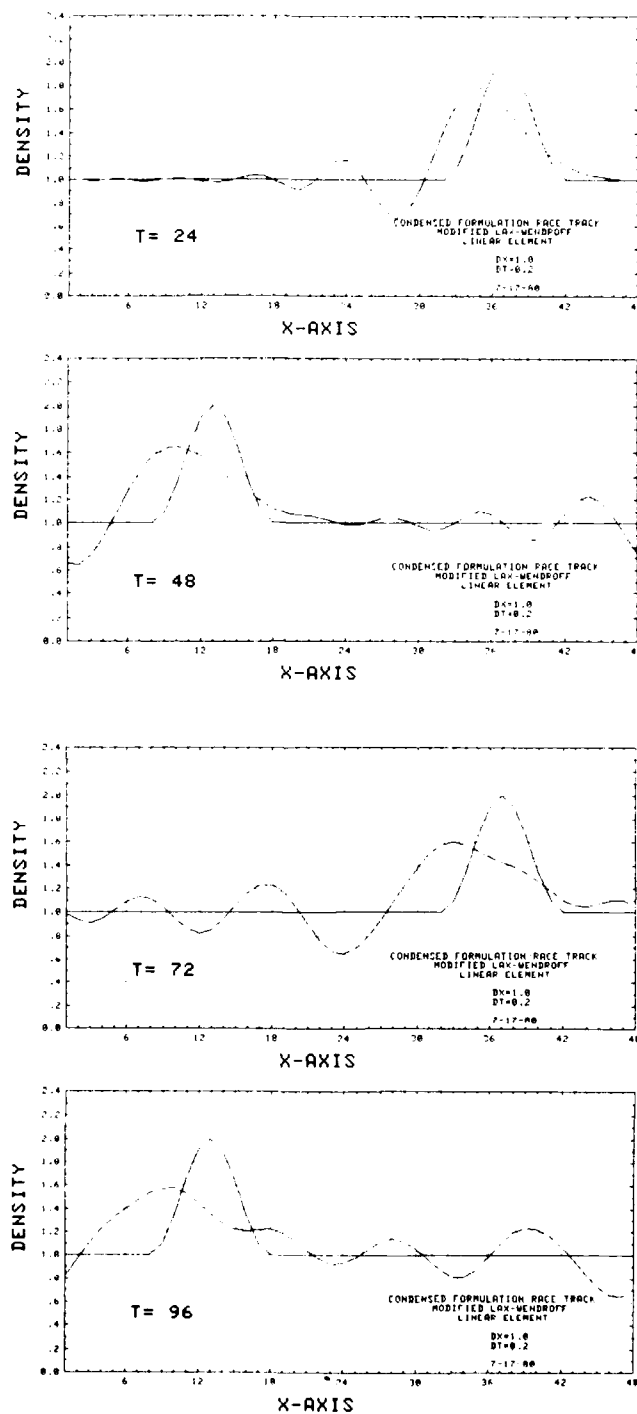
Fig. 5.1.9 — Advected cosine hill: modified Lax-Wendroff, linear CFM
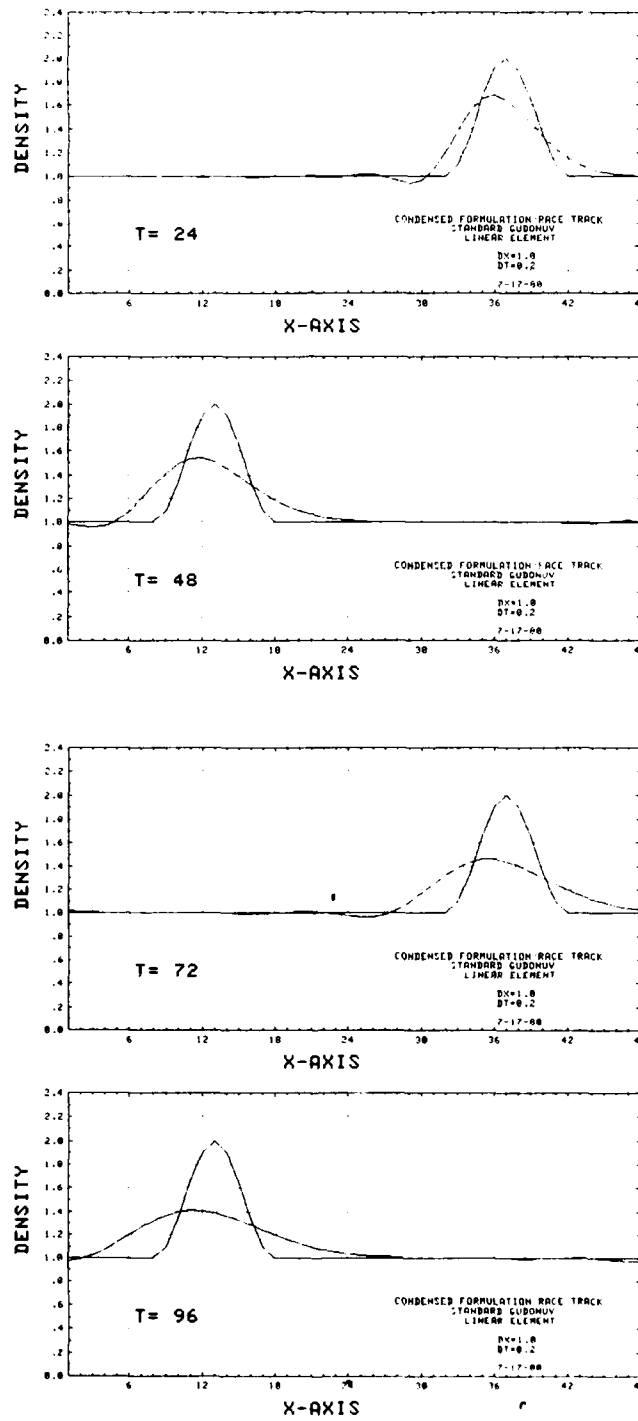
Fig. 5.1.10 — Advected cosine hill standard Godunov, linear CFM
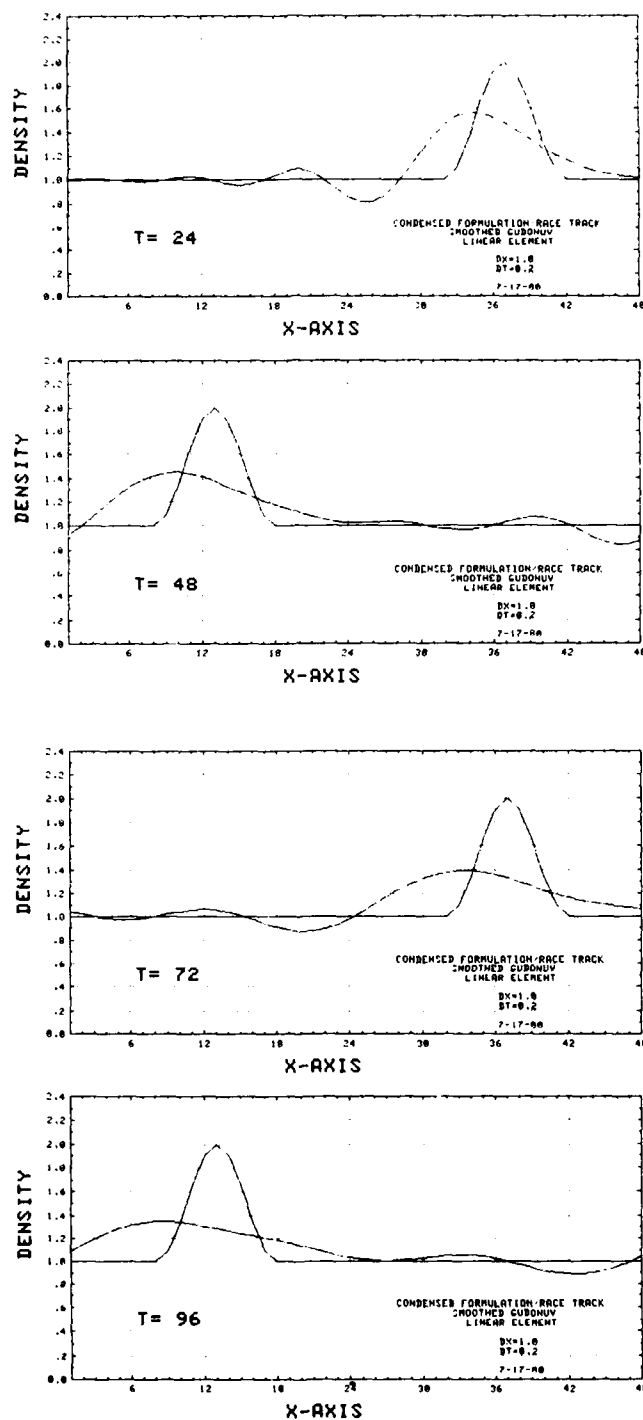
Fig. 5.1.11 — Advected cosine hill: smoothed Godunov, linear CFM
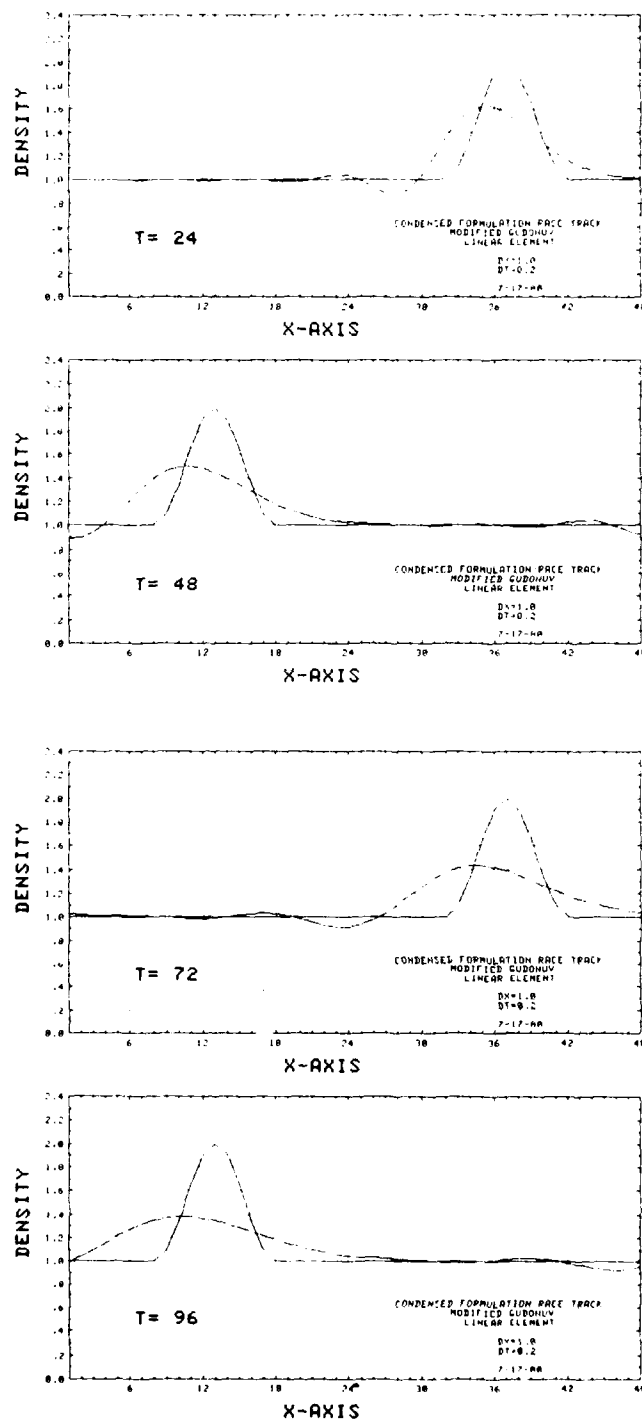
Fig. 5.1.12 — Advected cosine hill: modified Godunov, linear CFM
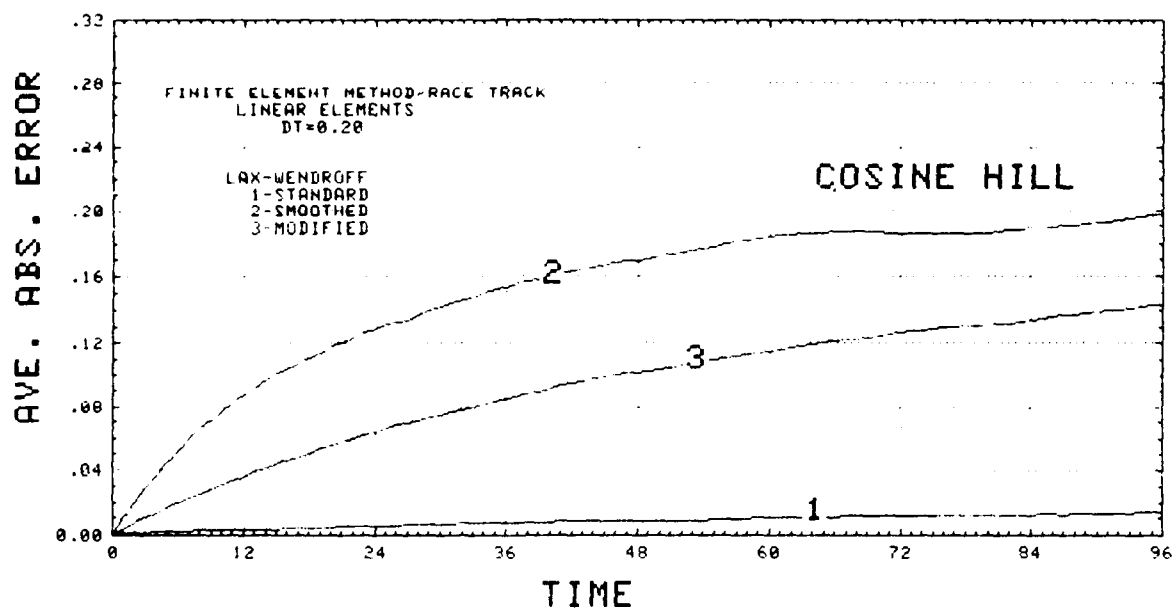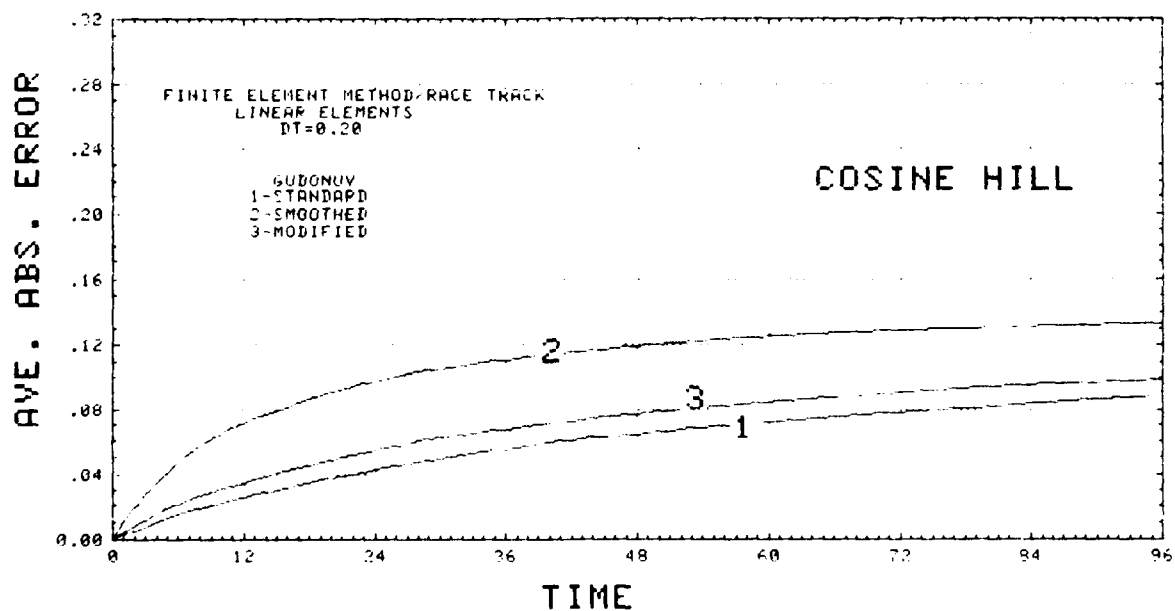
Fig. 8.13 — Average absolute errors for cosine hill advection (a) linear FEM, Lax-Wendroff time integrators (b) linear FEM, Godunov time integrators (c) linear CEM, Lax-Wendroff time integrators (d) linear CEM, Godunov time integrators

CONDENSED FORMULATION/RACE TRACK
LINEAR ELEMENTS
DT=0.20
7-17-90

LAX-WENDROFF
1-STANDARD
2-SMOOTHED
3-MODIFIED

COSINE HILL

(c)

CONDENSED FORMULATION/RACE TRACK
LINEAR ELEMENTS
DT=0.20
7-17-90

GUDONUV
1-STANDARD
2-SMOOTHED
3-MODIFIED

COSINE HILL

(d)
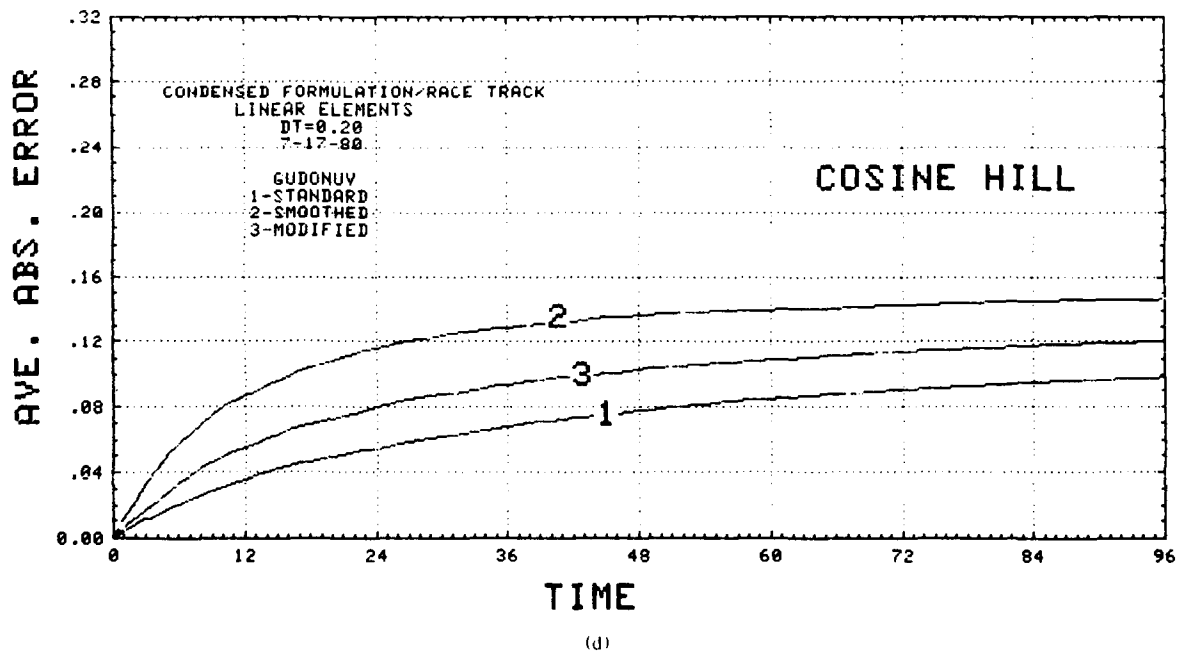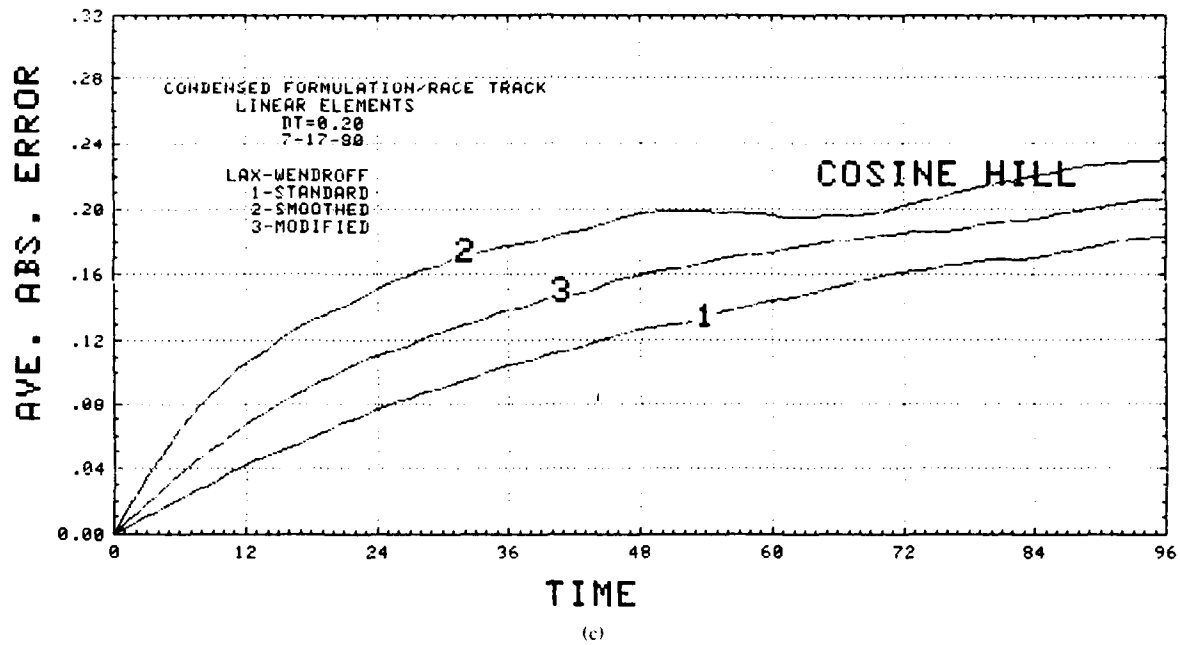
Fig. 5.1.13 (Continued) — Average absolute errors for cosine hill advection (a) linear FEM, Lax-Wendroff time integrators (b) linear FEM, Godunov time integrators (c) linear CFM, Lax-Wendroff time integrators (d) linear CFM, Godunov time integrators
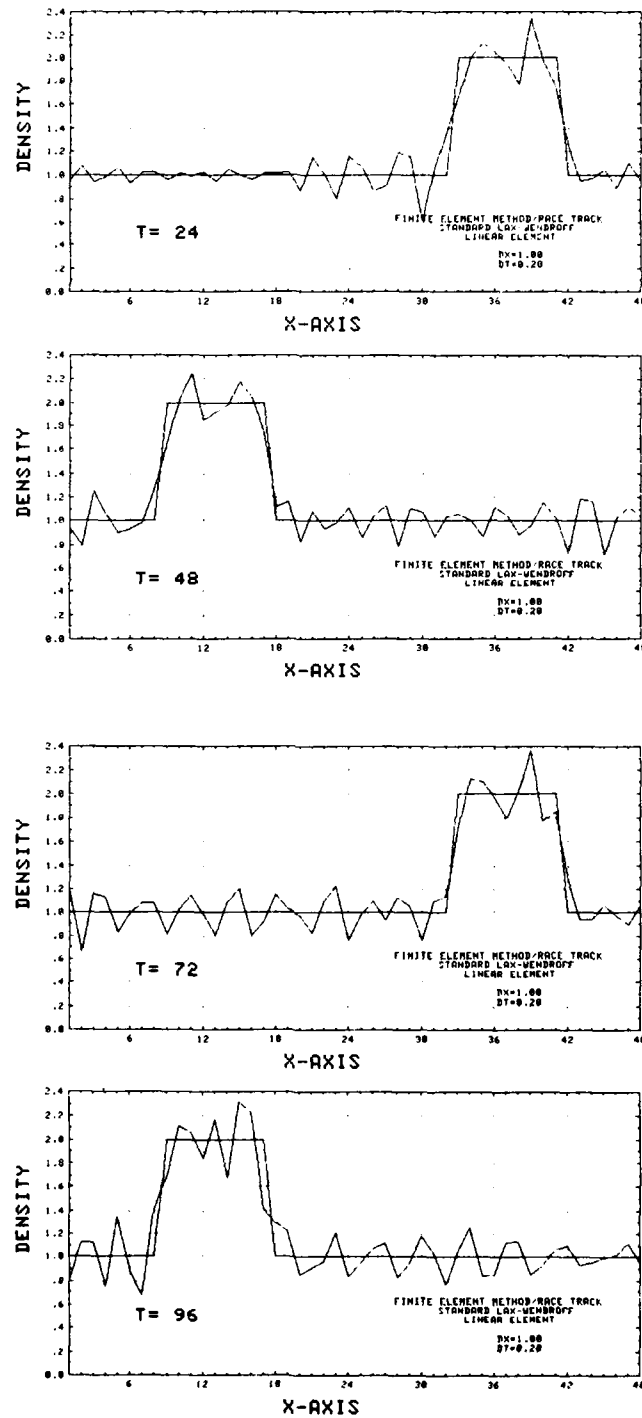
Fig. 5.1.14 — Advected square hill: standard Lax-Wendroff,
linear FEM
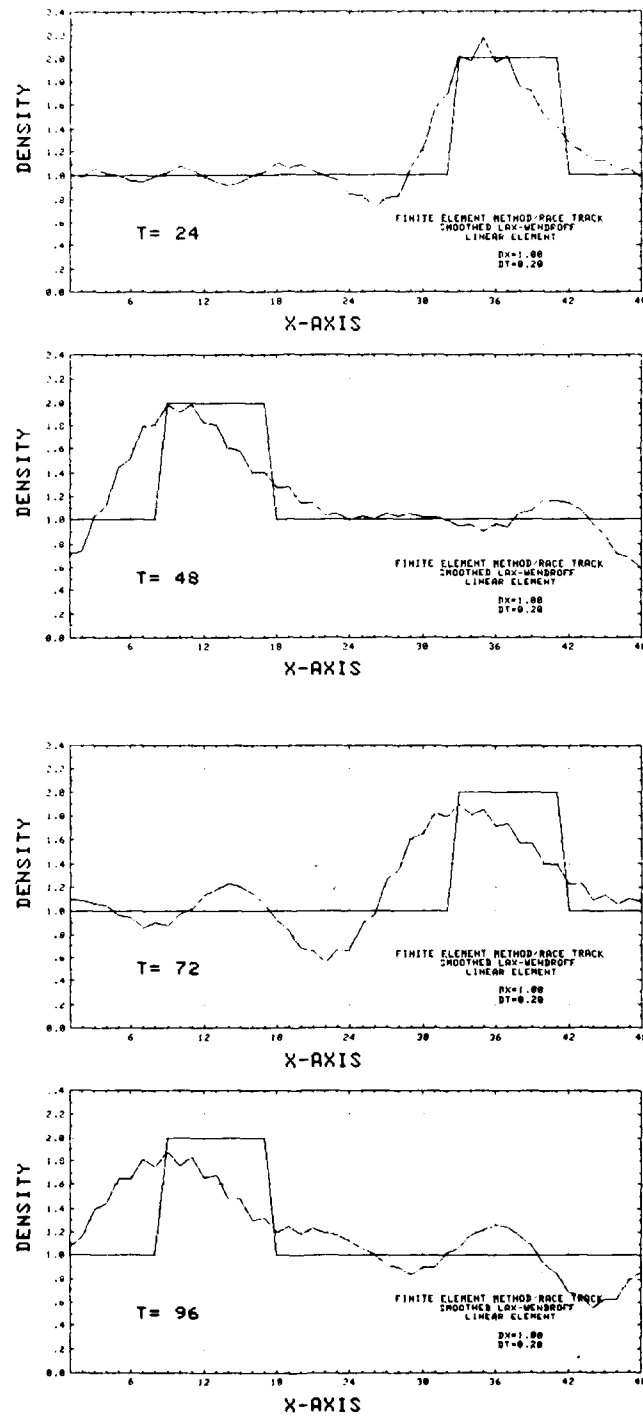
Fig. 5.1.15 — Advected square hill: smoothed Lax-Wendroff,
linear FEM
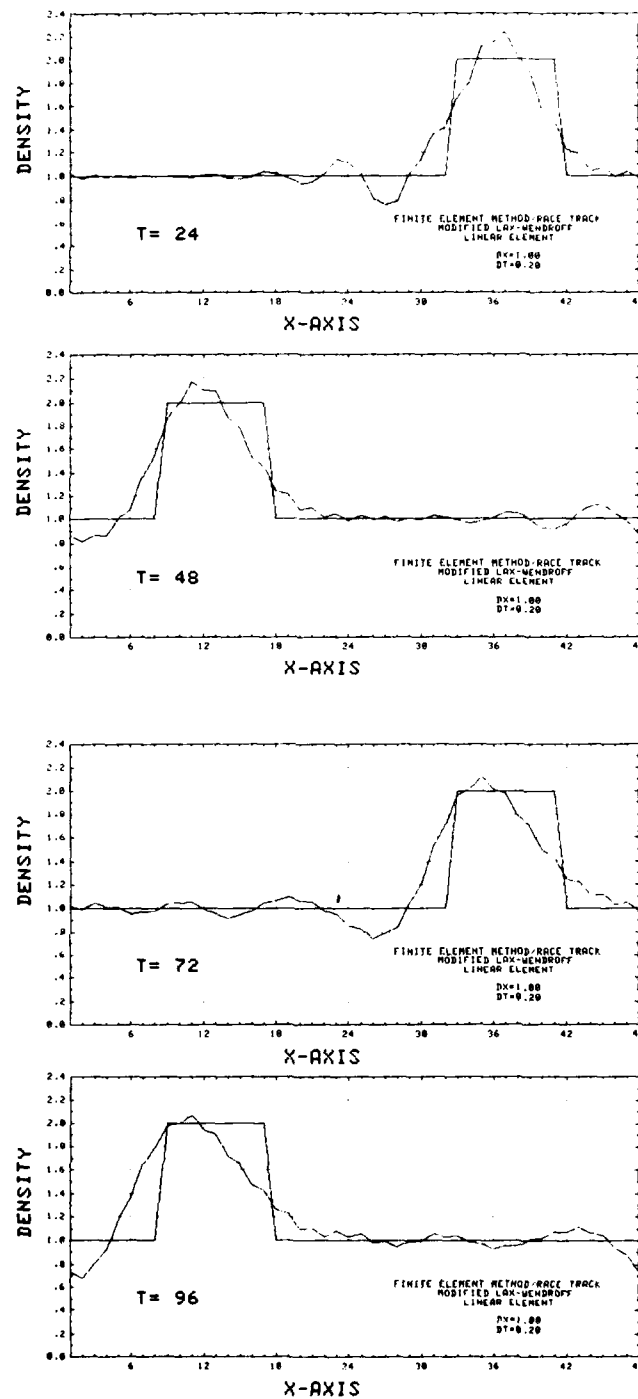
Fig. 5.1.16 — Advected square hill modified Lax-Wendroff, linear FEM

43

Fig. 5.1.17 — Advected square hill: standard Godunov, linear FEM
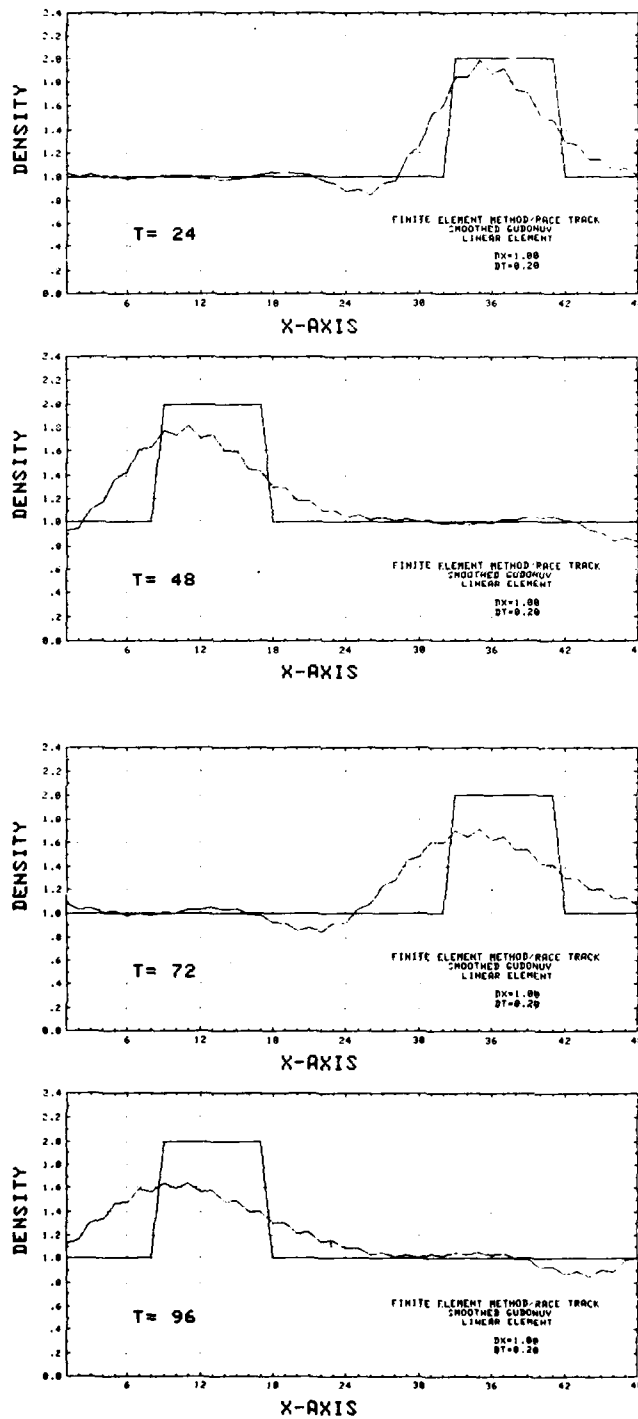
Fig. 5.1.18 — Advected square hill: smoothed Godunov, linear FEM
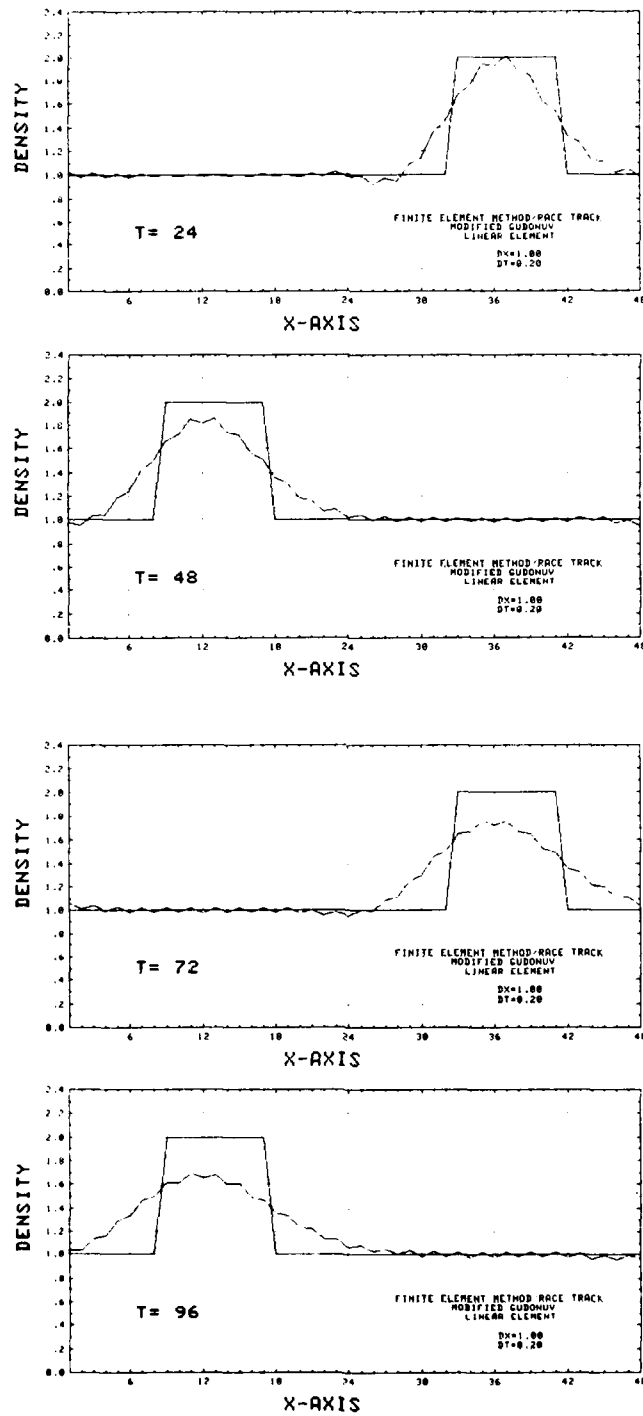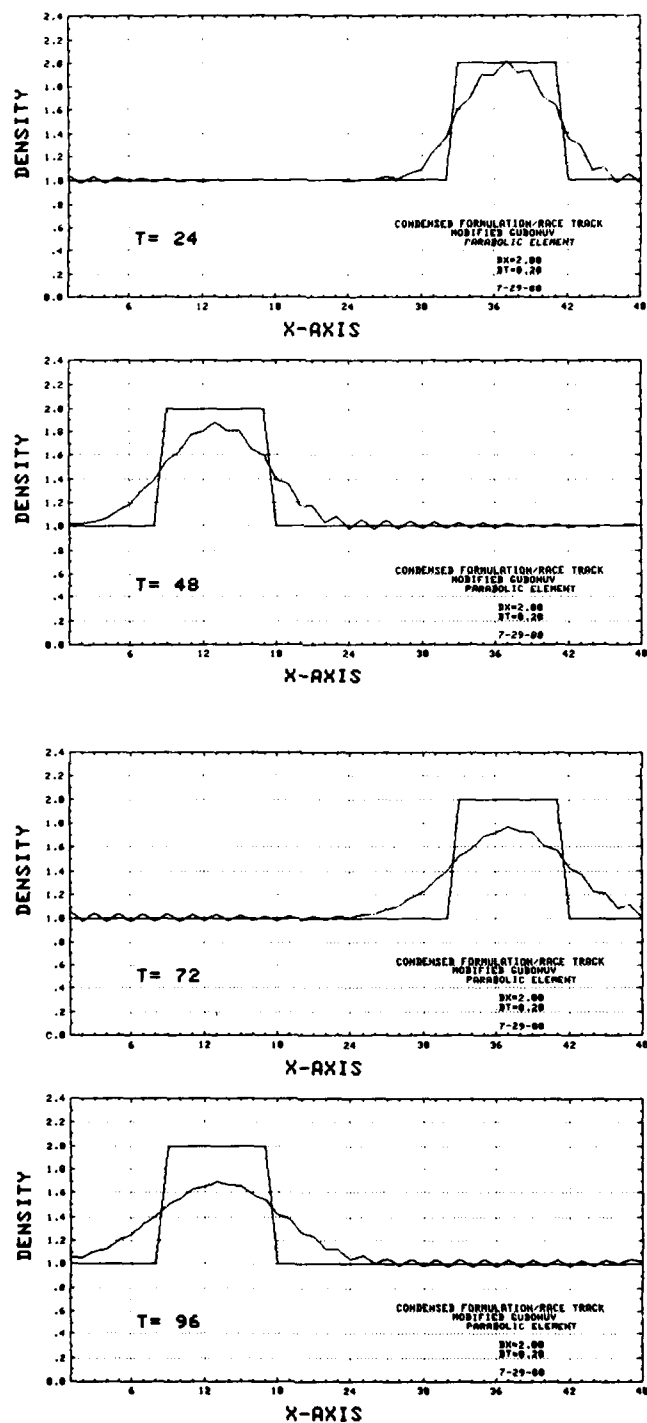
Fig. 5.1.19 — Advected square hill: modified Godunov, linear FEM
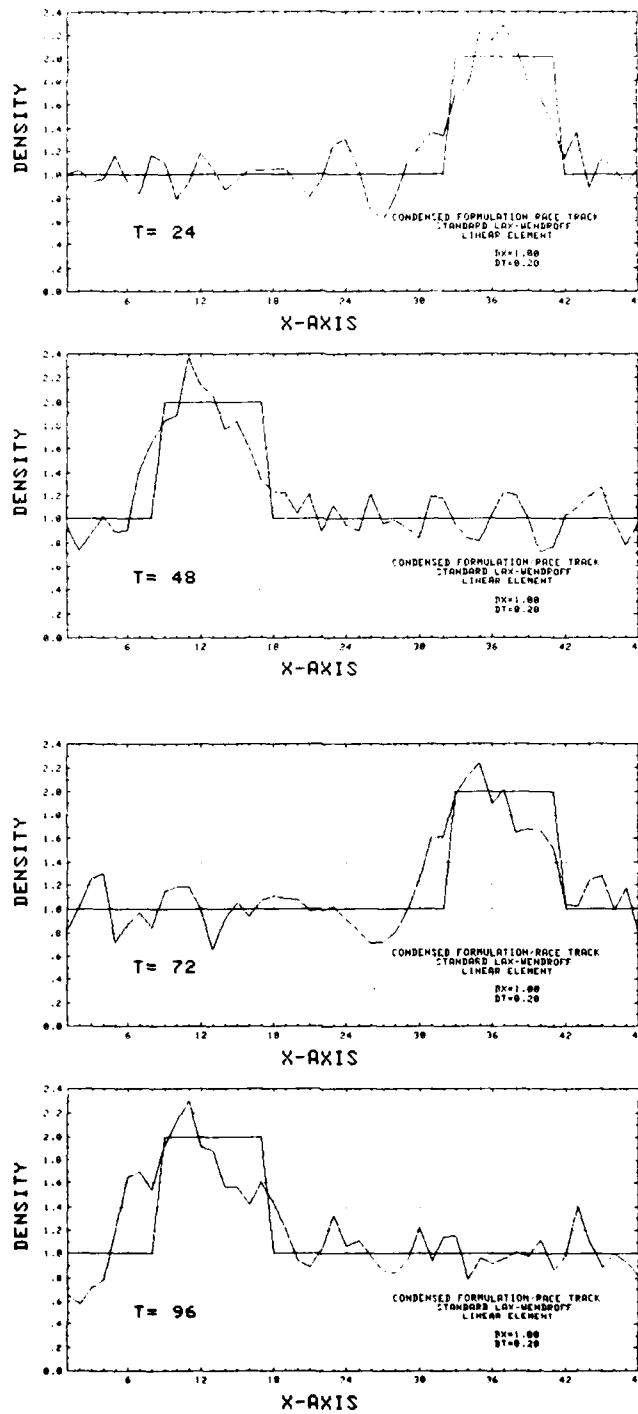
Fig. 5.1 20 — Advected square hill standard Lax-Wendroff, linear CFM
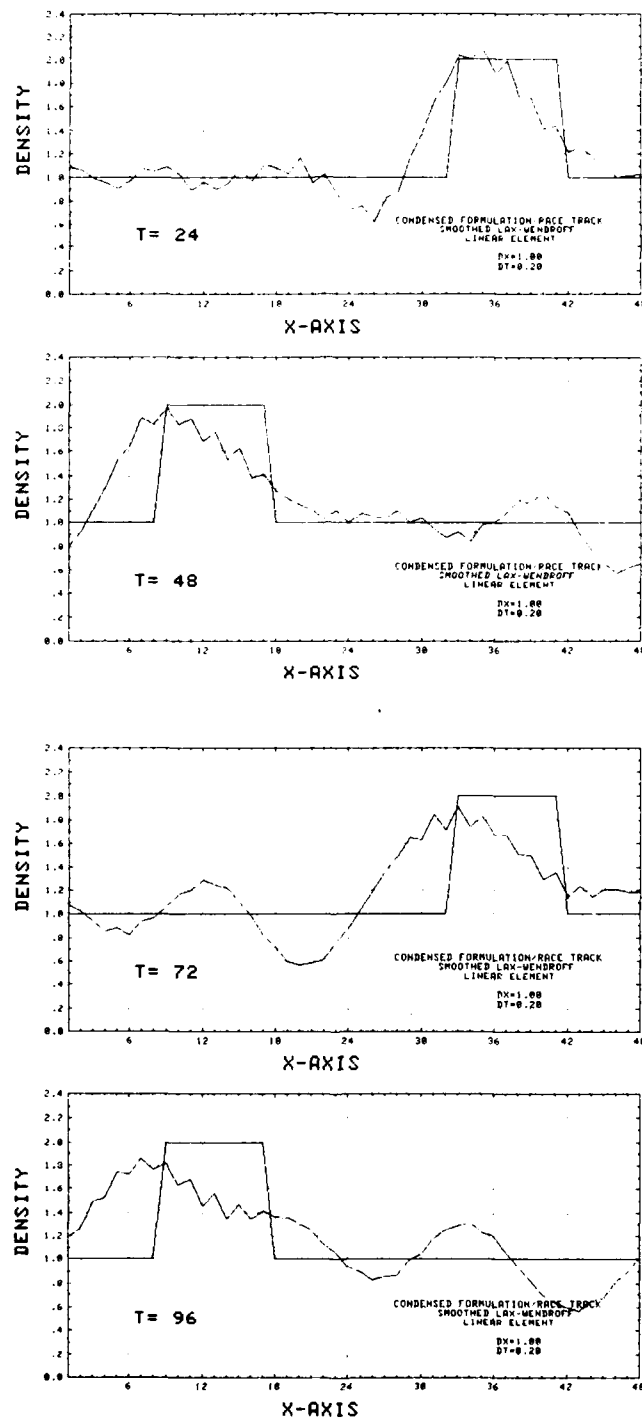
Fig. 5.1.21 — Advected square hill: smoothed Lax-Wendroff, linear CFM
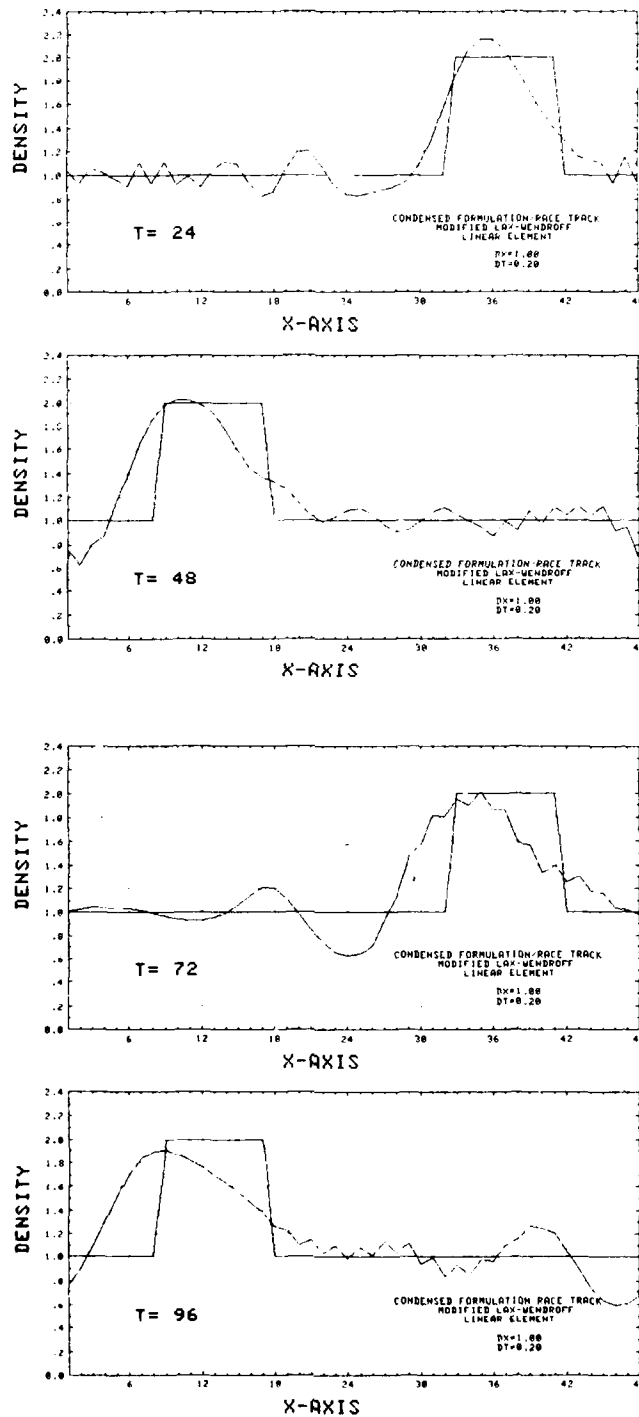
Fig. 5.1.22 — Advected square hill: modified Lax-Wendroff, linear CFM
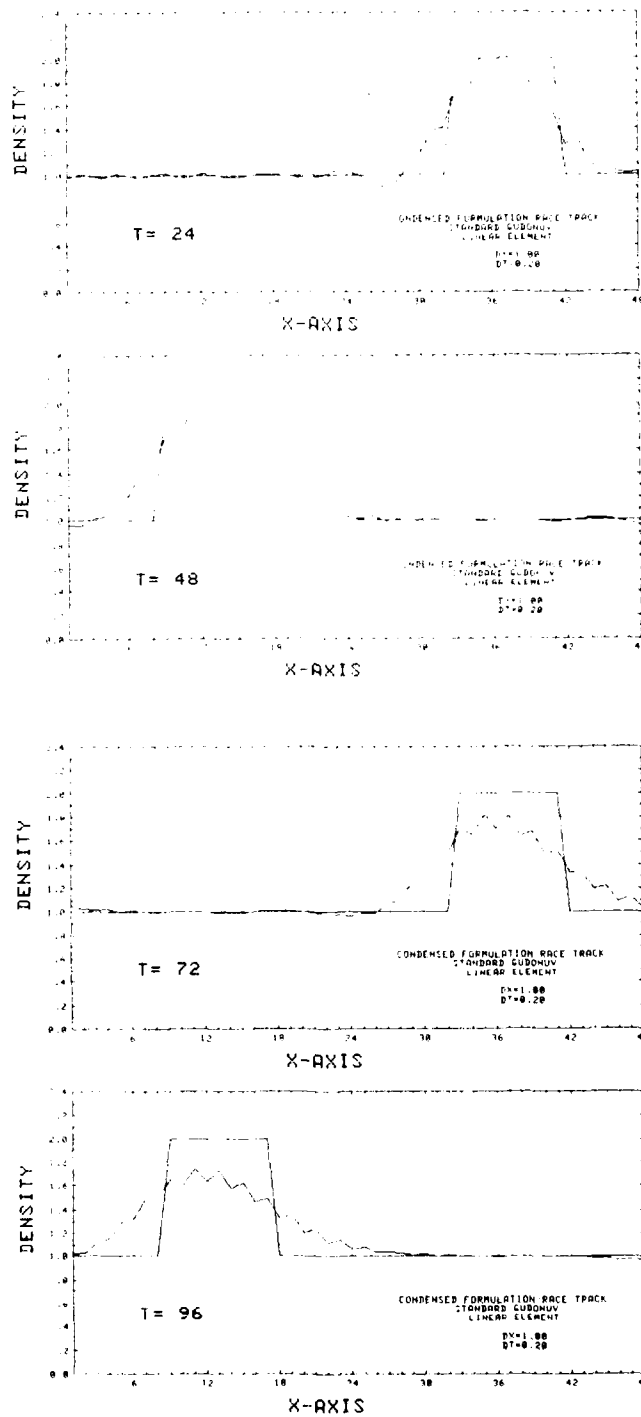
Fig. 5.1.23 — Advected square hill, standard Godunov, linear CFM
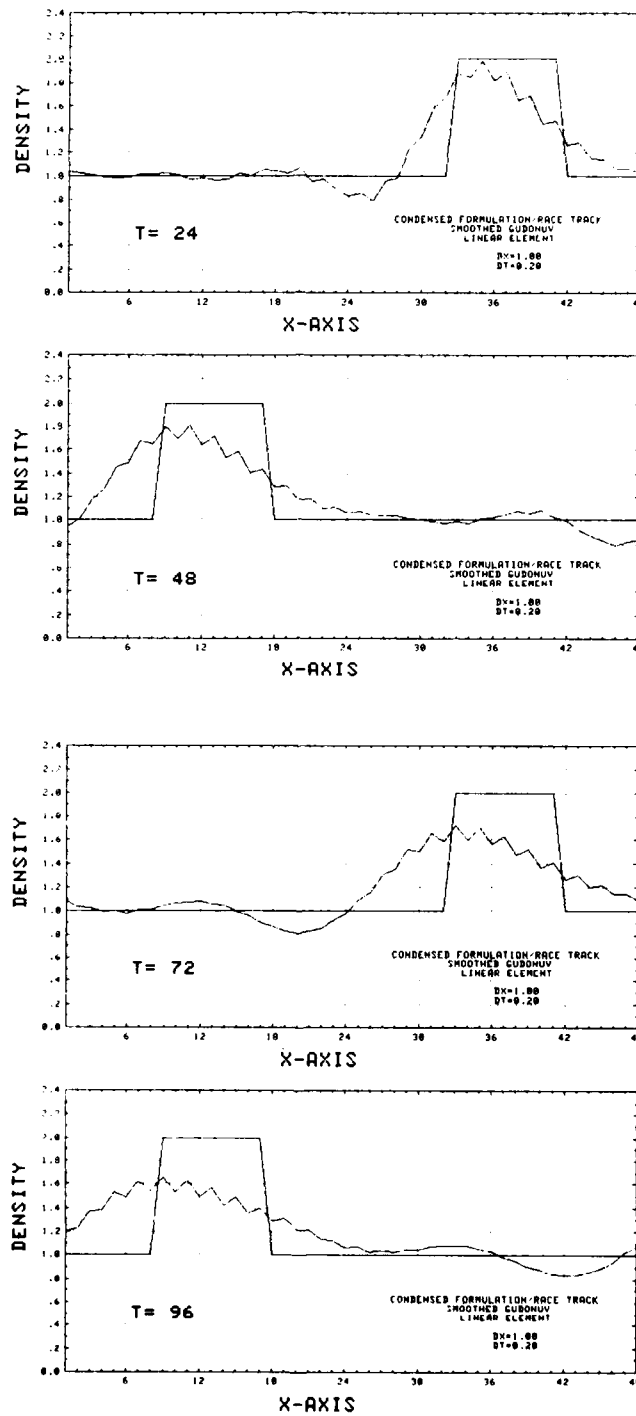
Fig. 5.1.24 — Advected square hill: smoothed Godunov, linear CFM
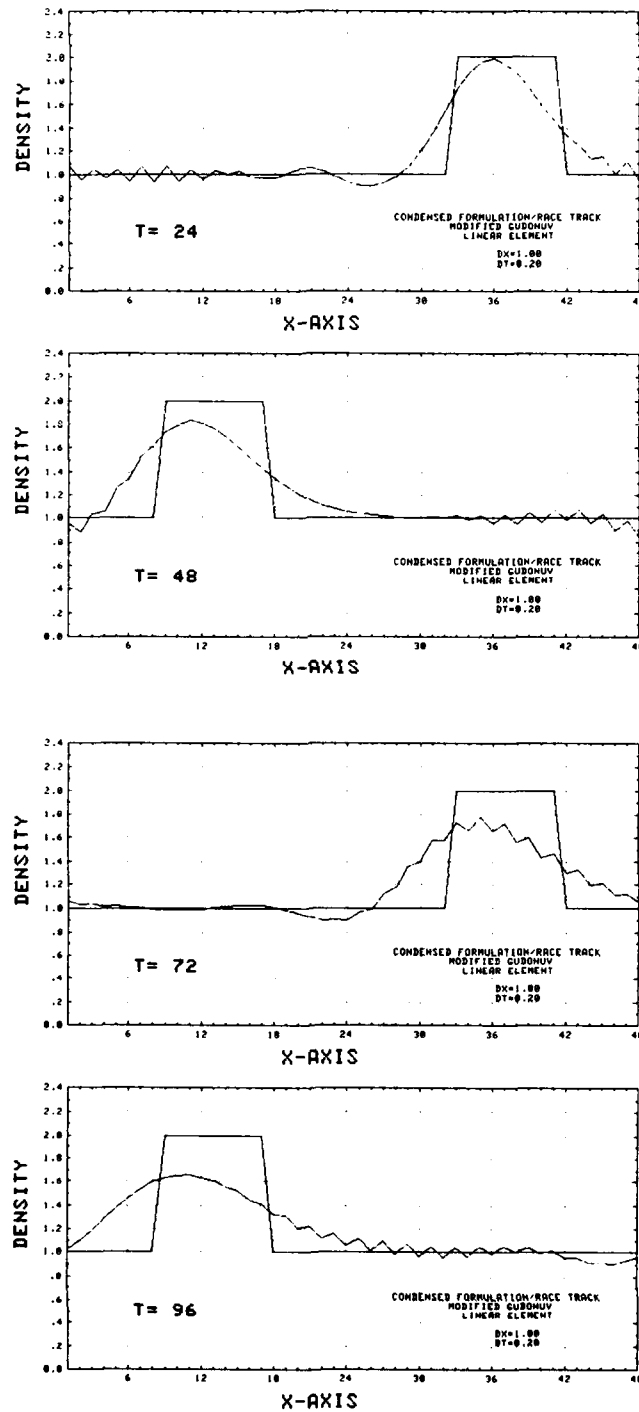
Fig. 5.1.25 — Advected square hill: modified Godunov, linear CFM
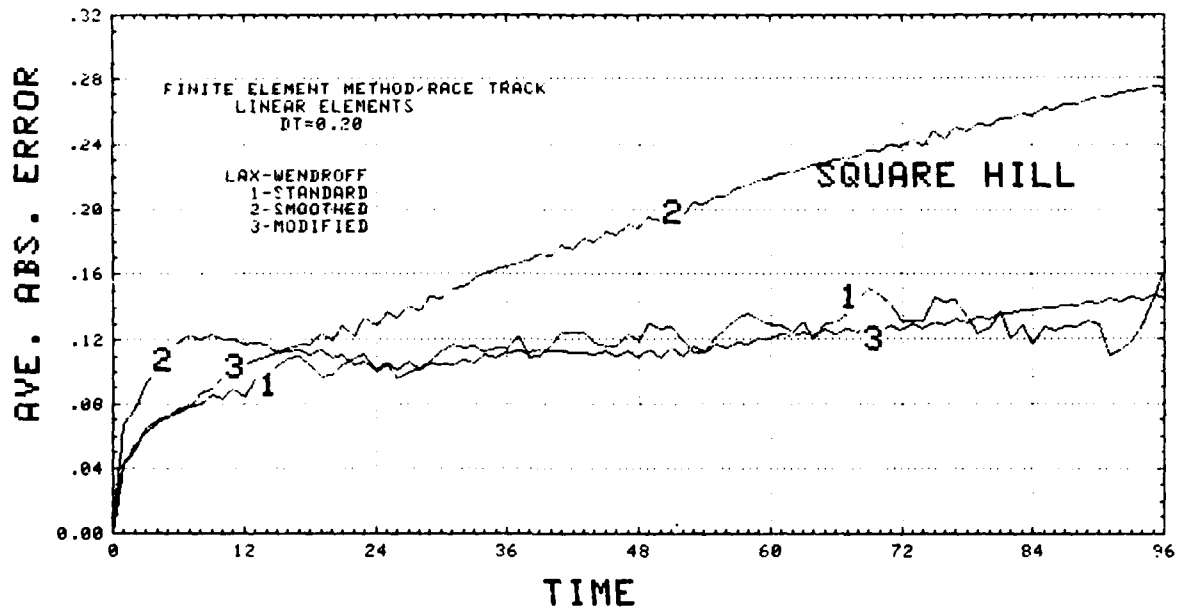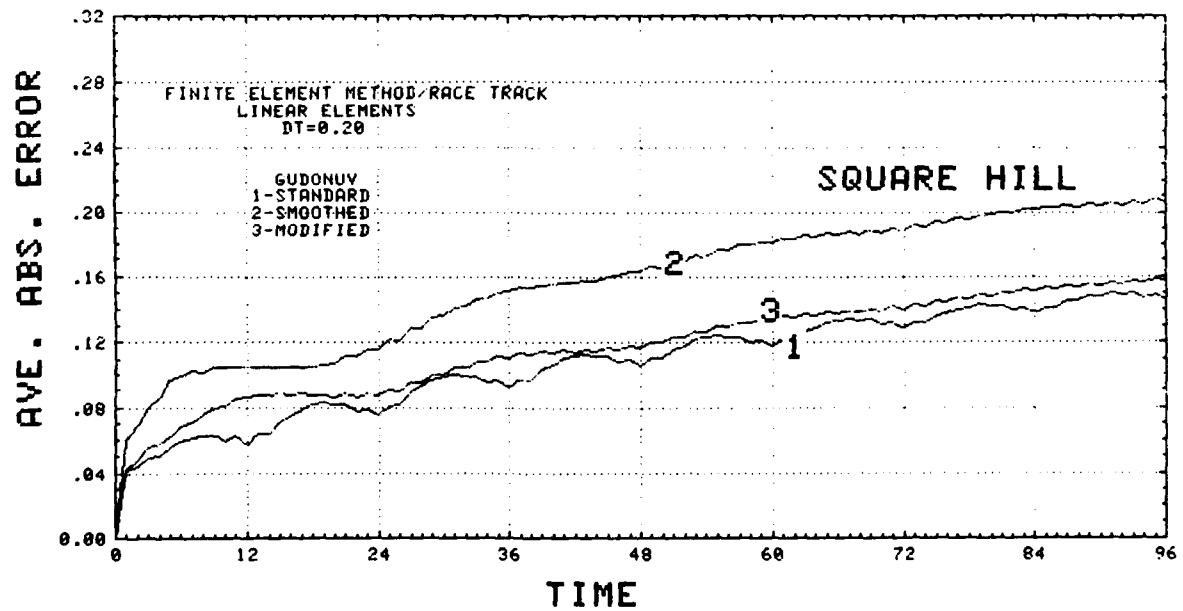
Fig. 5.1.26 — Average absolute errors for square hill advection. (a) linear FEM, Lax-Wendroff time integrators (b) linear FEM, Godunov time integrators (c) linear CFM, Lax-Wendroff time integrators (d) linear CFM, Godunov time integrators
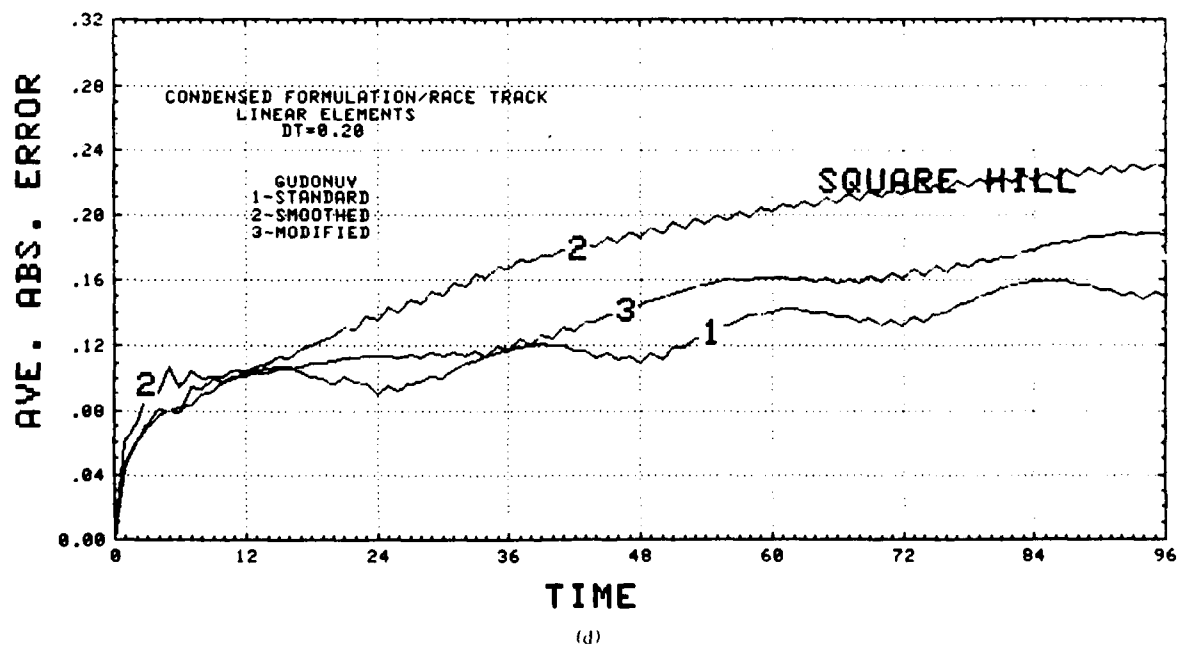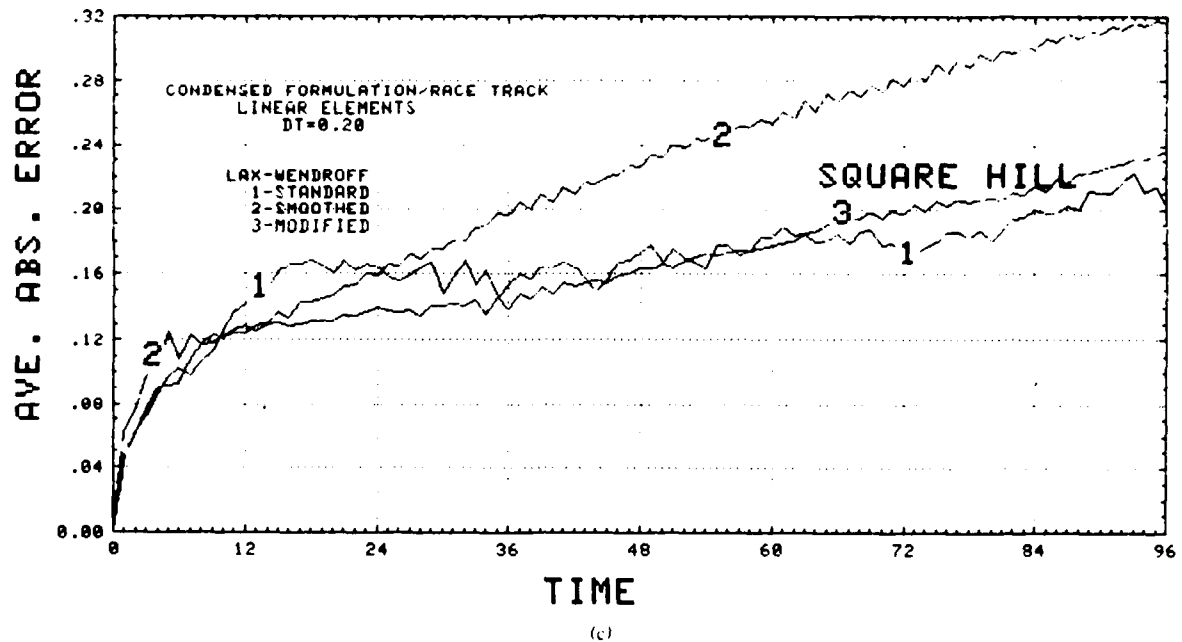
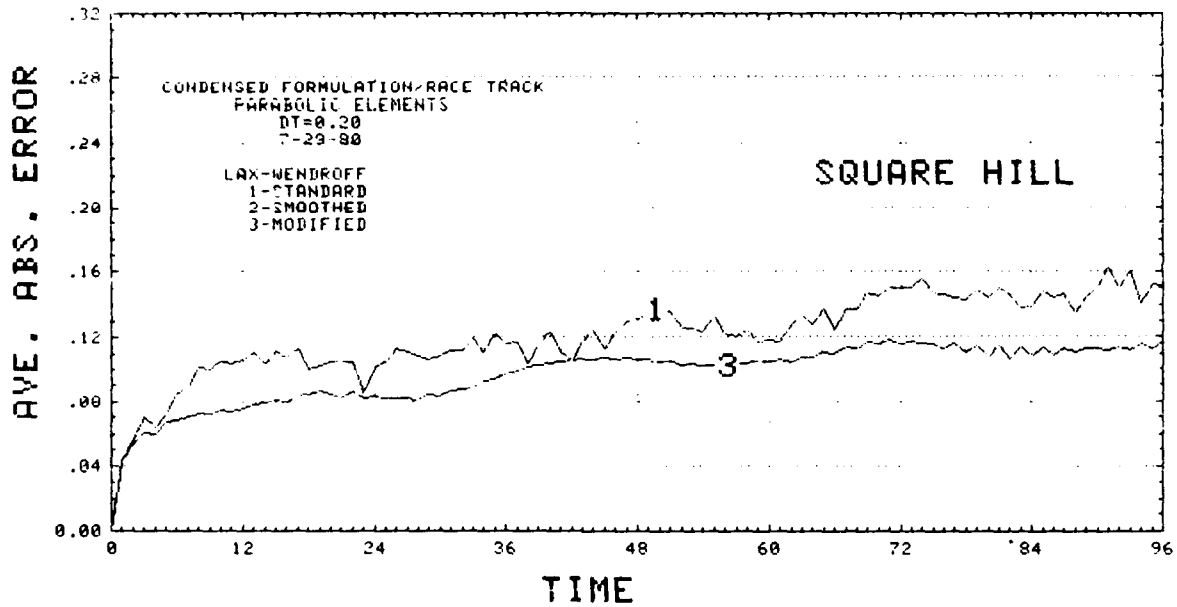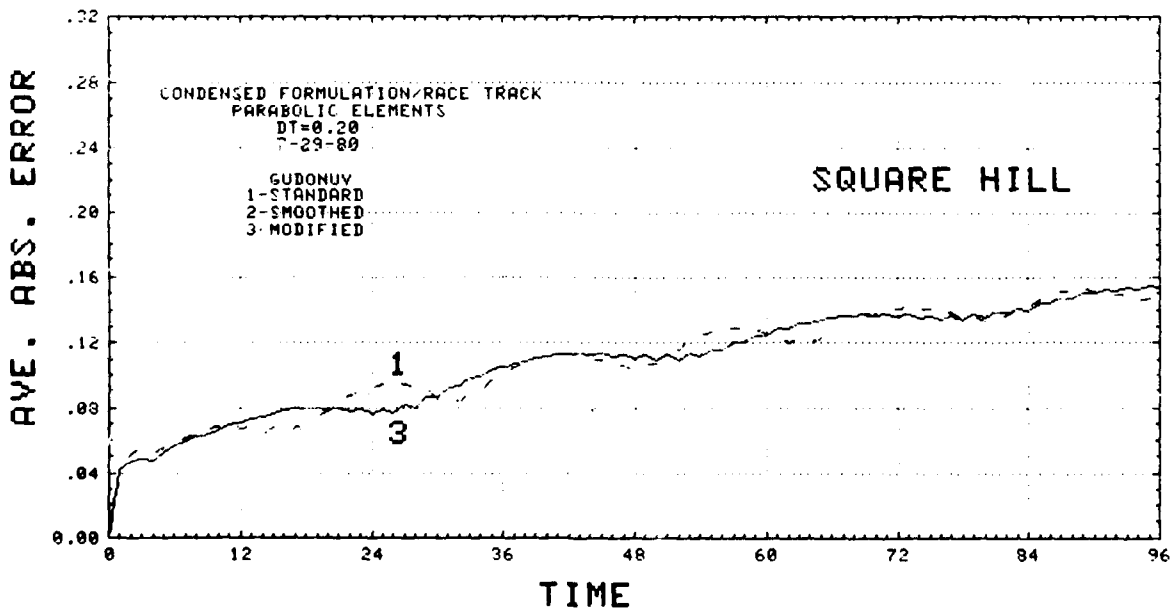Fig. 5.1.26 (Continued) — Average absolute errors for square hill advection. (a) linear FEM, Lax-Wendroff time integrators (b) linear FEM, Godunov time integrators (c) linear CFM, Lax-Wendroff time integrators (d) linear CFM, Godunov time integrators
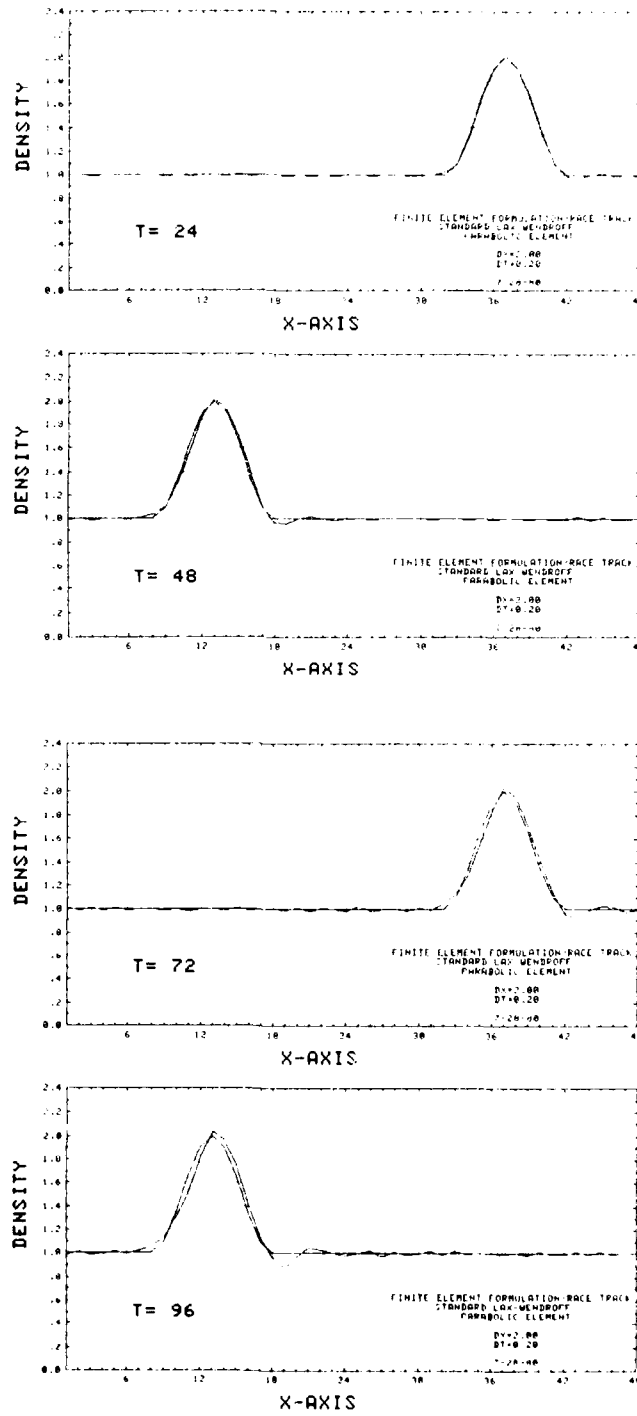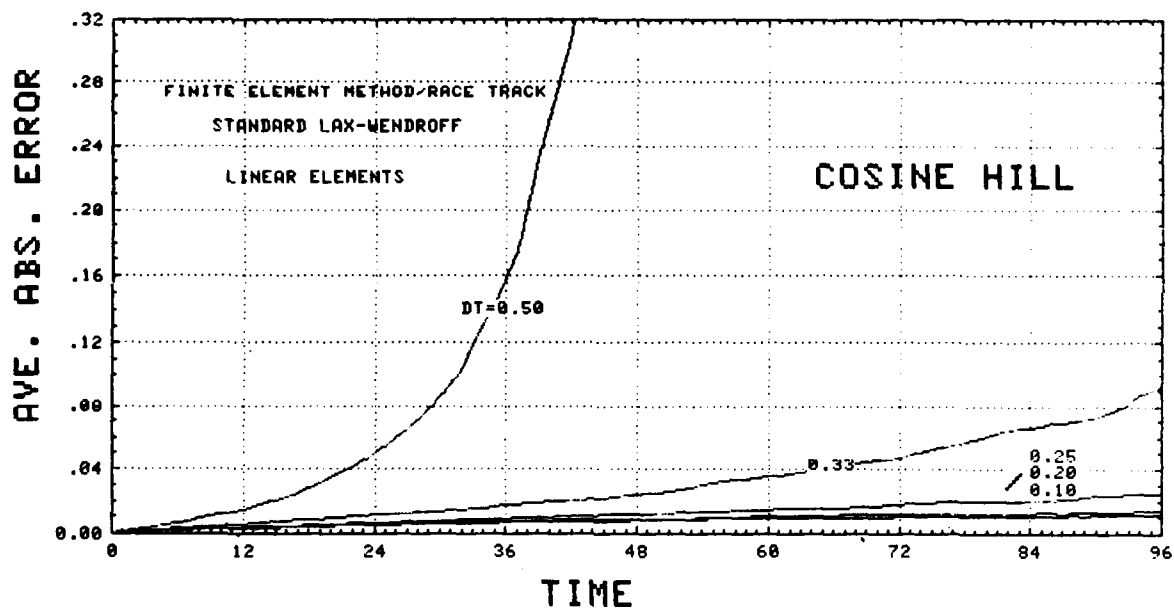
Fig. 5.2.1 — Advected cosine hill standard Lax-Wendroff, parabolic FEM
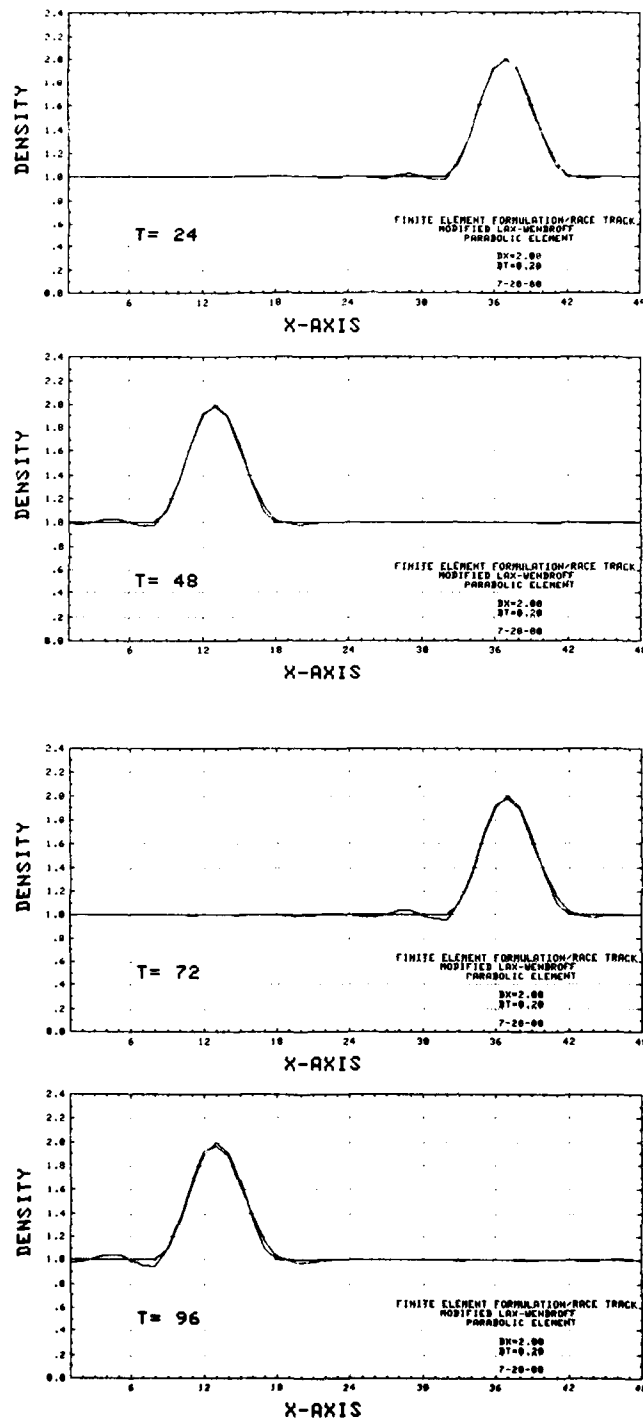
Fig. 5.2.2 — Advected cosine hill: modified Lax-Wendroff,
parabolic FEM
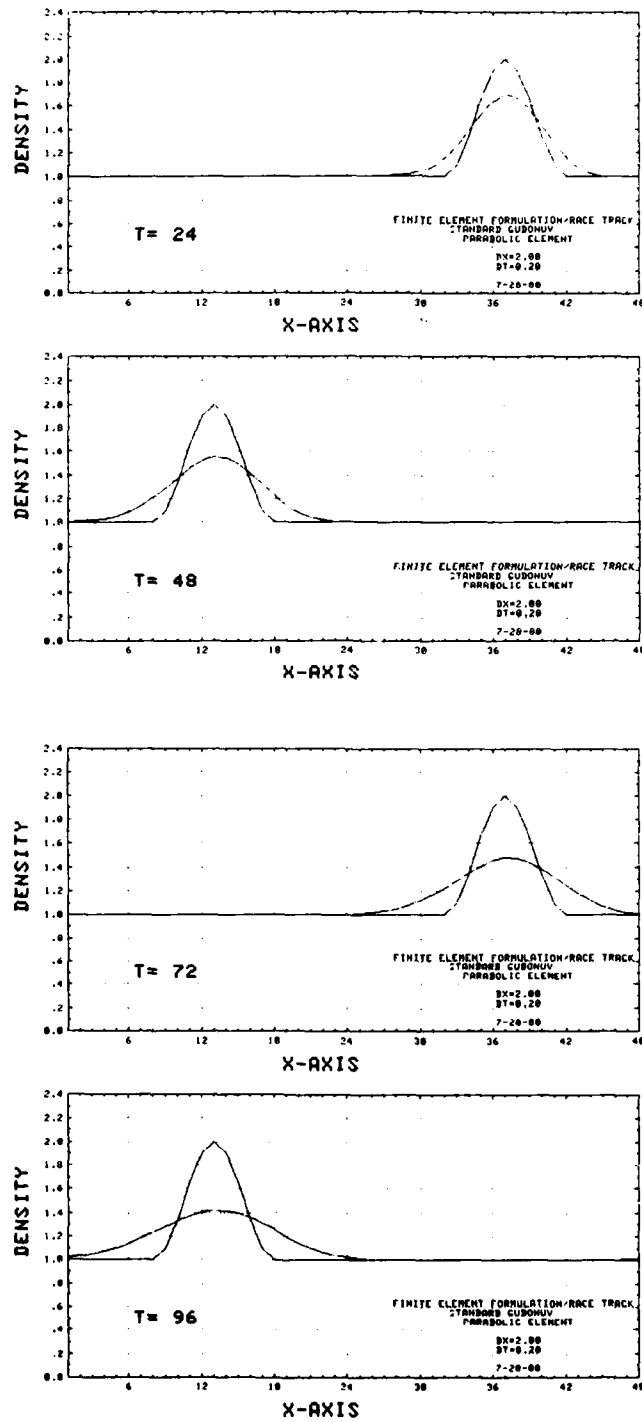
Fig. 5.2.3 — Advected cosine hill: standard Godunov, parabolic FEM

Fig. 5.2.4 — Advected cosine hill: modified Godunov, parabolic FEM
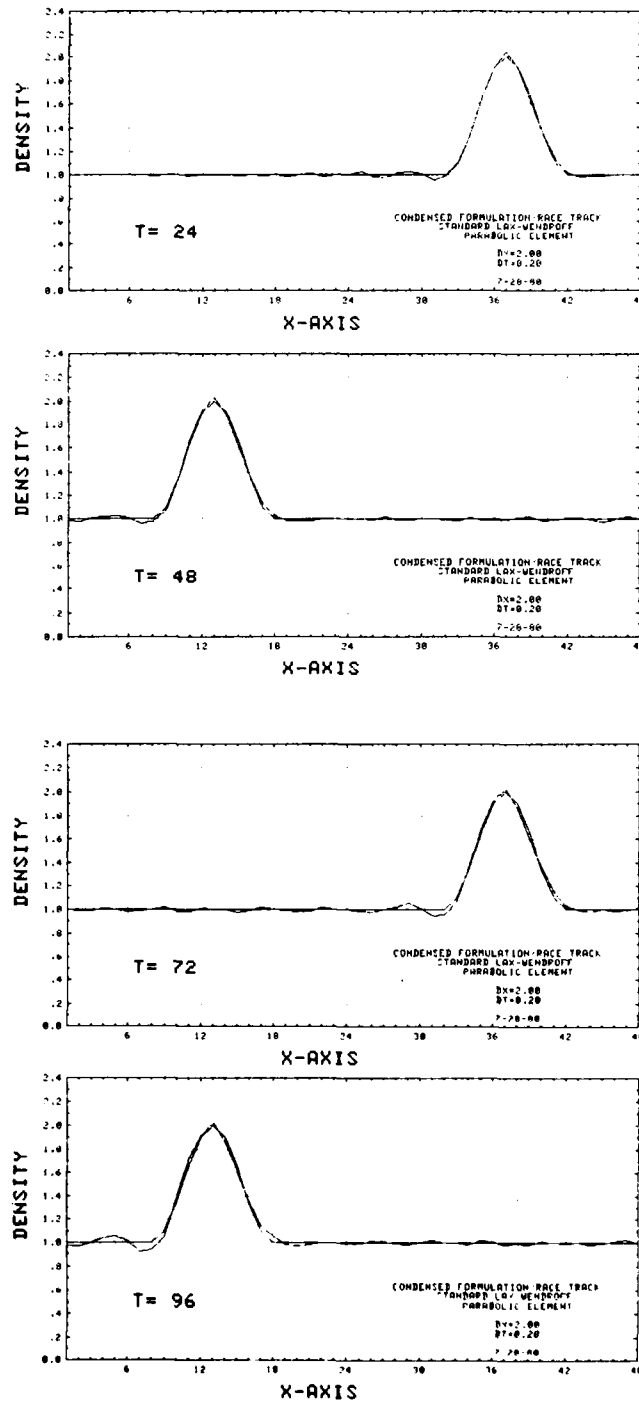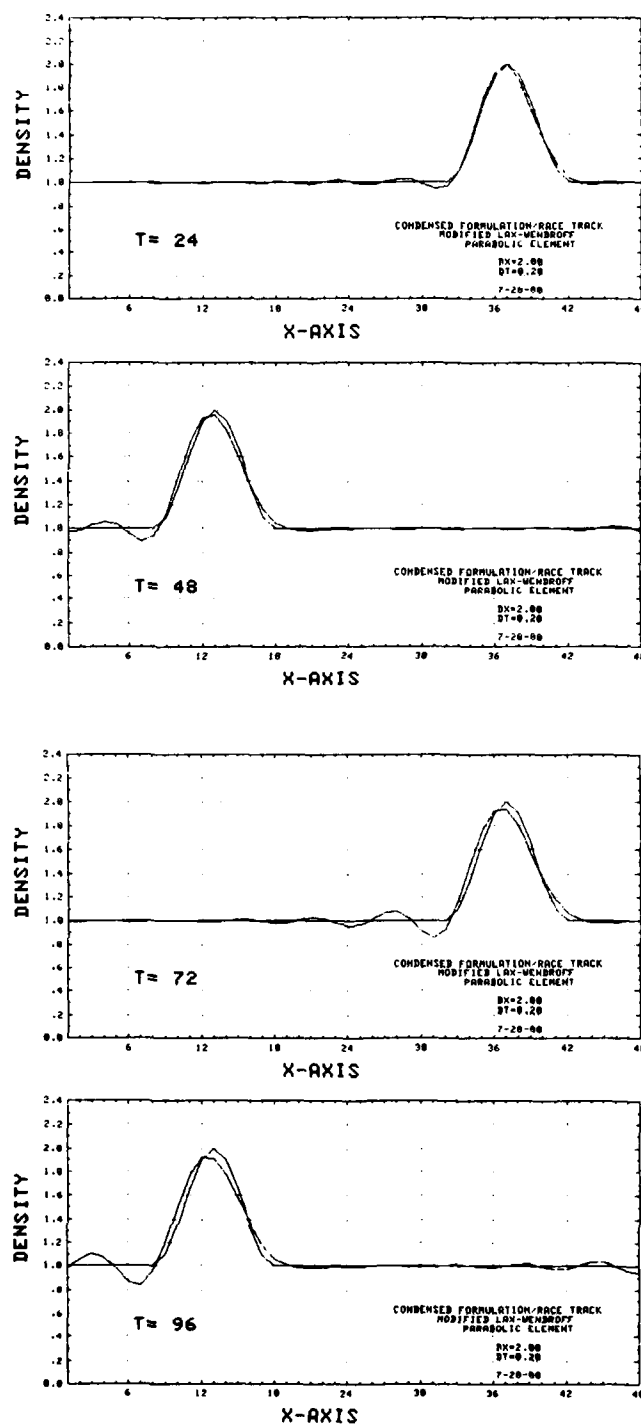
Fig. 5.2.5 — Advected cosine hill standard Lax-Wendroff, parabolic CFM

Fig. 5.2.6 — Advected cosine hill: modified Lax-Wendroff,
parabolic CFM
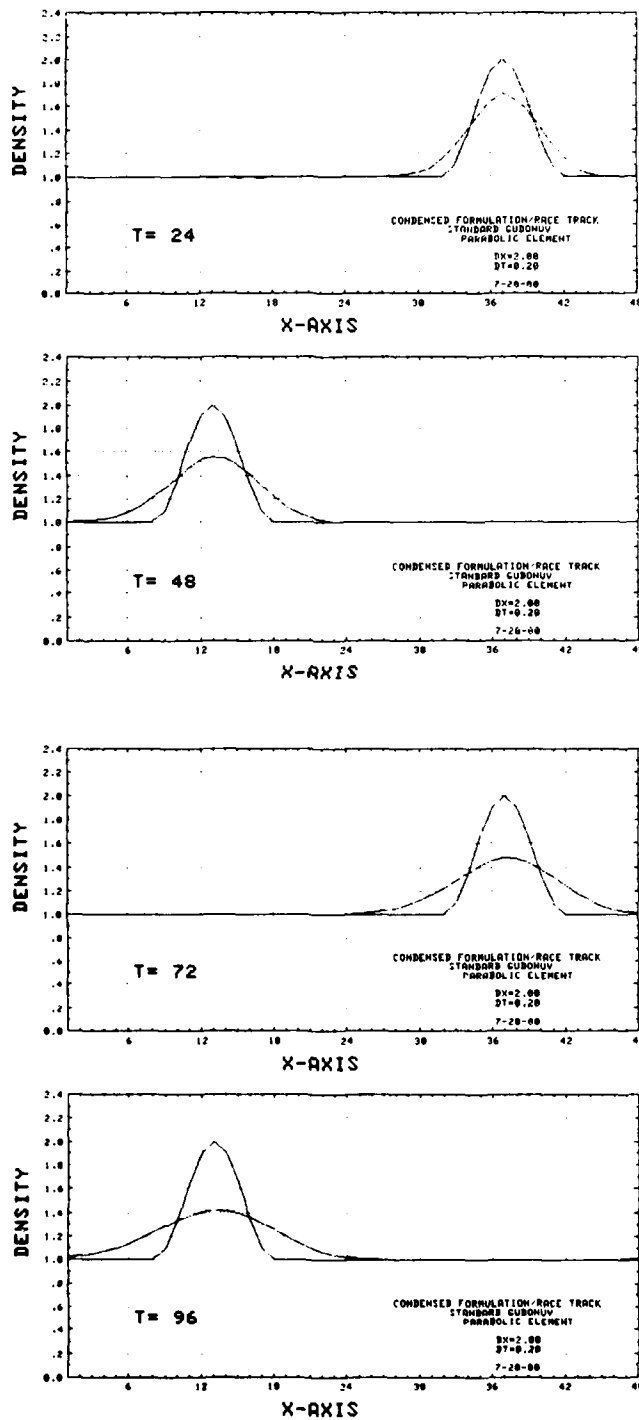
Fig. 5.2.7 — Advected cosine hill: standard Godunov, parabolic CFM
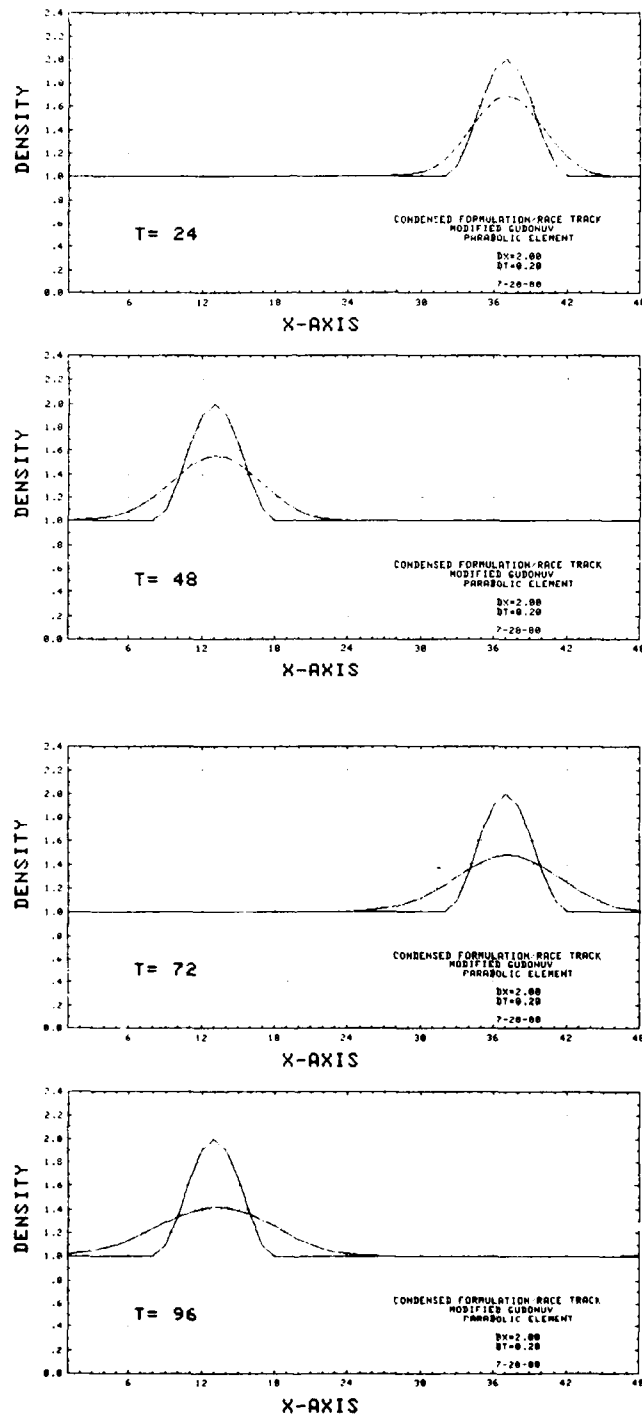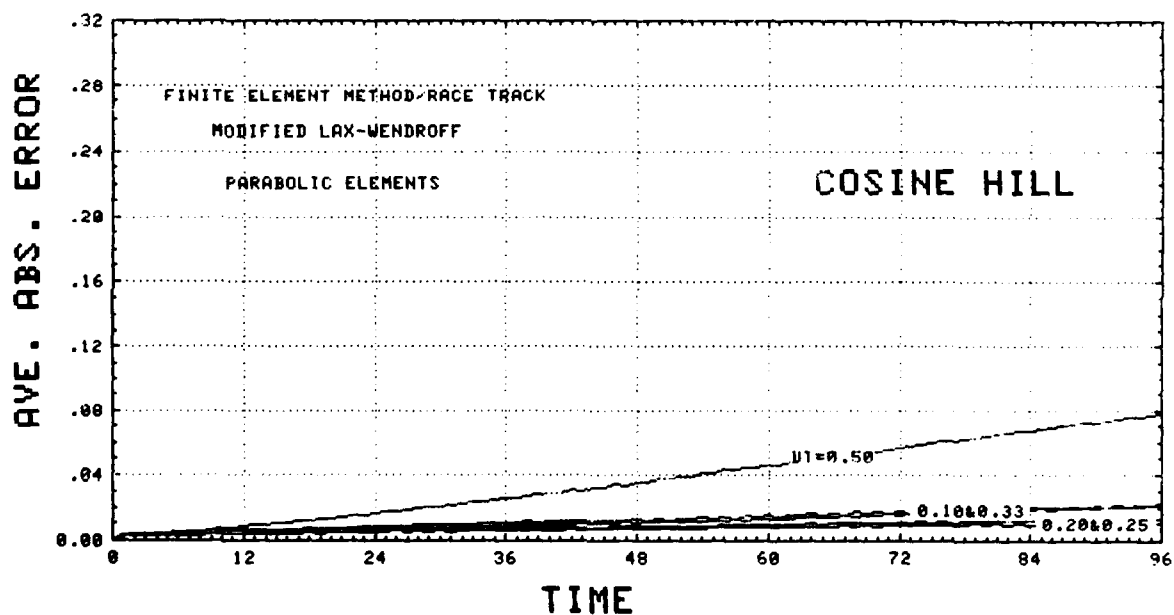
Fig. 5.2.8 — Advected cosine hill: modified Godunov, parabolic CFM
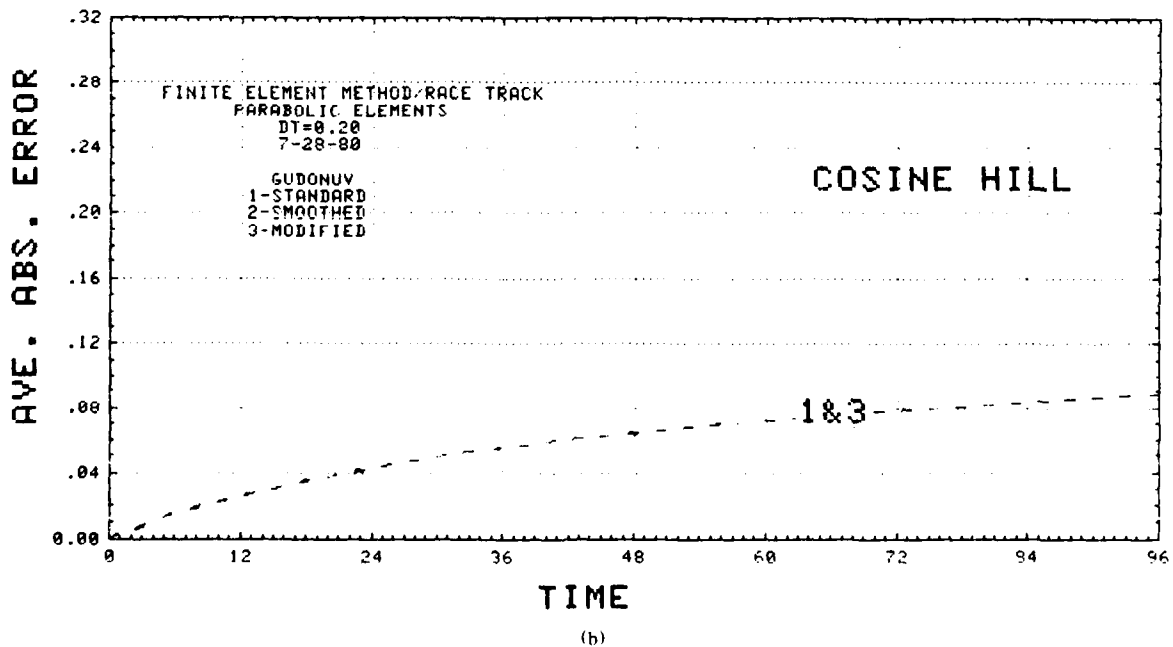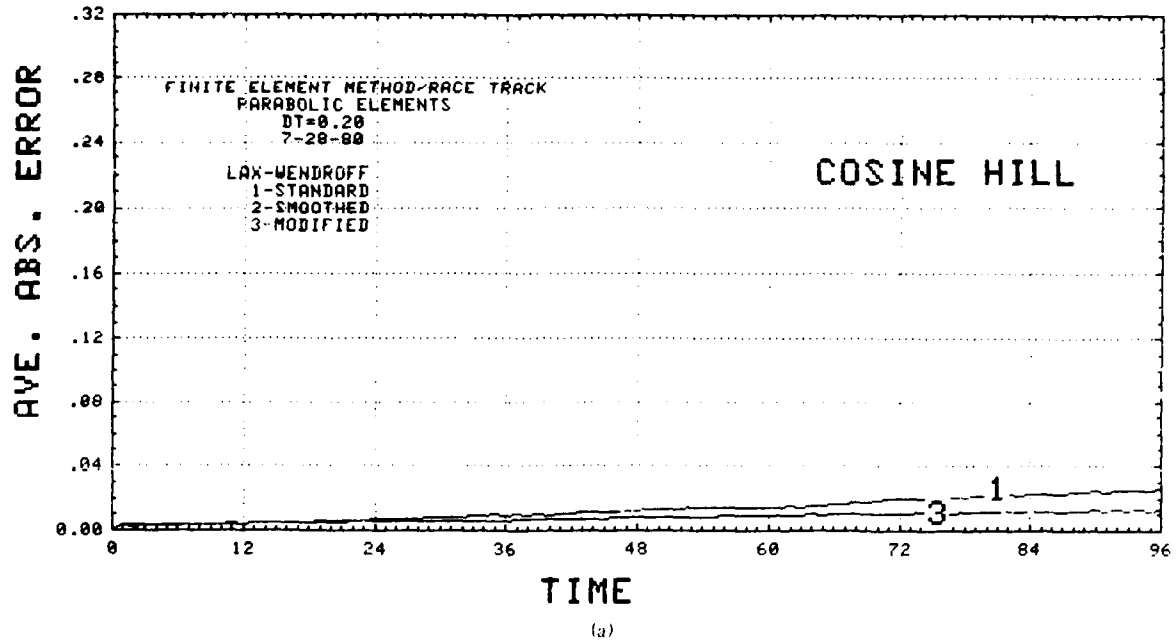
Fig. 5.2.9 — Average absolute errors for cosine hill advection (a) parabolic FEM, Lax-Wendroff time integrators (b) parabolic FEM, Godunov time integrators (c) parabolic CFM, Lax-Wendroff time integrators (d) parabolic CFM, Godunov time integrators

(c)

(d)
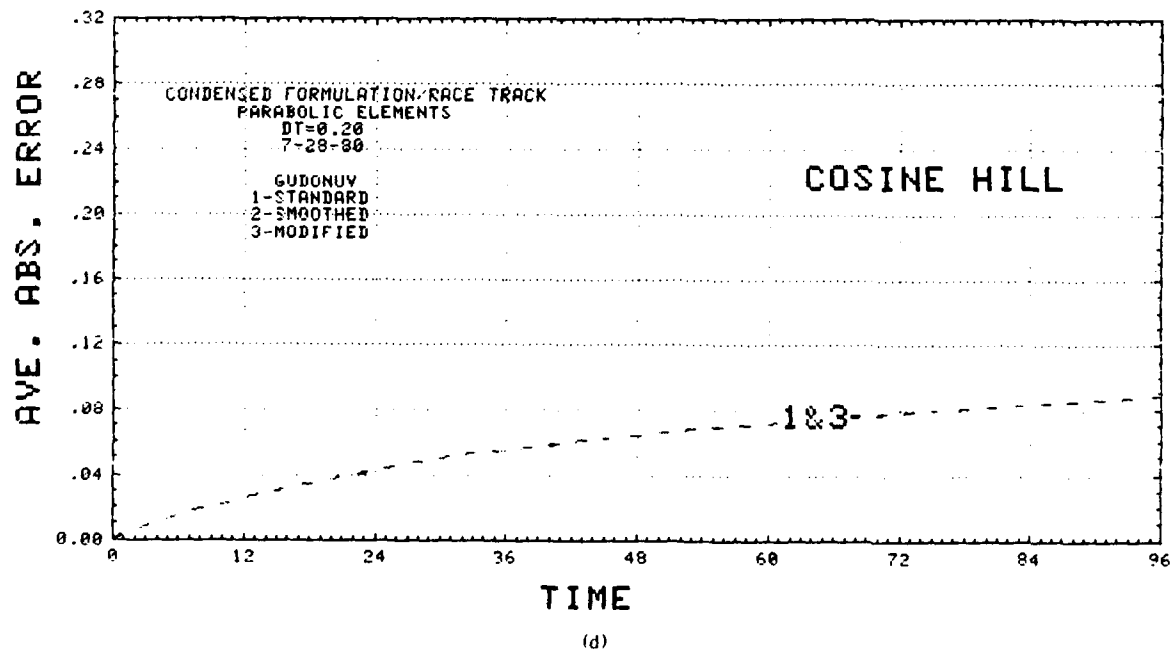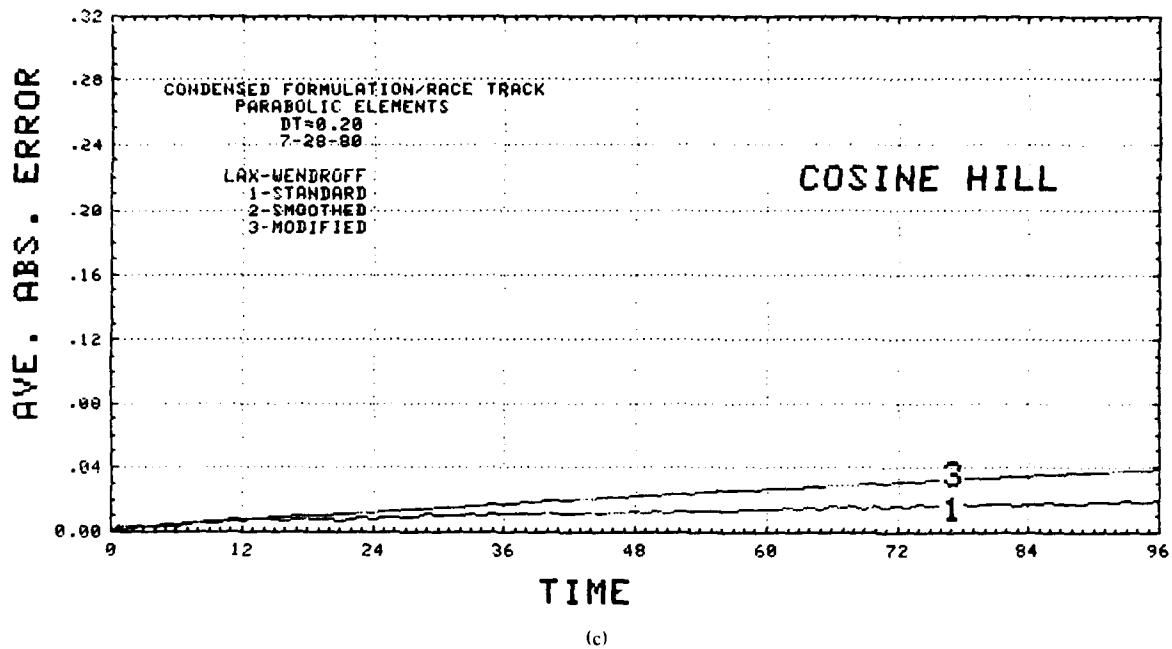
Fig. 5.2.9 (Continued) — Average absolute errors for cosine hill advection (a) parabolic FEM, Lax-Wendroff time integrators (b) parabolic FEM, Godunov time integrators (c) parabolic CFM, Lax-Wendroff time integrators (d) parabolic CFM, Godunov time integrators
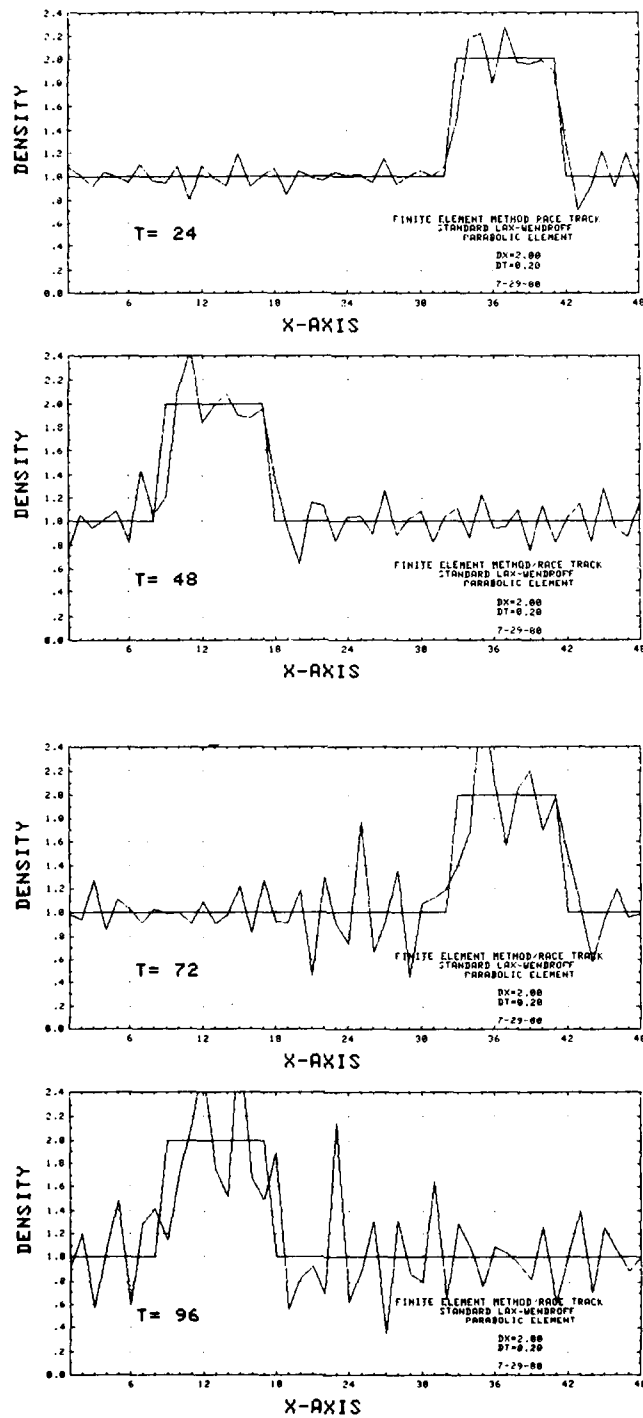
Fig. 5.2.10 — Advected square hill: standard Lax-Wendroff,
parabolic FEM
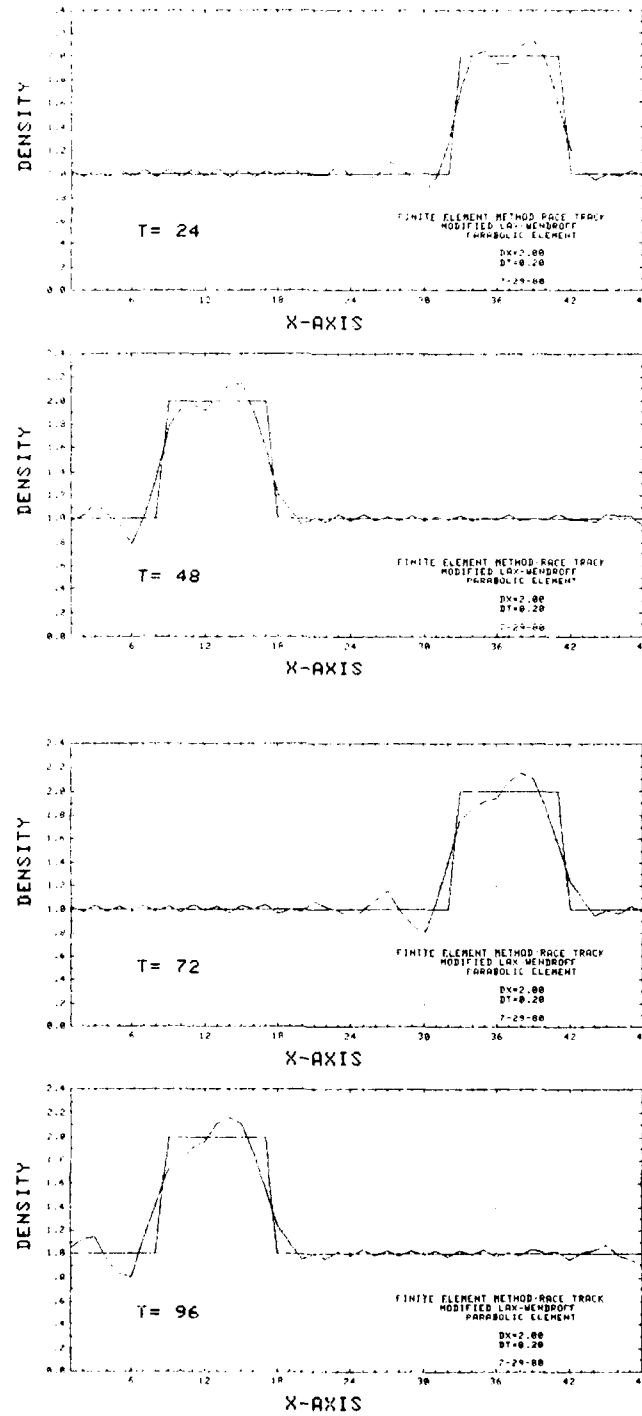
Fig. 5.2.11 — Advected square hill: modified Lax-Wendroff, parabolic FEM
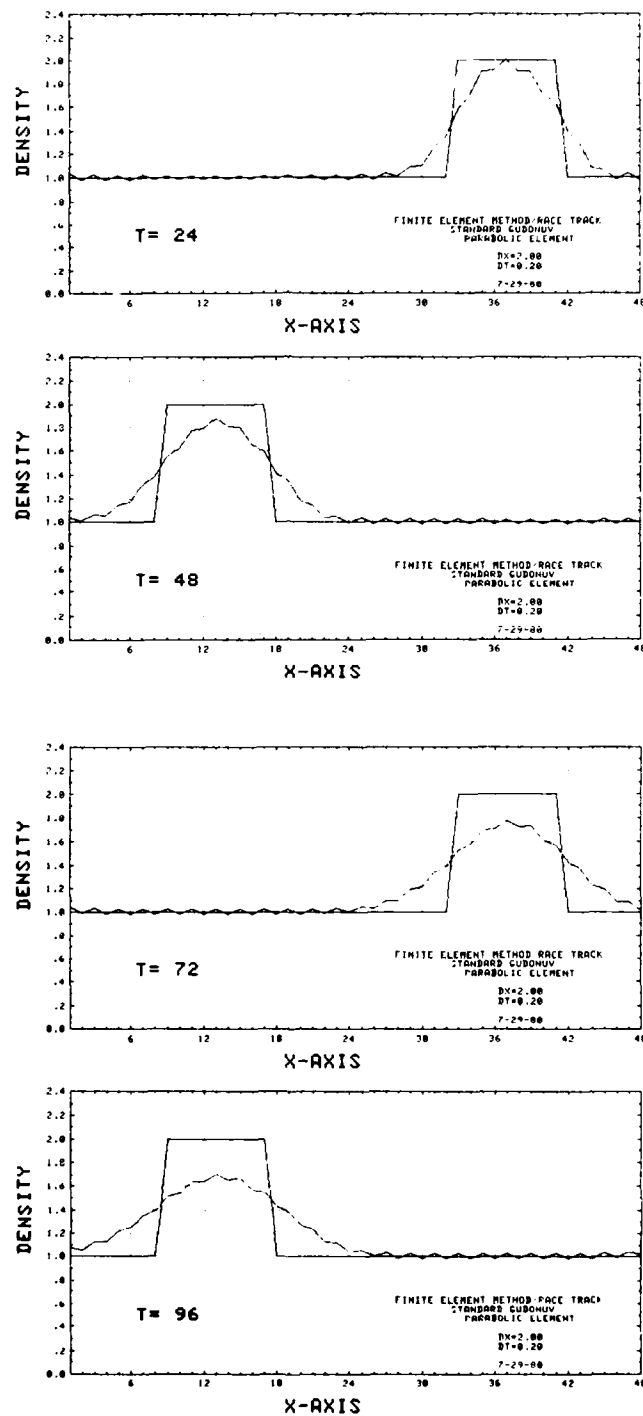
Fig. 5.2.12 — Advected square hill: standard Godunov,
parabolic FEM
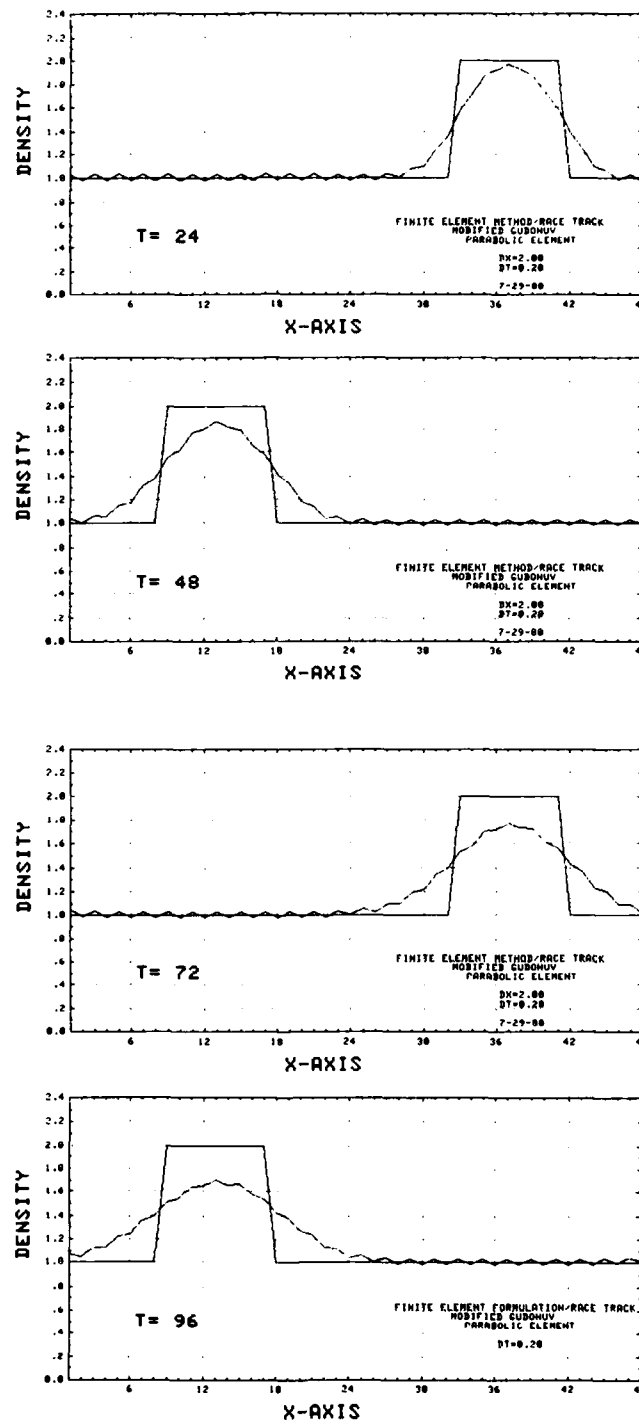
Fig. 5.2.13 — Advected square hill: modified Godunov,
parabolic FEM
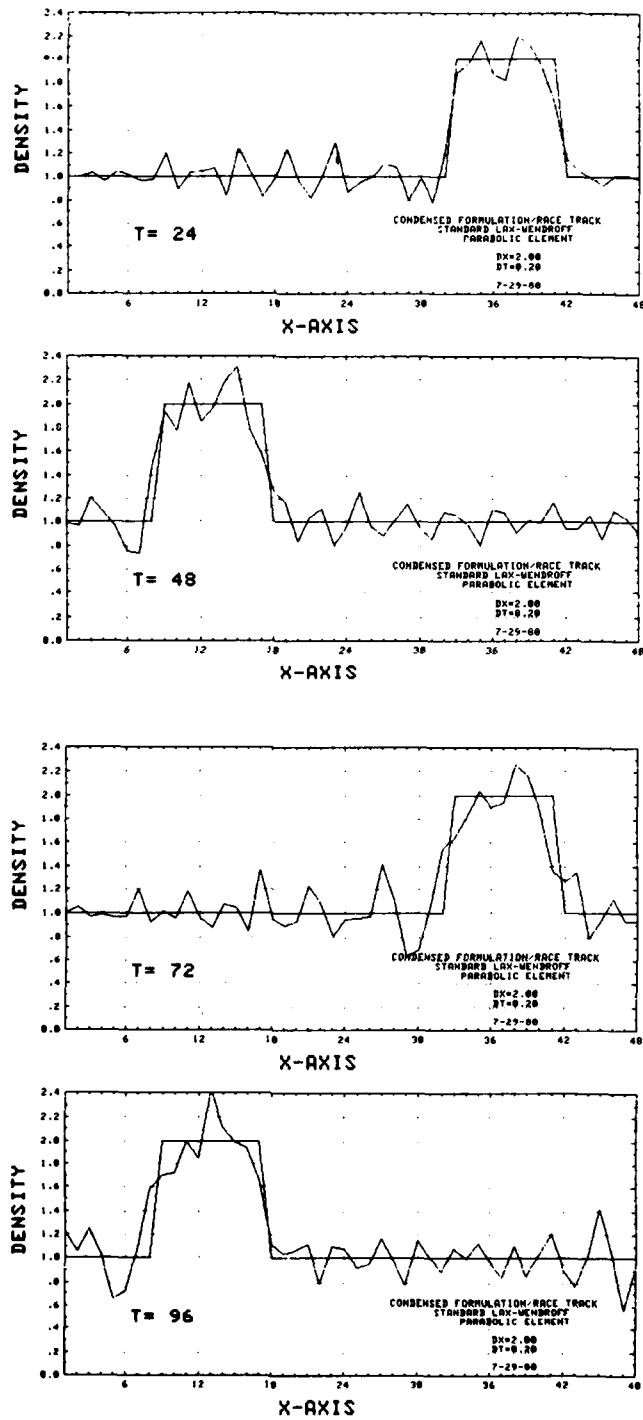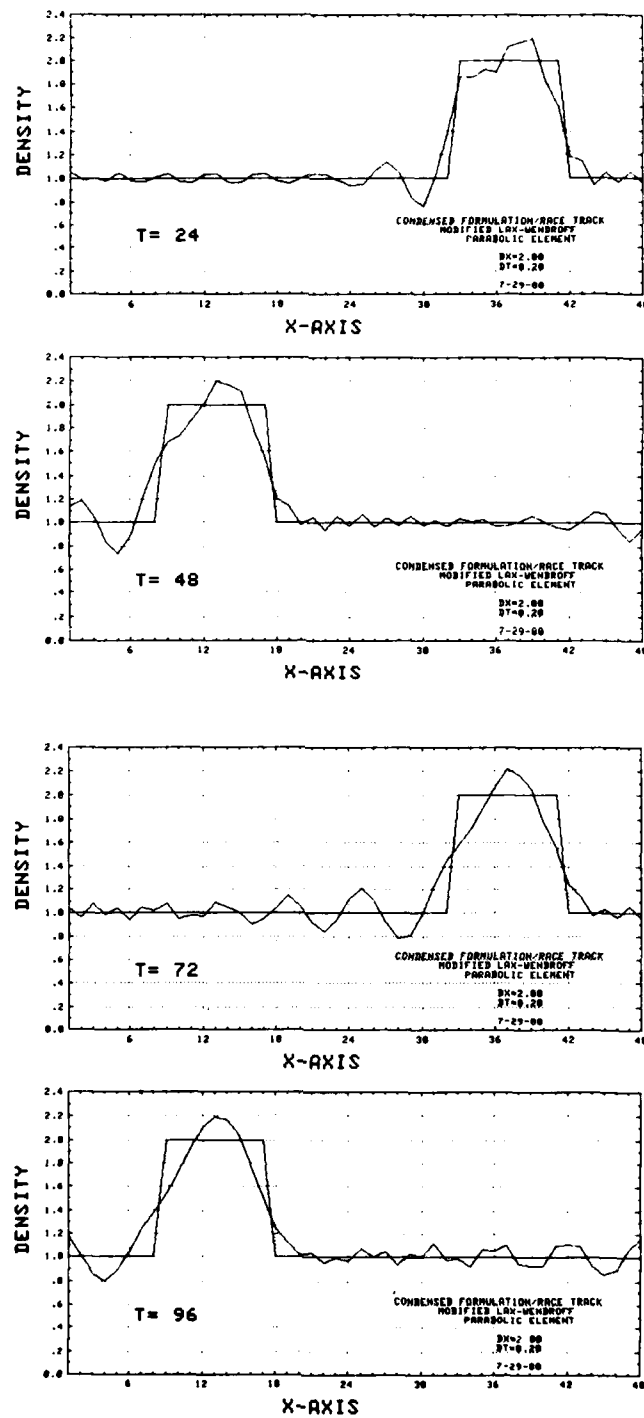
Fig. 5.2.14 — Advected square hill: standard Lax-Wendroff,
parabolic CFM

Fig. 5.2.15 — Advected square hill: modified Lax-Wendroff,
parabolic CFM
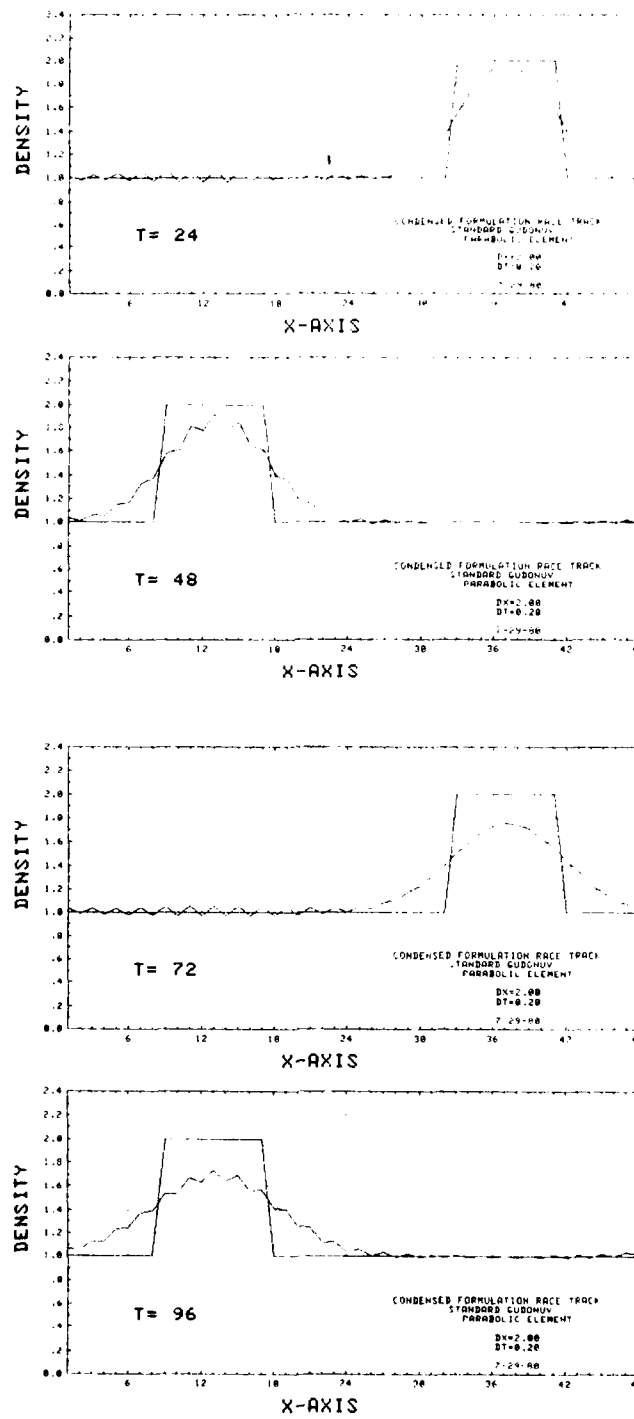
Fig. 5.2.16 — Advected square hill: standard Godunov, parabolic CFM

Fig. 5.2.17 — Advected square hill: modified Godunov,
parabolic CFM
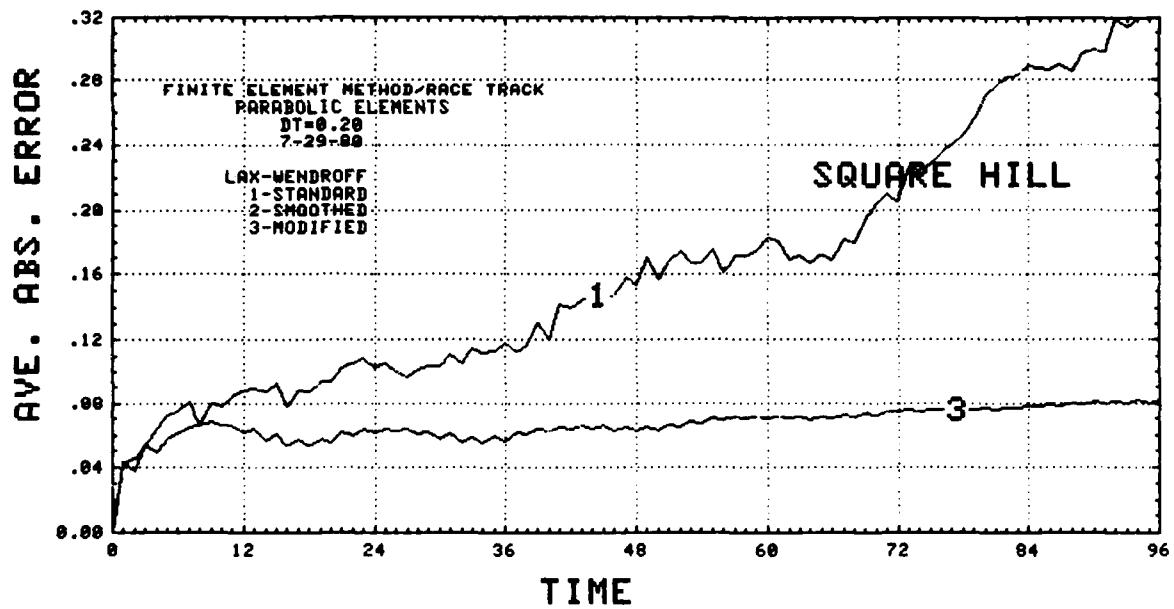
(a)
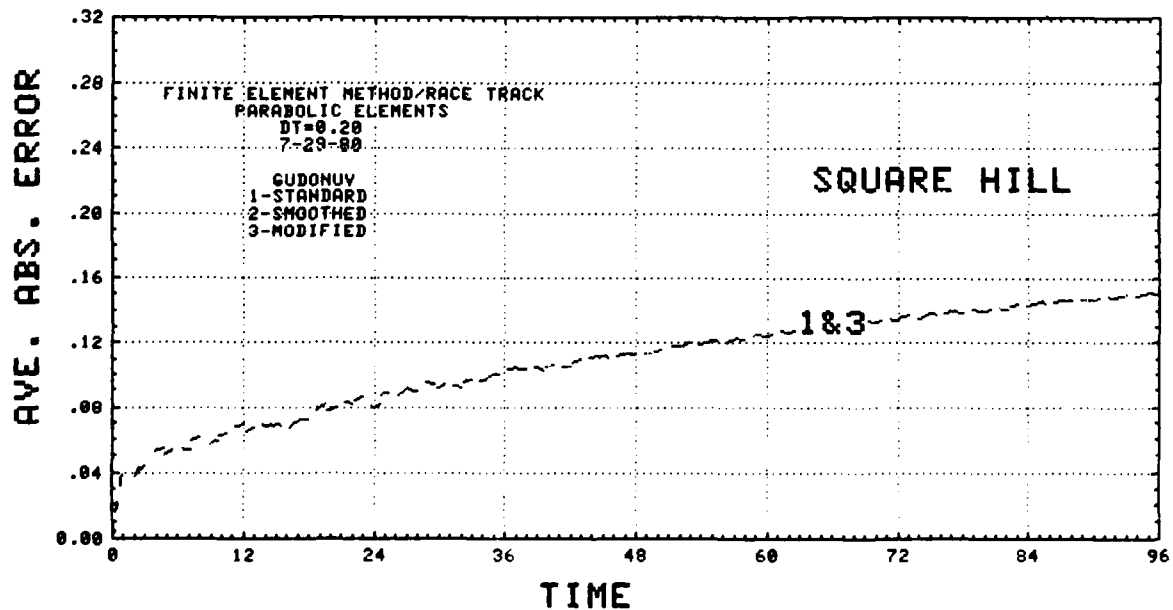
(b)

Fig. 5.2.18 — Average absolute errors for square hill advection (a) parabolic FEM, Lax-Wendroff time integrators (b) parabolic FEM, Godunov time integrators (c) parabolic CFM, Lax-Wendroff time integrators (d) parabolic CFM, Godunov time integrators

73

(c)

(d)

Fig 5.2.18 (Continued) — Average absolute errors for square hill advection (a) parabolic FEM, Lax-Wendroff time integrators (b) parabolic FEM, Godunov time integrators (c) parabolic CFM, Lax-Wendroff time integrators (d) parabolic CFM, Godunov time integrators

74

(a)

(b)

Fig. 5.4.1 — Average absolute errors for cosine hill advection versus time step size (a) standard Lax-Wendroff, linear FEM (b) modified Lax-Wendroff, parabolic FEM

75
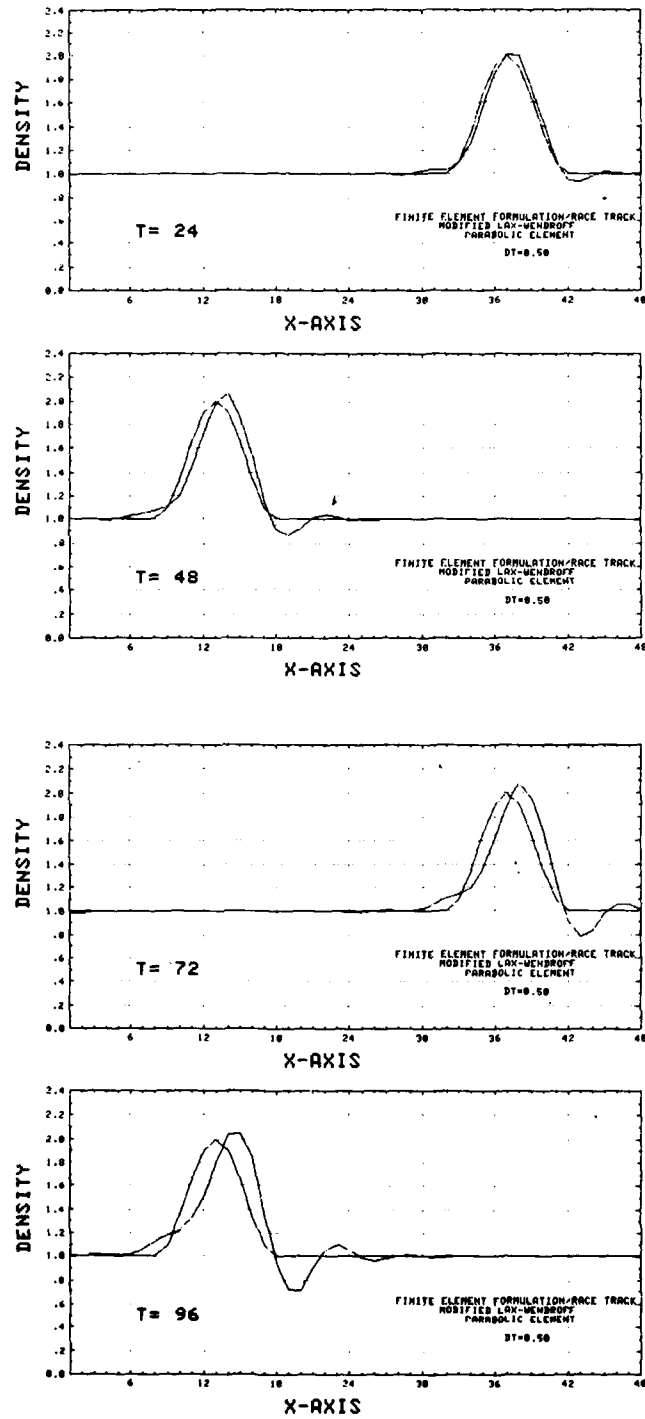
Fig. 5.4.2 — Advected cosine hill: modified Lax-Wendroff,
parabolic FEM with $\Delta t = 0.5$ s.
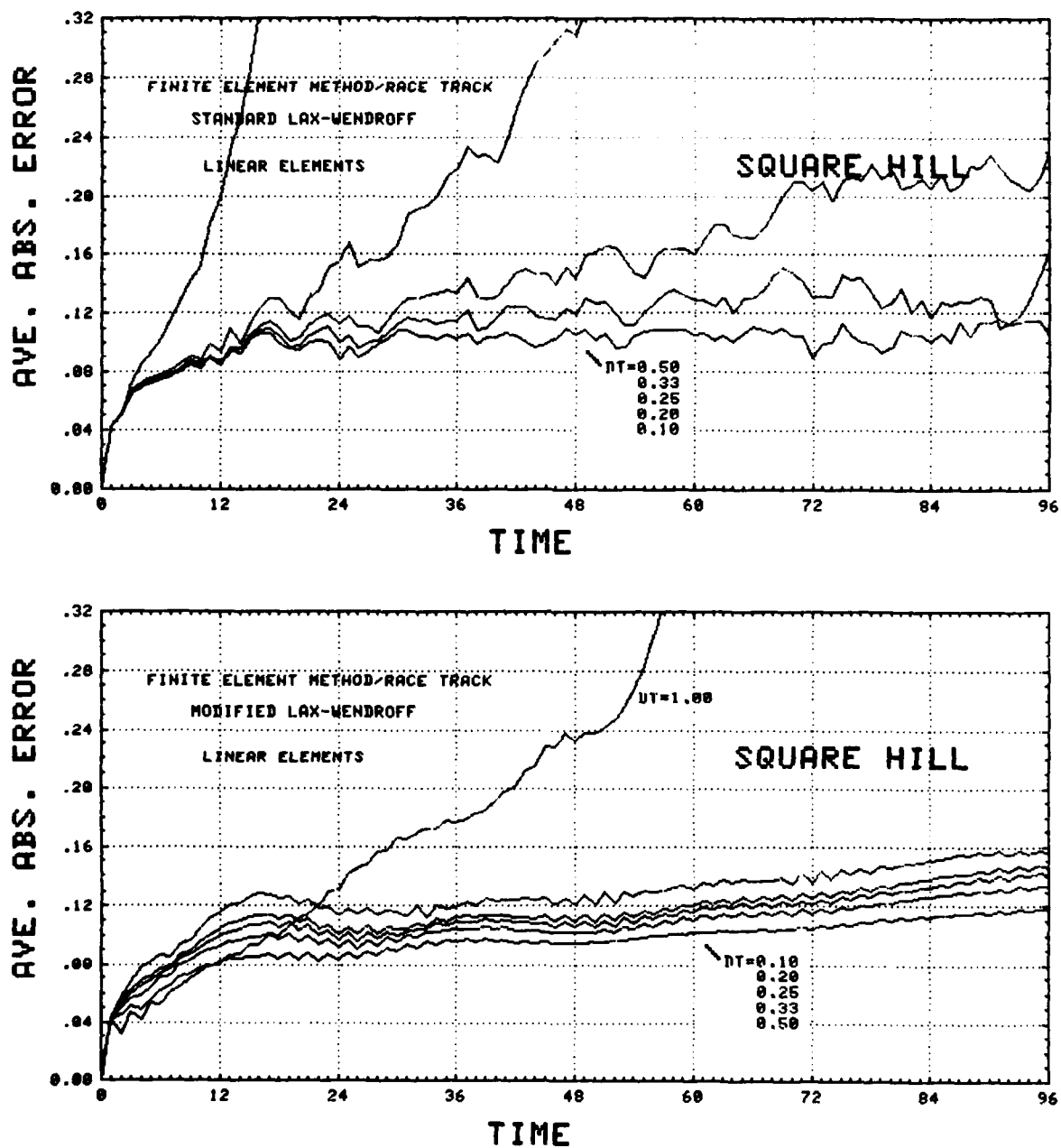
Fig. 5.4.3 — Average absolute errors for square hill advection versus time step size using linear FEM
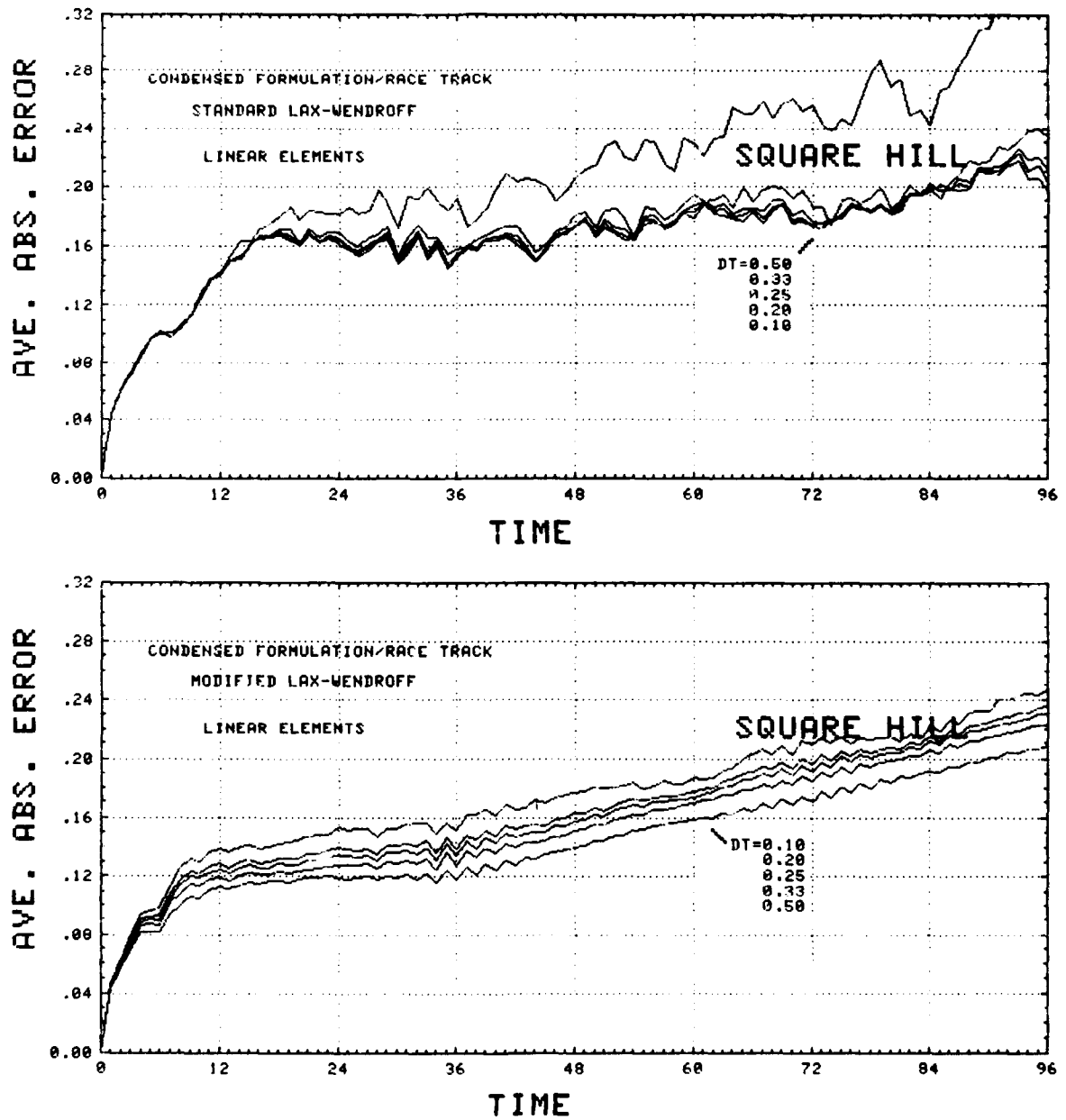
Fig. 5.4.4 — Average absolute errors for square hill advection versus time step size using linear CFM
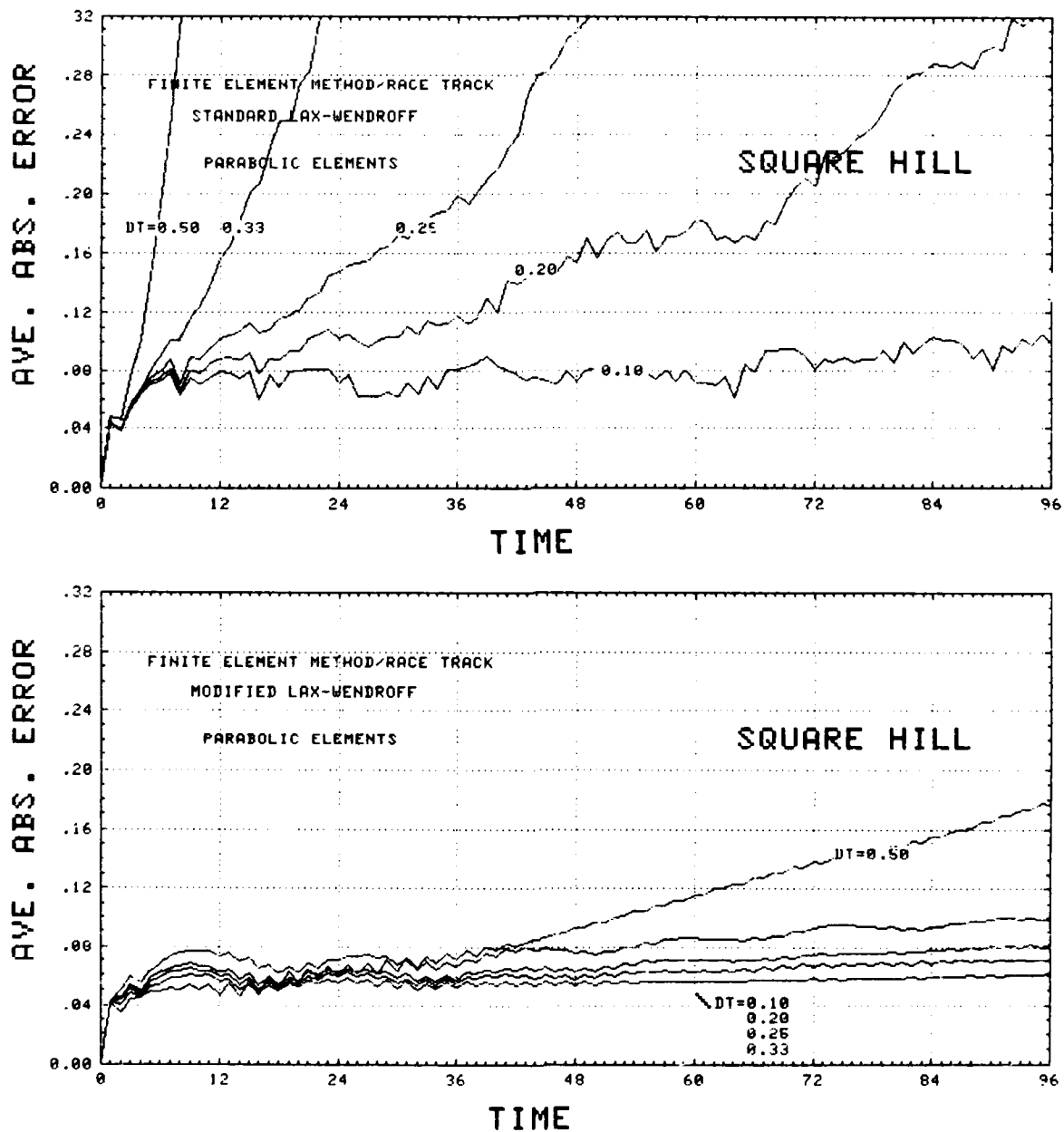
Fig. 5.4.5 — Average absolute errors for square hill advection versus time step size using parabolic FEM
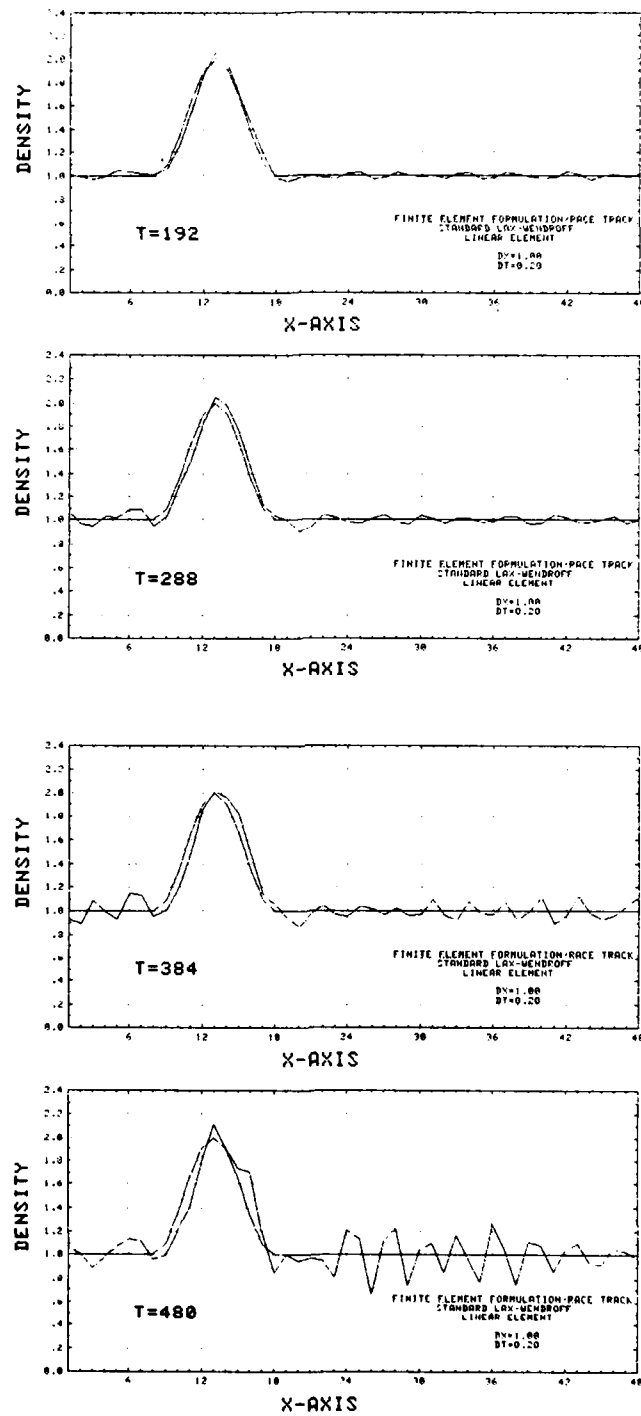
Fig. 5.5.1 — Advected cosine hill: standard Lax-Wendroff, linear FEM
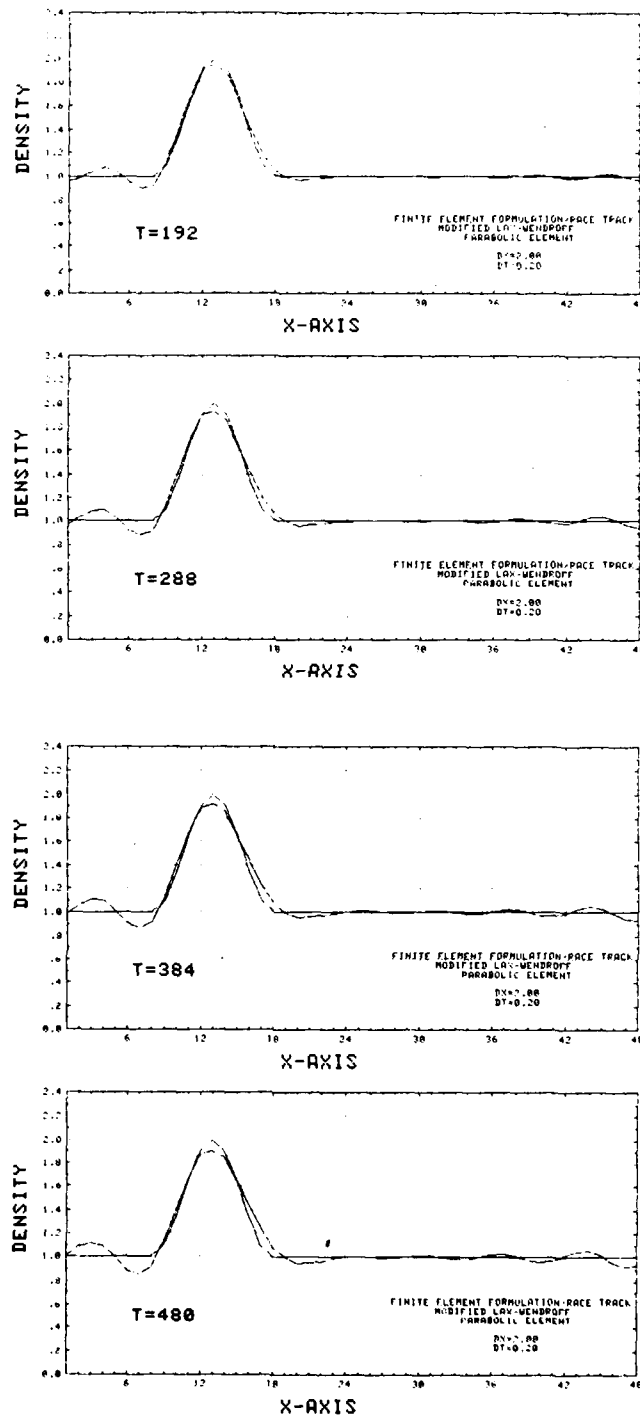
Fig. 5.5.2 — Advected cosine hill: modified Lax-Wendroff, parabolic FEM
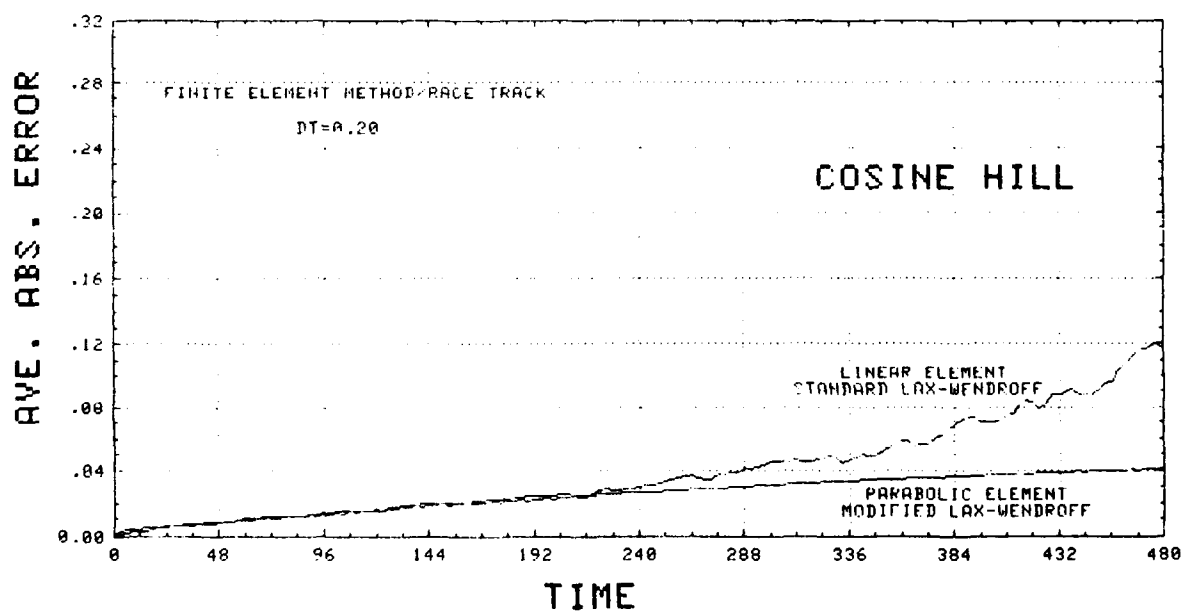
Fig. 5.5.3 — Average absolute errors for cosine hill advection
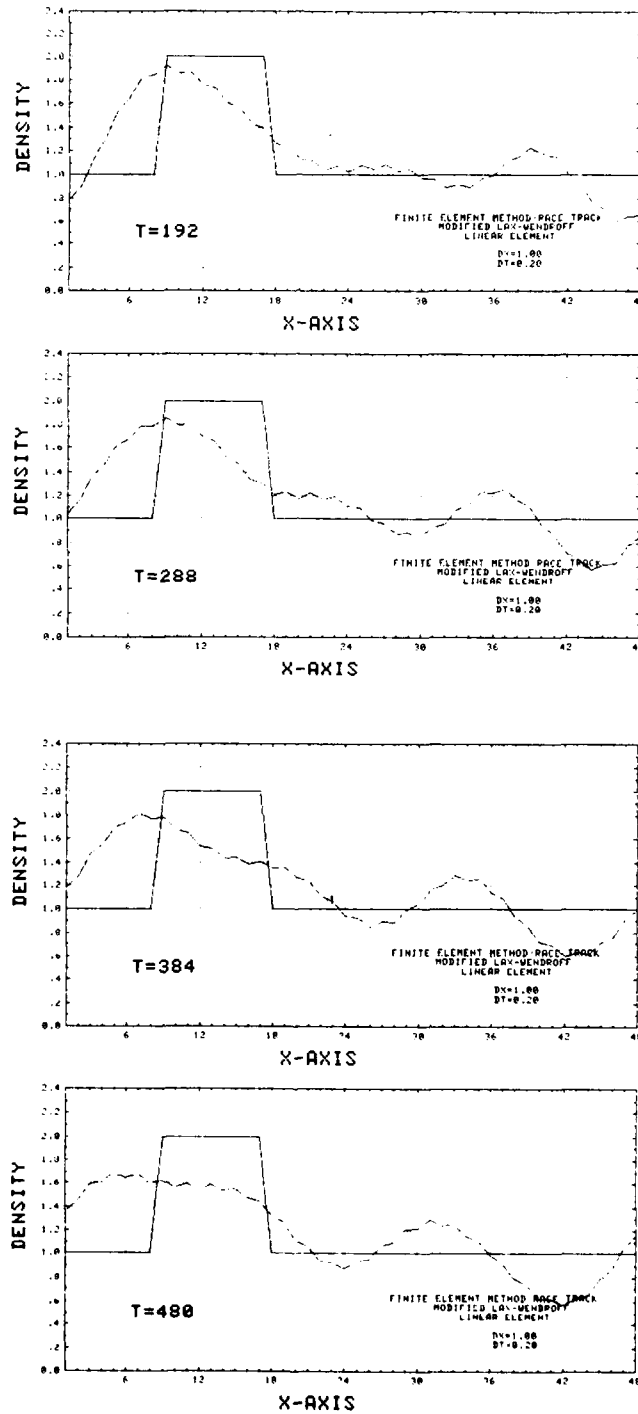
Fig. 5.5.4 — Advected square hill: modified Lax-Wendroff,
linear FEM
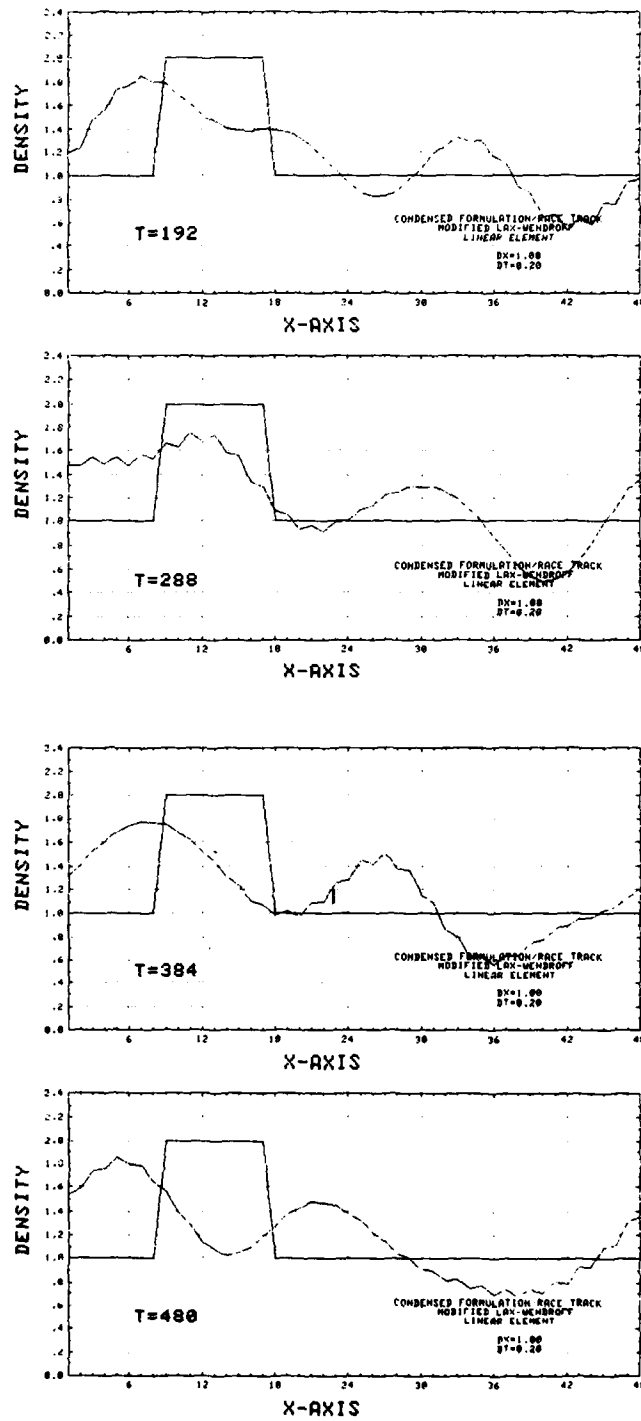
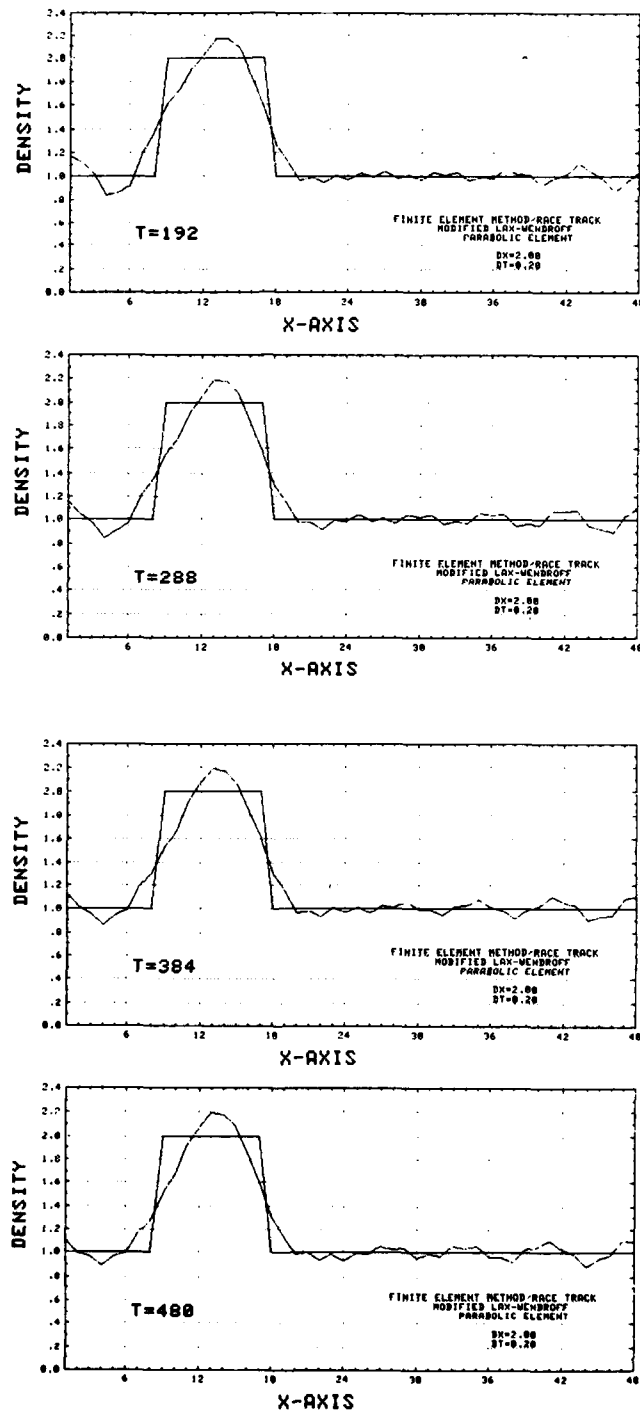Fig. 5.5.5 — Advected square hill: modified Lax-Wendroff,
linear CFM

Fig. 5.5.6 — Advected square hill: modified Lax-Wendroff,
parabolic FEM

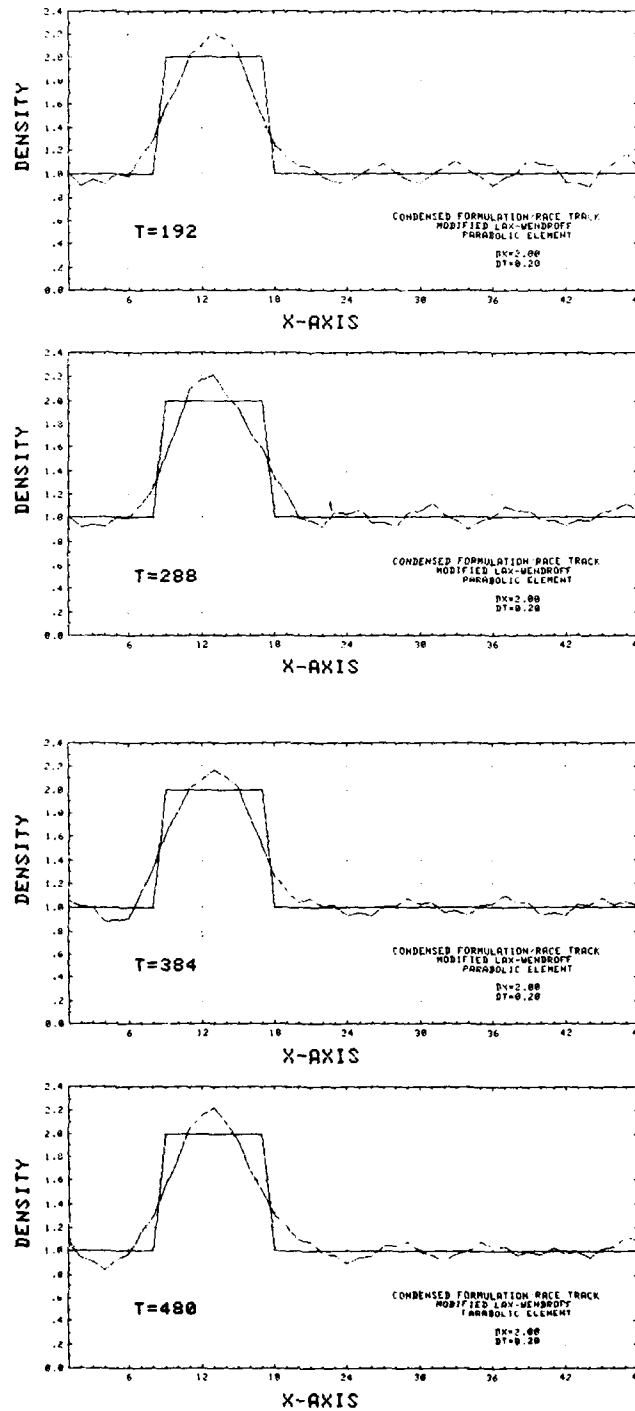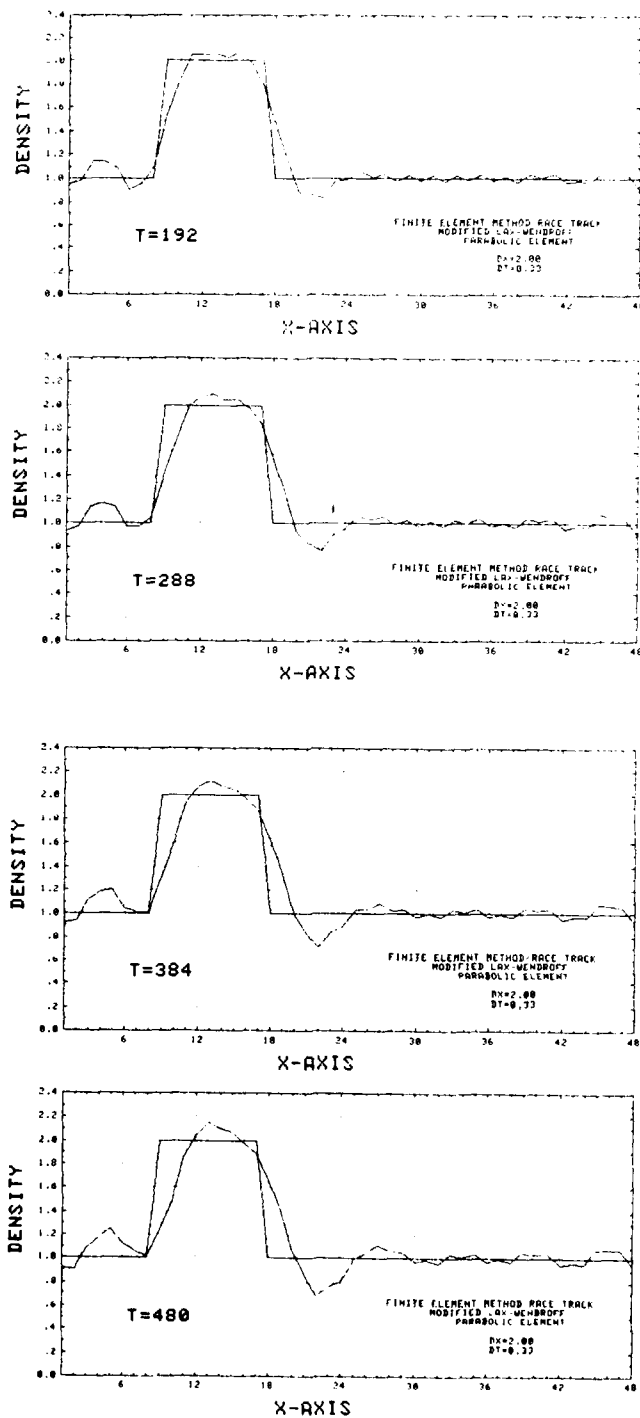Fig. 5.5.7 — Advected square hill: modified Lax-Wendroff,
parabolic CFM

Fig. 5.5.8 — Advected square hill modified Lax-Wendroff,
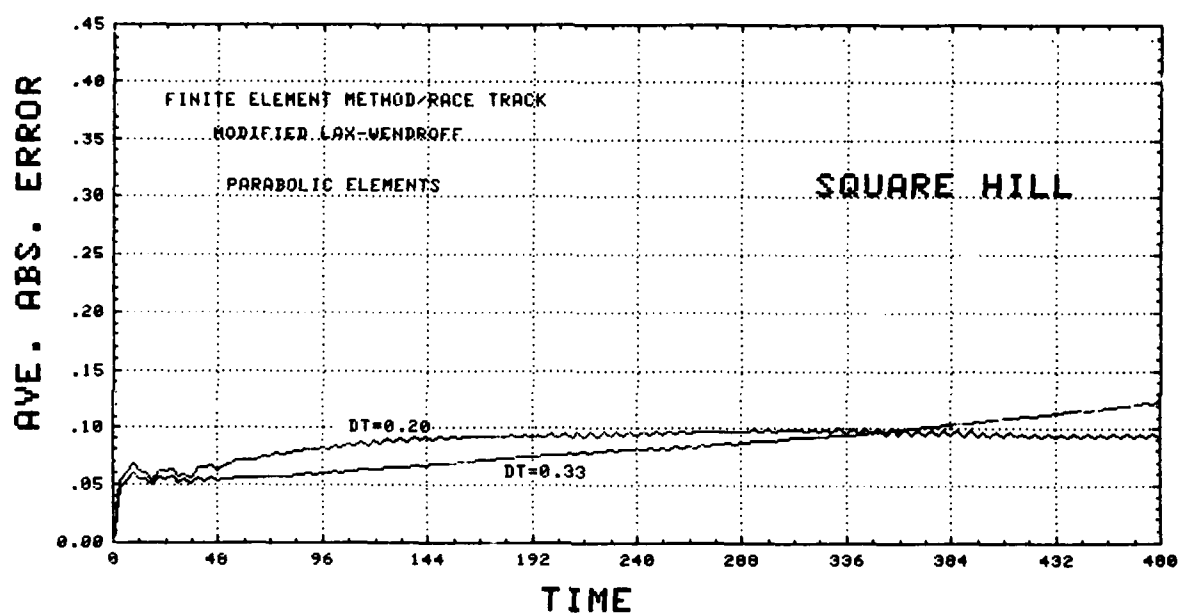parabolic FEM with $\Delta t = 0.33$ s.

Fig. 5.5.9 — Average absolute errors for square hill advection

DATE
ILME